UNIVERSITY OF SOUTHAMPTON

FACULTY OF PHYSICAL SCIENCES AND ENGINEERING

Physics and Astronomy

Synthesis and physicochemical properties of programmed DNA-gold nanoparticle assemblies

by

Johanna Midelet

Thesis for the degree of Doctor of Philosophy

January 2018

UNIVERSITY OF SOUTHAMPTON

ABSTRACT

FACULTY OF PHYSICAL SCIENCES AND ENGINEERING

Physics and astronomy

Thesis for the degree of Doctor of Philosophy

SYNTHESIS AND PHYSICOCHEMICAL PROPERTIES OF PROGRAMMED DNA-GOLD NANOPARTICLE ASSEMBLIES

by

Johanna Midelet

Gold nanoparticles (AuNPs) are attractive nanomaterials due to their specific physical and chemical properties. The use of synthetic deoxyribonucleic acid (DNA) to functionalise nanoparticles and bring them into programmed 2 or 3D structures has further enhanced their attractiveness as materials. These novel nanomaterials exhibit tuned properties, depending on their structures. The design process of such structures for specific applications can be facilitated by the study of physicochemical properties.

In this project, the aim was to synthesise programmed DNA-gold nanoparticle assemblies and to study and compare their physicochemical properties.

Gold nanoparticles of various sizes (5 to 50 nm) were synthesised and functionalised with designed oligonucleotides. They were then self-assembled to form dimer assemblies. A new strategy was developed to functionalise large spherical gold nanoparticles with a specific number of oligonucleotides.

Physicochemical properties of both single and dimer assembled gold nanoparticles were studied using a range of methods. Extinction and scattering as well as two photon photoluminescence spectroscopies were used to characterise optical properties of gold nanoparticles. The diffusion properties were studied using microfluidics and two photon excited photoluminescence-fluctuation correlation spectroscopy. Finally, the sedimentation process of gold nanoparticles was followed using digital photography. The results obtained showed differences in the properties between single and assembled gold nanoparticles.

Finally, a new way of synthesising DNA-AuNP assemblies was developed using a seeded-growth method. DNA-gold nanoparticle dimers of 5 nm were introduced into the growth process and either large spherical or branched DNA-gold nanoparticle dimers were obtained. After purification, the assemblies were studied using extinction and scattering spectroscopies. This new way of synthesising DNA-gold nanoparticle assemblies has exciting potential for the development of a larger library of gold nanoparticle structures.

DECLARATION OF AUTHORSHIP

I, **Johanna Midelet**

declare that this thesis and the work presented in it are my own and has been generated by me as the result of my own original research.

Synthesis and physicochemical properties of programmed DNA-gold nanoparticle assemblies

I confirm that:

1. This work was done wholly or mainly while in candidature for a research degree at this University;

2. Where any part of this thesis has previously been submitted for a degree or any other qualification at this University or any other institution, this has been clearly stated;

3. Where I have consulted the published work of others, this is always clearly attributed;

4. Where I have quoted from the work of others, the source is always given. With the exception of such quotations, this thesis is entirely my own work;

5. I have acknowledged all main sources of help;

6. Where the thesis is based on work done by myself jointly with others, I have made clear exactly what was done by others and what I have contributed myself;

7. Parts of this work have been published as:

Articles in academic press:

1. Johanna Midelet, Afaf H. El-Sagheer, Tom Brown, Antonios G. Kanaras, and Martinus H. V. Werts. “The sedimentation of colloidal nanoparticles in solution and its study using quantitative digital photography” *Part. Part.Syst. Charact.* 2017, 34, 10.

2. Johanna Midelet, Anne Débarre, Afaf H. El-Sagheer, Tom Brown, Antonios G. Kanaras, Martinus H.V. Werts. “Spectroscopic and hydrodynamic characterisation of DNA-linked gold nanoparticle dimers in solution using two-photon photoluminescence”. *ChemPhysChem*. 2018, 19, 1-11.

Posters or presentations at Conferences:

1. DGA-DSTL conference (2014,Bagneux, France). Poster: "Programmed Nanoparticle assemblies with DNA". Johanna Midelet, Martinus H. V. Werts, Antonios G. Kanaras.

2. E-MRS conference, (2015, Lille, France). Poster: "A new strategy for the isolation of discrete AuNP-DNA conjugates". Johanna Midelet, Nittaya Gale, Tom Brown, Antonios G. Kanaras.

3. COST Action MP1202, HINT training school. (2015, Ljubljana, Slovenia). Poster: "A new strategy for the isolation of discrete AuNP-DNA conjugates". Johanna Midelet, Nittaya Gale, Tom Brown, Antonios G. Kanaras.

4. DGA-DSTL conference (2015, Porton down, UK). Poster and Presentation: "Nanoparticle chiral structures as liquid metamaterials". Johanna Midelet, Nittaya Gale, Tom Brown, Martinus H. V. Werts, Antonios G. Kanaras.

5. Nanax7 conference (2016, Marburg, Germany). Poster: "Synthesis of large spherical and anisotropic gold nanoparticle dimers using a seeded growth method". Johanna Midelet, Amelie Heuer-Jungemann, Afaf H. El-Sagheer, Tom Brown, Martinus H. V. Werts, and Antonios G. Kanaras.

6. DGA-DSTL conference (2016, Paris, France). Poster and Presentation: "Nanoparticle structures as liquid metamaterials". Johanna Midelet, Tom Brown, Martinus H. V. Werts, Antonios G. Kanaras.

7. Nanax8 conference (2017, Braga, Portugal). Presentation: “Seeded-growth method applied to the synthesis of large spherical and anisotropic gold nanoparticle dimers”. Johanna Midelet, Afaf H. El-Sagheer, Tom Brown, Martinus H. V. Werts, and Antonios G. Kanaras.

Signed:

Date: 18/06/2018

Acknowledgements

Firstly, I would like to acknowledge Dr. Antonios Kanaras for giving me the financial support to carry on this project and giving me the opportunity to present my work in international conferences. I would also like to thank Dr. Martinus Werts, my second supervisor for the helpful discussions and his support throughout this project. I would also like to thank him for initially contacting me for this PhD and convincing me to accept!

DSTL is gratefully acknowledge for the financial support of this PhD. I would like to particularly thank Kevin Bown and Dr. Sarah Goodchild for being my technical partners over the four years of my PhD.

The help and encouragement of Dr. Nittaya Gale with the DNA work I carried on is particularly acknowledge. Furthermore, the participation of Prof. Tom Brown and Dr. Afaf H. El-Sagheer in the project for scientific discussions or DNA synthesis is greatly acknowledge. I would also like to thank the people of the Biomedical Imaging Unit for their help with microscopy. Thank you to Oliver Freeman, MPhys student for his help with the seeding growth part of this thesis.

I would like to say a big thank you to the past and present members of my research group and particularly to Dr. Amelie Heuer-Jungemman, Dr. Pascal Harimech, Dr. Patrick Vilela, Dr-soon-to-be Marilena Kyriazi and Miss AFDF. You all became more than just colleagues over these past four years. Girls a special thank you for being there for the highs and lows of this adventure.

I cannot forget to thank my special colleague, Clyde Midelet for the scientific discussions and for always replying to my annoying demands. Many thanks to Suzie Turnbull, for being there on all these Fridays after work but also way more than this.

Furthermore I would like to thanks all the housemates I met along these four years of PhD. You guys made me feel welcome and at home when I needed it. A special thank you to Lisa Jones, with who I shared the highs and lows of the PhD life. I would also like to thanks Chloe Harvey for sharing the crazy 55 Westridge Road with me. Thanks to Françoise Theobald for all the craziness.

I have to thanks my friends from home and especially Orianne Drean, Pauline Kervarrec, Lea Fevrier, Anne-Valerie Pogam and Margaux Le Couric for being able to cheers me up and understand the time where I did not give news because I was to busy trying to become a doctor! Thanks to Dr. Eleonore Mourad for the support even with the distance. And thanks to Dr. Mathieu Denis to have share the Southampton experience with me.

A particular thank you to Mrs. Pamela Watson for proof-reading this thesis and making the last moments of my writing adventure feel nicer.

Finally I would like to thank my family for the amazing support I received during this four years of PhD. My parents Brigitte and Jean-Marc Midelet (petits parents) who encouraged me to start this PhD. My two brothers, Christopher and Clyde Midelet for their supports, jokes and visits. It was always a pleasure to come back home Home! A very special thank you to my boyfriend Dr. Alastair Watson for all the support especially when I was being an absolute infernalo.

Abbreviations

A- Adenine

AUC- Analytical ultracentrifugation

AuCl – Gold monochloride

AuNP – Gold nanoparticle

BSPP- Bis(p-sulfonatophenyl)phenyl phosphine dehydrate dipotassium salt

Bp – Base pair

C- Cytosine

CCD – Charge coupled device

CTAB- Cetyl trimethylammonium bromide

CTAC- Cetyl trimethylammonium chloride

D – Diffusion coefficient

DIBO - Dibenzocyclooctyne

DLS-Dynamic light scattering

DNA- Deoxyribonucleic acid

dNTP – Deoxynucleotide triphosphate

dsDNA – Double stranded DNA

FCS- Fluctuation correlation spectroscopy

G- Guanine

HPLC- High pressure liquid chromatography

LED – Light-emitting diode

LSPR - Localised surface plasmon resonance

$MgCl_2$ – Magnesium chloride

NaCl – Sodium chloride

NIR – Near infrared

NP – Nanoparticle

OD – Optical density

PAE- Programmable atom equivalents

PAGE – Polyacrylamide gel electrophoresis

PCR- Polymerase chain reaction

PDMS – Polydimethyl siloxan

PTOFS – Photon time-of-flight spectroscopy

QENLS- Quantum-efficiency normalized light scattering

RCF- Relative centrifugal force

RLS – Resonant light scattering

s – Sedimentation coefficient

S-Au – Sulfur-gold

SDS- Sodium dodecyl sulphate

SERS- Surface enhanced Raman scattering

ssDNA – Single stranded DNA

T- Thymine

TBE- Tris borate ethylenediaminetetraacetic acid

TEM- Transmission electron microscopy

TPPL- Two-photon excited photoluminescence

UV-Vis - Ultraviolet-visible

λ – Wavelength

ξ – Extent of the diffusion

List of Figures

List of Equations

Equation 5.7. Centrifugal acceleration g_{cfg} necessary for the chosen centrifugation time t_{cfg} and a liquid height in the centrifuge tube z_{tube} This can be expressed as `relative centrifugal force', RCF = gcfg/g, where g = 9.81m.s^{-1} 171

List of Tables

Table of Contents

Chapter 1. Introduction

Colloidal metal nanoparticles (NPs) have been extensively studied during the last decades because of their unique physical and chemical properties diverging from their bulk counterparts. Due to surface effects, metallic nanoparticles give strong optical response in the UV-Visible range. Furthermore their surface can be easily functionalised allowing a large range of applications from catalysis and photonics to medicine [1, 2]. The capability to bring together nanoparticles into programmed 2 or 3D structures has permitted the construction of novel nanomaterials [3]. Great efforts have been made to design innovative strategies to control the organisation of nanomaterials. Current procedures are based either on top-down or bottom-up approaches. Top down methods give access to nanomaterials from the bulk. In this case lithographic techniques are often utilised to break the bulk material into smaller, micro- and nano-sized structures. However, this strategy has not yet reached a level that allows the fabrication of materials with molecular or atomic precision. In contrast, bottom-up methods utilise nano-sized building blocks and employ molecular chemistry/biology techniques to create ordered nanostructures [4, 5]. One of these techniques is the employment of biomolecules such as proteins, peptides or deoxyribonucleic acid (DNA) [6]. The use of DNA especially, as a scaffold to link inorganic nanoparticles forming complex assemblies has been investigated widely [7-9].

Recently Mirkin and co-workers introduced the term ‘programmable atom equivalents’ (PAE) [10]. These PAEs are building blocks composed of DNA-nanoparticle conjugates. It has been demonstrated that PAEs can be built into highly

ordered structures by means of DNA hybridisation. Macfarlane et al. suggested that these PAEs could be used to create a ‘new periodic table’ as showed in **Figure 1.1** [11].

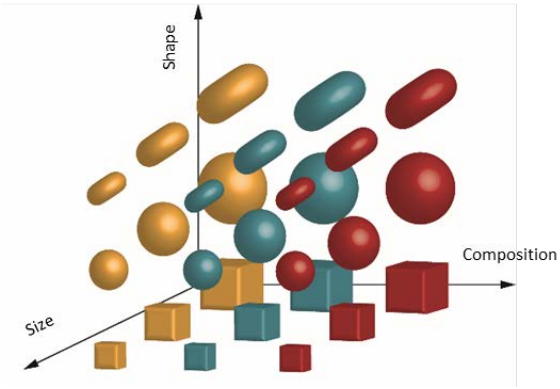

Figure 1.1. Illustration of the new concept of “Programmable atom equivalents”. A new periodic table defined by the shape, size and composition of the particles. Adapted from [11]

According to this theory, the nanoparticles are viewed as ‘atoms’ and can be assembled into ‘artificial molecules’. Many research groups have already shown that nanoparticle dimers, trimers, tetramers or even complex superlattices can be assembled by DNA hybridisation [12-16]. However, most of the studies utilised only one type of nanomaterial to make homogeneous structures. Yet, lately a great interest in the formation of heterogeneous nanoassemblies has started to develop. These nanomaterials will exhibit exciting novel properties depending on the properties of each building block and their interaction [17]. It could for example be envisaged to couple optical and magnetic properties within one type of assembly.

This thesis was focused on the synthesis of programmed DNA-gold nanoparticle (AuNP) assemblies and the study of their physicochemistry properties. AuNPs are used because they interact with the electromagnetic field of light inducing a resonant oscillation of free metal electrons in the conduction band, resulting in a localised surface

plasmon resonance (LSPR) [18]. The plasmon of individual particles could interact with plasmons from others particles when they are brought together in programmed assemblies [19, 20]. Applications of resulting assemblies range from enhancers for surface enhanced Raman scattering (SERS), biosensors, molecular rulers or optical metamaterials [21, 22]. The AuNPs are combined with designed DNA leading to the formation of dimers, trimers or tetramers. In these structures the particle size and shape could be controlled

For the Defence of Science and Technology Laboratory, it is of high interest to fund fundamental research. A concentrated solution made of assemblies synthesised in this thesis hold the promise of controlling the generation, absorption and propagation of light at sub-wavelength scales as metamaterials do. The formation of liquid materials with unconventional electromagnetic properties is an analogue to the fabrication of metamaterials, where well-designed periodical structures on a surface can manipulate light at the sub-wavelength scale. For these reasons, “metafluids” can be the next step of evolution in metamaterial research This may find all kinds of optofluidic applications such as sensors, fluidic optical modulators, low-cost tuneable filters that can be integrated in low-cost miniaturized cameras. A more distant goal may be the development into a sprayable or paintable liquid that forms a metamaterial coating on objects

Chapters 2 and 3 introduce the theoretical background and the experimental procedures used in this work.

Chapter 4 explains the synthesis and characterisation of different sizes of spherical gold nanoparticles. Moreover after showing the characterisation of the designed oligonucleotides**,** their use in functionali**s**ation of previously synthesised gold

nanoparticles is discussed. Lastly the formation of gold nanoparticles-DNA assemblies is shown. Physicochemical properties of DNA-AuNPs assemblies were then studied.

Chapter 5 investigates the optical, diffusion and sedimentation properties of different sizes of particles and their DNA assemblies using various technique such as ultraviolet-visible (UV-Vis), resonant light scattering (RLS), two-photon photoluminescence (TPPL) spectroscopies, microfluidics and digital photography.

Chapter 6 introduces the use of a seeded-growth method as a solution for the synthesis of dimers of either large spherical or anisotropic (branched) gold nanoparticles. The particles obtained were also characterised using UV-Vis and RLS spectroscopies.

Lastly, **Chapter 7** provides a summary of the results obtained in this thesis and introduces future work suggestions.

1.1 References

1. Eustis, S. and M.A. El-Sayed, *Why gold nanoparticles are more precious than pretty gold: Noble metal surface plasmon resonance and its enhancement of the radiative and nonradiative properties of nanocrystals of different shapes*. Chemical Society Reviews, 2006. **35**(3): p. 209-217.

2. Sau, T.K., et al., *Properties and Applications of Colloidal Nonspherical Noble Metal Nanoparticles*. Advanced Materials, 2010. **22**(16): p. 1805-1825.

3. Wang, L.B., et al., *Dynamic Nanoparticle Assemblies*. Accounts of Chemical Research, 2012. **45**(11): p. 1916-1926.

4. Diaz Fernandez, Y.A., et al., *The conquest of middle-earth: combining top-down and bottom-up nanofabrication for constructing nanoparticle based device*s. Nanoscale, 2014. **6**(24): p. 14605-14616.

5. Jia, C.-J. and F. Schuth, *Colloidal metal nanoparticles as a component of designed catalyst*. Physical Chemistry Chemical Physics, 2011. **13**(7): p. 2457-2487.

6. Cunningham, A. and T. Bürgi, *Bottom-up Organisation of Metallic Nanoparticles, in Amorphous Nanophotonics*, C. Rockstuhl and T. Scharf, Editors. 2013, Springer Berlin Heidelberg: Berlin, Heidelberg. p. 1-37.

7. Cutler, J.I., E. Auyeung, and C.A. Mirkin, *Spherical Nucleic Acids*. Journal of the American Chemical Society, 2012. **134**(3): p. 1376-1391.

8. Wilner, O.I. and I. Willner, *Functionalized DNA Nanostructures*. Chemical Reviews, 2012. **112**(4): p. 2528-2556.

9. Tan, S.J., et al., *Building plasmonic nanostructures with DNA*. Nature Nanotechnology, 2011. **6**: p. 268.

10. Zhang, C., et al., *A general approach to DNA-programmable atom equivalents*. Nature Materials, 2013. **12**(8): p. 741-746.

11. Macfarlane, R.J., et al., *Nucleic acid-modified nanostructures as programmable atom equivalents: forging a new "table of elements"*. Angewandte Chemie - International Edition, 2013. **52**(22): p. 5688-5698.

12. Heuer-Jungemann, A., et al., *Copper-free click chemistry as an emerging tool for the programmed ligation of DNA-functionalised gold nanoparticles*. Nanoscale, 2013. **5**(16): p. 7209-7212.

13. Loweth, C.J., et al., *DNA-based assembly of gold nanocrystals*. Angewandte Chemie-International Edition, 1999. **38**(12): p. 1808-1812.

14. Lau, K.L., G.D. Hamblin, and H.F. Sleiman, *Gold Nanoparticle 3D-DNA Building Blocks: High Purity Preparation and Use for Modular Access to Nanoparticle Assemblies*. Small, 2014. **10**(4): p. 660-666.

15. Sun, D.Z. and O. Gang, *Binary Heterogeneous Superlattices Assembled from Quantum Dots and Gold Nanoparticles with DNA*. Journal of the American Chemical Society, 2011. **133**(14): p. 5252-5254.

16. Macfarlane, R.J., et al., *Nanoparticle Superlattice Engineering with DNA*. Science, 2011. **334**(6053): p. 204.

17. Maye, M.M., O. Gang, and M. Cotlet, *Photoluminescence enhancement in CdSe/ZnS-DNA linked-Au nanoparticle heterodimers probed by single molecule spectroscopy*. Chemical Communications, 2010. **46**(33): p. 6111-6113.

18. Kelly, K.L., et al., T*he Optical Properties of Metal Nanoparticles: The Influence of Size, Shape, and Dielectric Environment*. The Journal of Physical Chemistry B, 2003. **107**(3): p. 668-677.

19. Myroshnychenko, V., et al., *Modelling the optical response of gold nanoparticles*. Chemical Society Reviews, 2008. **37**(9): p. 1792-1805.

20. Barrow, S.J., et al., *DNA-directed self-assembly and optical properties of discrete 1D, 2D and 3D plasmonic structures*. Nano Today, 2013. **8**(2): p. 138-167.

21. Busson, M.P., et al., *Optical and Topological Characterization of Gold Nanoparticle Dimers Linked by a Single DNA Double Strand*. Nano Letters, 2011. **11**(11): p. 5060-5065.

22. Watanabe-Tamaki, R., et al., *DNA-Templating Mass Production of Gold Trimer Rings for Optical Metamaterials*. The Journal of Physical Chemistry C, 2012. **116**(28): p. 15028-15033.

Chapter 2. Theoretical background

In this thesis programmed DNA-AuNP assemblies were synthesised using DNA hybridisation and their physicochemical properties were studied (**Chapters 4 and 5**). Furthermore a new way of synthesising large spherical or anisotropic gold nanoparticle assemblies using seeded growth method was developed (**Chapter 6**).

This chapter will introduce pertinent background information about materials and techniques used to support the project. Firstly, **Sections 2.1** and **2.2** will discuss gold nanoparticles physicochemical properties and syntheses. Then, after introducing oligonucleotides and their properties in **Section 2.3**, their use for gold nanoparticles functionalisation will be discuss in **Sections 2.4**. Finally, the formation of programmed DNA nanoparticle assemblies *via* DNA hybridisation will be introduced in **Section 2.5** follow by the presentation of the new seeded-growth method applied to synthesis of gold-DNA nanoparticle assemblies in **Section 2.6**.

2.1 Physicochemical properties of gold nanoparticles and their assemblies

2.1.1 Optical properties

Metallic nanoparticles and particularly gold nanoparticles have attracted much attention for centuries due to their noticeable colour, red, largely different to bulk

material [1]. These remarkable optical properties arise from the way these particles interact with the light. When the electromagnetic field of the light interacts with metallic NPs a charge separation occurs and a dipole oscillation of the free metal electrons of the conduction band is observed (see **Figure 2.1**). This phenomenon is called localised surface plasmon resonance and generates strong extinction of the light (absorption and scattering) [2].

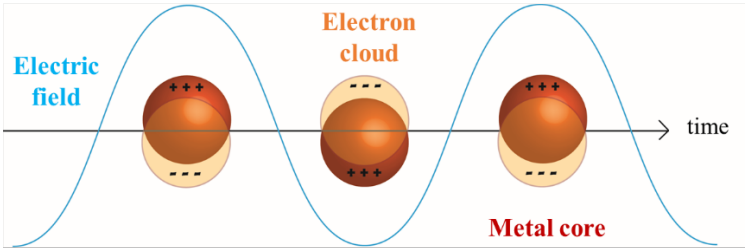

Figure 2.1 Schematic representation of the interactions of metal nanoparticles with light

As early as 1852, Michael Faraday was the first one to make a link between the size of these particles and their optical properties [3]. But it was only in 1908, that Gustav Mie solved Maxwell's equations using boundaries conditions for spherical particles and quantitatively explained this particular link. In the case of smaller particles (<20 nm) the extinction is mainly contributed by the absorption therefore **Equation 2.1** can be used [4].

$$C_{ext} = \frac{24\pi^2 r^3 \varepsilon_m^{3/2}}{\lambda} \frac{\varepsilon_i}{(\varepsilon_R + 2\varepsilon_m)^2 + \varepsilon_i^2}$$

Equation 2.1. Calculation of the total extinction cross-section for particles smaller than 20 nm. With r, radius of the particles. λ, wavelength of the incident light, $\varepsilon = \varepsilon_r(x) + i\varepsilon_i(x)$, complex dielectric constant of the metal. And ε_m, dielectric constant of the surrounding medium

As described by this expression, the SPR depends on the metal core composition, size, or shape but also on the electric properties of the medium. The dielectric constant is related to the refractive index by $\varepsilon_m = n_m^2$, the medium surrounding the particles therefore plays a role in the optical properties. The oscillation is at its maximum when $\varepsilon_r(x) = -2\,\varepsilon_m$. For gold and silver, the strong absorption of the light is observed in the visible range; thus UV-Visible spectroscopy is largely employed to characterised particles [5]. For small particles (<40 nm) the scattering contribution is negligible, but as the size of the particles increases the contribution of the scattering cross section rapidly increases too as it has a size dependence of r^6 [6] .

Light scattering provides further information on the plasmonic properties of the particles therefore it is important to be able to characterise it. Dynamic light scattering (DLS) is a well-known technique that uses scattering properties to determine particles size. Furthermore, as described in the literature, a corrected light scattering spectrum of a nanoparticle solution can be obtained in a conventional right-angle fluorimeter configuration using white light as the illumination source. The raw sample light scattering spectrum, $I_{raw}(\lambda)$ can be corrected using the spectrum of a Ludox (colloidal silica) reference sample, $I_{raw}^{Ludox}(\lambda)$ according to **Equation 2.2** [7, 8].

$$I_{LS}(\lambda) = \lambda^{-4} \frac{I_{raw}(\lambda)}{I_{raw}^{Ludox}(\lambda)}$$

Equation 2.2. Expression of corrected light scattering intensity, $I_{LS}(\lambda)$ using Ludox

Sufficiently diluted Ludox is a good light scattering reference since it is a perfect Rayleigh scatterer. In order to account for batch-to-batch variations in the Ludox

concentration, the Ludox reference sample is characterised by an optical density parameter, p_0 then each of their extinction spectra is described by **Equation 2.3**.

$$\mathrm{OD}_{\mathrm{Ludox}}(\lambda) = p_0 \lambda^{-4}$$

Equation 2.3. Expression to describe extinction spectra for Ludox reference sample

While the corrected light scattering spectrum, $I_{LS}(\lambda)$ has the spectral shape of the scattering cross section spectrum and does not depend on any instrumental parameters, its intensity still does depend on the nanoparticle concentration, which is usually not precisely known for purified nanoparticle solutions. The corrected light scattering spectrum can be normalised using the Ludox density parameter, p_0 and the optical density OD of the nanoparticle sample at the wavelength $\lambda_{\mathrm{max}}^{\mathrm{LS}}$ where its scattering, I_{LS} is maximal (see **Equation 2.4**).

$$\mathrm{I}_{\mathrm{QENLS}}(\lambda) = \frac{p_0 \mathrm{I}_{\mathrm{LS}}(\lambda)}{\mathrm{OD}(\lambda_{\mathrm{max}}^{\mathrm{LS}})}$$

Equation 2.4. Expression used to normalise light scattering intensity with Ludox and OD of samples studied

This is named the quantum-efficiency normalised light scattering (QENLS) spectrum. It describes the intrinsic light scattering behaviour of the nanoparticle in solution, independent of concentration, specific illumination or spectrometer properties. It allows light scattering of different nanoparticles to be compared directly, both in terms of the spectral shape and the scattering efficiency.

As stated above, the concentration independence is interesting for nanoparticle characterisation, since it is often difficult to precisely know the precise concentration of

nanoparticle sample preparations. Moreover, QENLS spectra may be obtained theoretically from the scattering and extinction cross section spectra, calculated using analytic or numerical electromagnetic models (see **Figure 2.2**) [9, 10]. This allows for a direct comparison between the experiment and theoretical model and helps in establishing structure-property relations for these plasmonic assemblies.

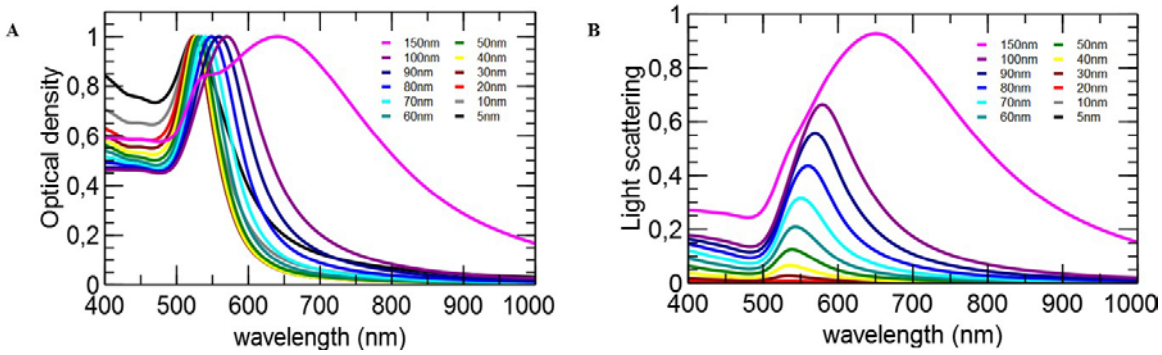

Figure 2.2. Theoretical **A)** extinction and **B)** scattering spectra for different size of single AuNPs. These spectra have been plotted by C.Midelet, PhD student at ENS Rennes (France)

In gold nanoparticle assemblies, the optical response is shifted due to plasmon coupling. This phenomenon depends on the particles themselves (size and shape), interparticle distance and assemblies' geometry [11]. By carefully designing 2 or 3D gold nanoparticles assemblies, plasmonic properties can be finely tuned [12].

2.1.2 Diffusion properties

Studying the transport properties of gold nanoparticles, such as diffusion and sedimentation is important to understand their behaviour in solutions and further design new particles or particle assemblies for specific applications.

The study of the diffusion properties of gold nanoparticles is especially crucial for biological applications. In biological media, different molecule such as protein are likely to interact with gold nanoparticles surface and therefore modify their diffusion properties [13]. Transport properties are also important for cellular uptake where the aim is to design particles that are specifically and efficiently targeting cancer cells for examples [14]. Diffusion depends on different factors such as the size, shape or composition of the particles but also on the surrounding media [15]. Theoretically, the diffusion of spherical objects in a viscous liquid medium is described by the Stokes-Einstein equation (see **Equation 2.5**) and decreases with increasing hydrodynamic radius, Rh.

$$D = \frac{k_b T}{6\pi \eta_{media} R_h}$$

Equation 2.5. Stokes-Einstein equation. With k_b: Boltzmann constant (1.38×10^{-23} $m^2.kg.s^{-2}.K^{-1}$), T: Temperature (297±2 K), η_{media}: Dynamic viscosity of media (Pa.s) and R_h: hydrodynamic radius depends of the sample

In this thesis, diffusion coefficients (*D*) were determinate using different techniques. First a microfluidic 'H-filter', previously applied to non-fluorescent food dyes and gold nanoparticles, was adapted to contain an in-line monitoring of the extinction spectrum (see **Figure 5.13**) [16]. The laminar regime created under this microfluidic architecture leads to two parallel flows (A and B) in a single microfluidic channel that appears as if separated by a physical barrier, even though they are in contact and on the same phase. AuNPs are therefore transferred only by diffusion from one flow to the other [17, 18]. In this technique the particle transfer is characterised using the extent of diffusion, ξ.

Experimental and theoretical extent of diffusion, (ξ_{exp} and ξ_{th}) were described by **Equations 2.6 and 2.7**, with $\xi = 0$ corresponding to no diffusion and $\xi = 1$ to complete diffusion [16].

$$\xi_{exp} = \frac{2\,(OD_{tot} - OD_A)}{OD_{tot}}$$

Equation 2.6. Expression of the experimental extent of the diffusion ξ_{exp} with ODtot, the optical density of the nanoparticle sample injected and OD_A the optical density at the exit A

$$\xi_{th} = 1 - \sum_{i=0}^{\infty} \frac{8}{\pi^2(2i+1)^2} \exp(-D(2i+1)^2\tau)$$

$$\text{with } \tau = \frac{\pi^2 Lh}{wU}$$

Equation 2.7. Expression of the theoretical extent of the diffusion ξ_{exp} with *D*, the diffusion coefficient and τ, interaction time. The expression for τ ($m^2.s$) includes L (m), channel length, w (m), channel width, h (m), channel height and U ($m^3.s^{-1}$), volumetric flow rate

After collecting the data for ξ_{exp} at certain specified flow rates, *D* can be found by numerically solving $\xi_{exp} - \xi_{th} = 0$ using a dedicated python script (see **Section 5.3**).

Other analytical techniques, such as dynamic light scattering or fluctuation correlation spectroscopy (FCS) are employed to determine diffusion coefficients [19]. By analysing the TPPL intensity fluctuations in the confocal volume, due to Brownian motion, information on the hydrodynamics of the particles can be obtained. TPPL-FCS is similar to fluorescence correlation spectroscopy but instead of fluorescence it uses the multi-photon excited light emission from the plasmonic structures for probing the dynamics of the confocal volume.

The autocorrelation data for single stranded DNA (ssDNA)-AuNP monoconjugates can be described using a model involving only translational diffusion (see **Equation 2.8**), assuming a 3D Gaussian beam (see **Section 5.2**).

$$G_{trans}(\tau) = 1 + \frac{1}{N}\left[\left(1 + \frac{\tau}{\tau_D}\right)\sqrt{1 + q\frac{\tau}{\tau_D}}\right]^{-1}$$

$$\text{With } \tau_D = \frac{\omega_{xy}^2}{8D_{trans}} \text{ and } q = \frac{\omega_{xy}^2}{\omega_z^2}$$

Equation 2.8. Model used for autocorrelation of ssDNA-AuNP monoconjugates. In the case of two-photon excitation, the translational diffusion time constant τ_D directly relates to the diffusion coefficient D_{trans} and the lateral waist of the observation volume $\boldsymbol{\omega_{xy}^2}$. Furthermore, ω_z is the longitudinal waist of the observation volume. N is the mean number of particles diffusing simultaneously inside the excitation volume. Calibration of the focal volume using Rhodamine 6G in water gives ω_{xy}= 225 nm and q = 0.075

For the dimers a model including a rotational term was required, described by rotational time constant τ_R (see **Equation 2.9**).

$$G_{trans-rot}(\tau) = 1 + [G_{trans}(\tau) - 1]\left[1 + p\exp(\frac{-\tau}{\tau_R})\right]$$

and

$$D_R = \frac{1}{6\tau_R}$$

Equation 2.9. Model used for autocorrelation of DNA-AuNP dimers. With τ_R, rotational time constant and D_R rotational diffusion coefficient

2.1.3 Sedimentation properties

Observations of the sedimentation of colloidal solutions were important historically in establishing the physical reality of molecules and providing a molecular basis for thermodynamics in the form of statistical mechanics [20, 21]. Nowadays, there is an intense interest in the development of colloidal solutions of engineered nanocrystals for a variety of applications. These solutions should display sedimentation behavior in line with expectations for these particles on basis of their shape, composition and suspending medium. For stable and dilute solutions, the sedimentation behavior is a result of the particular interplay of nanoparticle hydrodynamics, and gravitational and Brownian forces (see **Figure 2.3**). Under these conditions, the surface chemistry of the nanoparticles, while ensuring colloidal stability, does not significantly influence the sedimentation behaviour.

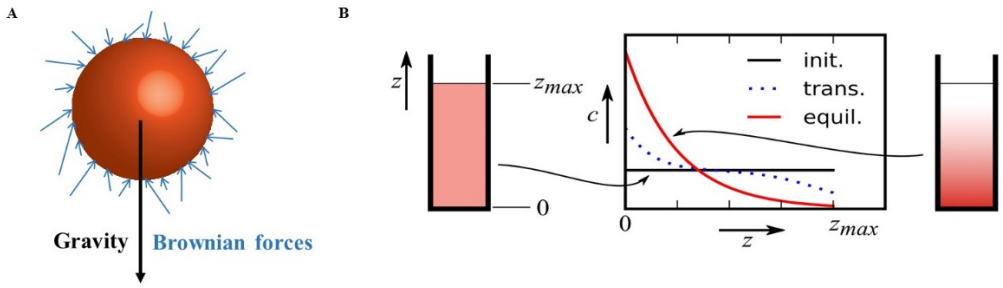

Figure 2.3 Sedimentation versus Brownian diffusion in colloidal solutions. **A)** Gravity tends to direct dense particles to the bottom of the cell, whereas the random Brownian forces tend to disperse the particles throughout the entire volume. **B)** Establishment of an equilibrium gradient starting from an initial homogeneous distribution of particles with theoretical initial, transient and equilibrium concentration profiles as a function of vertical position

An understanding of the sedimentation of nanoparticle solutions is useful as it may give rapid and visual clues about the size distribution and colloidal stability of newly synthesised colloids. These clues go beyond the simple assessment of whether a prepared solution is colloidally stable. Careful monitoring of sedimentation behaviour may be used to verify the nature of the suspended object in its native medium, and is complementary to methods that characterise a limited number of specimens deposited on a substrate, such as electron microscopy.

Furthermore, sedimentation, decantation and controlled centrifugation are often purification steps in wet-chemical synthesis of nanoparticles and nanoparticle assemblies, for instance for the purification of gold nanorods [22]. A further example is the purification of nanoparticles by flocculation and subsequent sedimentation. Flocculation under the influence of depletion forces, due to specific flocculants produces, la**r**ge aggregates of these nanoparticles that settle rapidly leaving non-flocculated impurities in the supernatant [23].

There is a clear connection between the gravitational sedimentation of colloidal particles and analytical ultracentrifugation (AUC), where sedimentation is sped up by increasing g to multiples of the earth gravitational pull. AUC has been successfully applied to the study of nanoparticle solution [24-26]. Optimisation of the measurement using a spectroscopic approach, in combination with detailed numerical analysis of the multi-wavelength sedimentation profiles, has made AUC extremely versatile for the analysis of nanoparticle preparations.

For all these reasons, it is instructive and of fundamental interest to study the sedimentation behaviour of nanoparticle solutions in greater detail. Recently, Alexander et al. reported a study of gravitational sedimentation of gold nanoparticles [27]. They focused on measuring the optical density at a pre-defined height in the solution as a

function of time, using an UV-visible absorption spectrophotometer. This study was then further extended by making estimates of the size distribution of colloidal gold samples by including a multi-wavelength analysis.

A simple model for sedimentation can be formulated under the assumptions that there are no interactions between nanoparticles and that their motion is only governed by random Brownian forces and a directional gravitational force. The relevant parameters of the system depend only on the effective density and overall shape of the particles, and on the density, viscosity and temperature of the suspending liquid. The surface chemistry of the particles has no influence, nor does the exact composition of the suspending medium. However, these chemical parameters may influence the model indirectly, e.g. by changing density or viscosity of the medium, or by altering particle shape and effective density.

The establishment of a concentration gradient in such a dilute colloidal solution of independent, non-interacting particles in a homogeneous gravitational field is described by the Mason-Weaver equation, a one-dimensional partial differential equation [28]. This equation is the direct predecessor to the more well-known Lamm equation which applies to a centrifugal field and is extensively used in the analysis of ultracentrifuge data.

$$\frac{\partial \mathrm{C}}{\partial \mathrm{t}} = D\frac{\partial^2 \mathrm{C}}{\partial \mathrm{z}^2} + \mathrm{sg}\frac{\partial \mathrm{C}}{\partial \mathrm{z}} \quad \text{and} \quad D\frac{\partial \mathrm{C}}{\partial \mathrm{z}} + \mathrm{sgC} = 0 \ (\mathrm{z} = \mathrm{zmax}, \mathrm{z} = 0)$$

Equations 2.10 and 11. Mason-Weaver equation and boundary conditions. D is the diffusion coefficient, s sedimentation coefficient, g gravitational constant, and z = zmax and z = 0, are the top and bottom of the cell, respectively

These equations were solved numerically using a Crank-Nicolson finite-difference method. The numerical solver accepts an arbitrary concentration profile as the initial condition. The initial condition at t=0 is C= C_0 for $0 \leq z \leq z_{max}$ and C=0 elsewhere.

The term *sg* is the terminal velocity of a particle accelerated by gravitational force in a viscous liquid ($v_{term} = sg$), and represents the velocity (directed towards the bottom of the cell) this particle would have in absence of Brownian motion. It is written in terms of the sedimentation coefficient, *s*. For spherical particles sedimentation and diffusion coefficient are given by the well-known Stokes' law and the Einstein-Smolukowski-Sutherland theory (see **Equations 2.12 and 13**).

$$s_{sphere} = \frac{2}{9}\frac{\alpha^2(\rho - \rho_{fl})}{\eta} \quad \text{and } D_{sphere} = \frac{k_B T}{6\pi\eta\alpha}$$

Equations 2.12 and 13. Sedimentation and diffusion coefficients for spherical particles. With α, particle radius, η, viscosity of the media, ρ and ρ_{fl} the mass density of the particle and the suspending fluid, respectively, k_B, Boltzmann constant and T, temperature

Quantitative digital photography and a simple mathematical diffusion-sedimentation equation were used to monitor and model the sedimentation of AuNPs and DNA-AuNP assemblies. Practical implications of the theoretical model for the analysis and purification of nanoparticle assemblies were also discussed (see **Section 5.4**).

2.2 Chemical synthesis of colloidal gold nanoparticles

AuNPs can be synthesised in a wide range of sizes, shapes and bear different surface stabilizers using chemical synthesis. All protocols are based on the same principle; a gold salt is reduced by a reducing agent in presence of a capping agent.

2.2.1 Synthesis of 5 to 50 nm spherical gold nanoparticles

In 1951, Turkevich et al. synthesised spherical gold nanoparticles by reducing gold salt ($HAuCl_4$) in an aqueous boiling solution of sodium citrate [29, 30]. Twenty years later, Frens et al. extended the method by modifying the ratio gold to citrate in order to change particles sizes [31].

If the principle of the synthesis is simple its mechanism appears more complicated (see **Figure 2.4**).

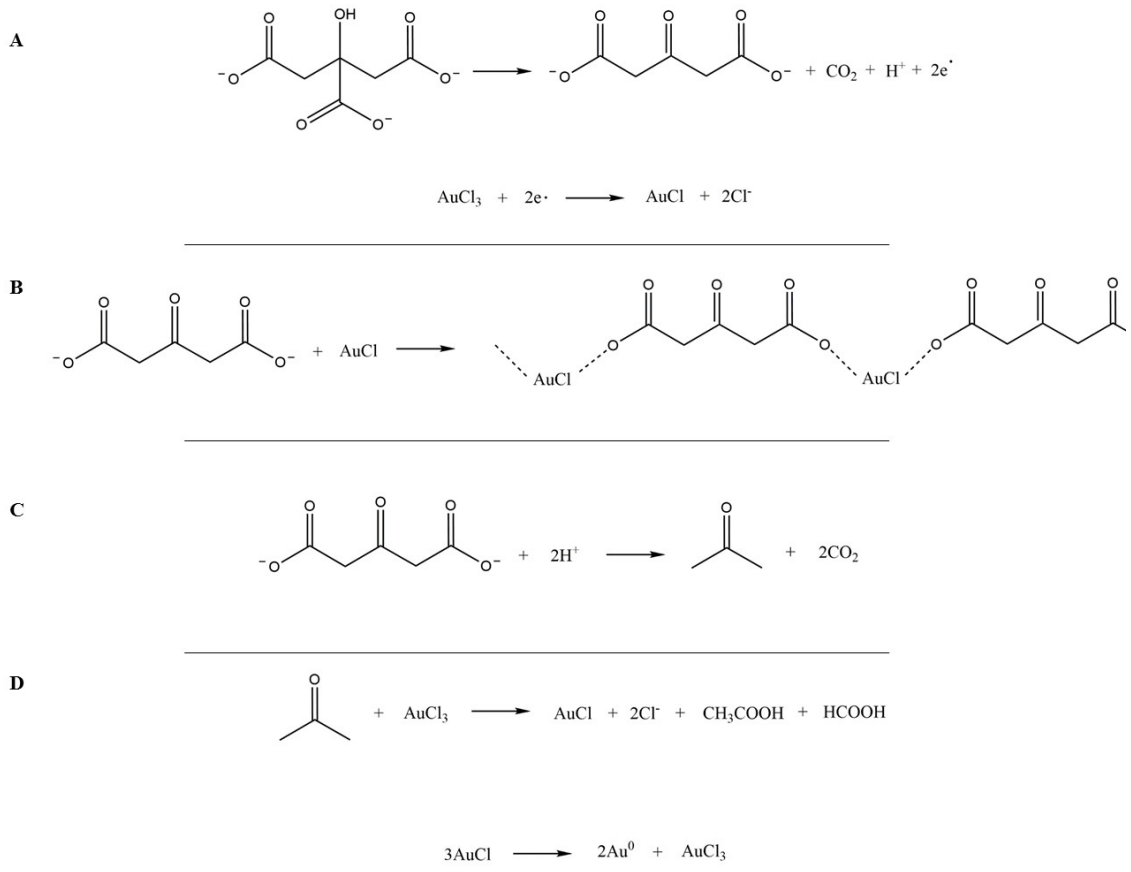

Figure 2.4. Reaction mechanism for the formation of AuNPs using Turkevich method. Adapted from [32]

First in the reaction, citrate is oxidised into acetone dicarboxylate and Au^{3+} precursor is reduced into Au^{+1} to form gold monochloride (AuCl) (Reaction **A**). The second step involves the formation of complexes between dicarboxylate anions and AuCl (Reaction **B**). Coagulation of this complexes and disproportionation of AuCl into Au^0 form gold nuclei necessary for the gold nanoparticle formation (Reaction **D**). In a side reaction, acetone dicarboxylate is also decompose into acetone (Reaction **C**) and reduce Au^{3+} into Au^0 (Reaction **D**).

The drawback of the Turkevich method is the loss of monodispersity in particles' shape and size when increasing the diameter over 20 nm. To tackle this problem

synthesise of larger spherical particles have been developed using seeded growth methods [33]. The principle behind this technique is to separate the nucleation from the growth process to obtain a narrow size distribution. Therefore small particles called seeds are used as nucleation centres for the growth of larger particles. Another important aspect of this type of synthesis is the control of kinetics parameters to avoid second nucleation [34]. In 2011, Bastus et al. performed a kinetic study and found the best conditions to synthesise citrate coated spherical gold nanoparticles up to 200 nm. They showed that reducing the temperature to 90 °C instead of 100 give a better size distribution by avoiding second nucleation [35]. The same group furthermore developed seeded growth method for the synthesis of citrate coated smaller (<10 nm) gold nanoparticles but also for large silver particles [36, 37]. Seeding methods are also used for the synthesis of anisotropic gold nanoparticles (see **Section 2.2.2**).

Easier way than seeded methods are available for the synthesis of small gold nanoparticles. The Brust-Schiffrin method is well developed and produced small particles, in organic solvent, in the range of 1 to 5 nm using the strong reducing agent sodium borohydride [38]. The main disadvantage of this method is the use of thiols as capping agents making ligand exchange for applications difficult due to the strong S-Au bond. Sodium borohydride is a strong reducing agent and can reduce quickly a gold salt in water to form Au^0 and initiate nucleation. It has also been shown than sodium borohydride act in the same way as citrate in the Turkevich method, it plays the role of reducing and capping agent [39]. For these reasons it is a good reducing agent for the synthesis of small AuNPs.

2.2.2 Synthesis of branched gold nanoparticles

Anisotropic gold nanoparticles and particularly branched NPs have attracted scientists' attention due to their special plasmonic properties in the longer wavelength range [40]. They are especially interesting for use in SERS experiments [41].

The synthesis of anisotropic particles such as the nanobranched in this thesis (see **Chapter 6**) also involve the use of a seeding method. In the first step small spherical seeds are produced by reduction of Au salt using a strong reducing agent, sodium borohydride in presence of a surfactant, Cetyl trimethylammonium bromide (CTAB). Then these seeds are introduced in a growth solution containing Au ions, a weak reducing agent, ascorbic acid and shape directing additives, CTAB and silver ions [42]. The protocol used in this work has been previously developed in the group [43]. Silver and CTAB are used as capping agents. Silver binds preferably to the planes [100] of the Au surface. This phenomenon favour the CTAB capping of these planes *via* silver-bromide interactions and promote the growing of gold branches onto the [111].

This principle have been used to develop a new approach to synthesise DNA-AuNP dimers using seeding method (see **Chapter 6**).

2.3 Oligonucleotides as scaffolds for nanoparticles self-assemblies

In this section structures and properties of DNA are going to be depicted (see **Section 2.3.1**). Furthermore a brief review of their modifications for application in self-assemblies formation can be found in **Section 2.3.2**.

2.3.1 Structures and properties of oligonucleotides

Deoxyribonucleic acid is present in almost every living system where it carries genetic information. It is a polymeric macromolecule constituted of monomers called nucleotides. These monomers consist of a phosphate group, a pentose sugar and a heterocyclic base (see **Figure 2.5A**) [44]. Four naturally occurring bases could be found in DNA: adenine (A) and guanine (G) are purines and cytosine (C) and thymine (T) are pyrimidines (see **Figure 2.5B**). The oligomer is formed by phosphodiester bond made between the 5'-phosphate group of one nucleotide to the 3'-hydroxyl group of another. At pH above 2, the phosphodiester group is negatively charged therefore single stranded DNA is highly negatively charged.

In 1953, James Watson and Francis Crick revealed that in solution DNA adopts a duplex structure. By constructing models, they showed that the strands are held together by hydrogen bonds between individual bases on opposite strands [45]. Furthermore, purine base A is always paired with pyrimidine T and the purine G is always paired with the pyrimidine C (see **Figure 2.5B**). This particularity led to complementary single stranded DNA sequences and it is of specific interest in the formation of self-assemblies using DNA as a scaffolds. Within the duplex the strands are anti-parallel, the 5'-end of one is next to the 3'-end of the complementary one. In solution the duplex is not linear but presents a double helix shape where the hydrophobic bases are places in the centre and the negative phosphate backbone is external. In term or dimension the distance between successive base pairs is around 0.34 nm and one helical turn is repeated every 10 to 11 base pairs [46].

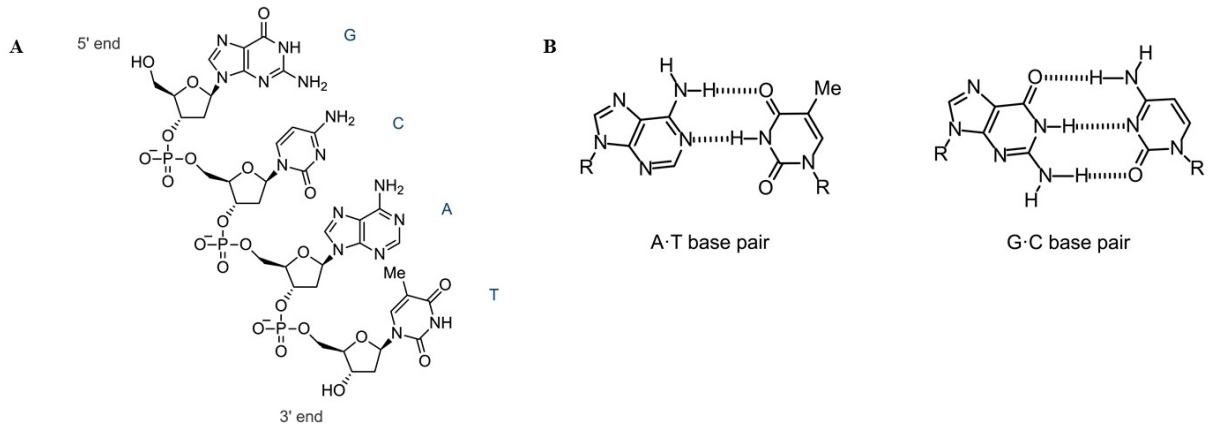

Figure 2.5. A) Chemical structure of a LSPR strand with the sequence GCAT and B) Chemical structure of the four naturally occurring DNA bases in their base pair form

The duplex stability is ensured by the hydrogen bonding between complementary bases and also by base stacking. However, because of the electrostatic repulsion forces coming from both negatively charged backbones, double stranded DNA (dsDNA) is sensitive to its environment (Ionic strength, pH and temperature). During hybridisation process (formation of duplex using two complementary single strands) the negative charge of the DNA backbone is generally screened using cations (e.g. Mg^{2+}, Na^{+}) facilitating the formation of the duplex structure [47]. Furthermore the ionic properties of the solution play a role in the stability of the DNA. The pH is also an important parameter to consider as it affects the stability of the dsDNA at acidic (<5) or basic (>10) pH due to the protonation or deprotonation of the bases.

Finally, the temperature is a crucial factor. High temperatures will break the weak hydrogen bonds between bases and DNA duplexes will dehybridise. The melting temperature Tm is the temperature at which 50% of the dsDNA are dehybridised. To determine this specific value DNA duplexes can be submitted to a melting curve experiment. A DNA solution is submitted to heat up and cool down cycles while the OD at 260 nm is recorded. A characteristic sigmoidal shaped curve is obtained and the melting temperature is found at inflection point of the curve (see **Figure 2.6**).

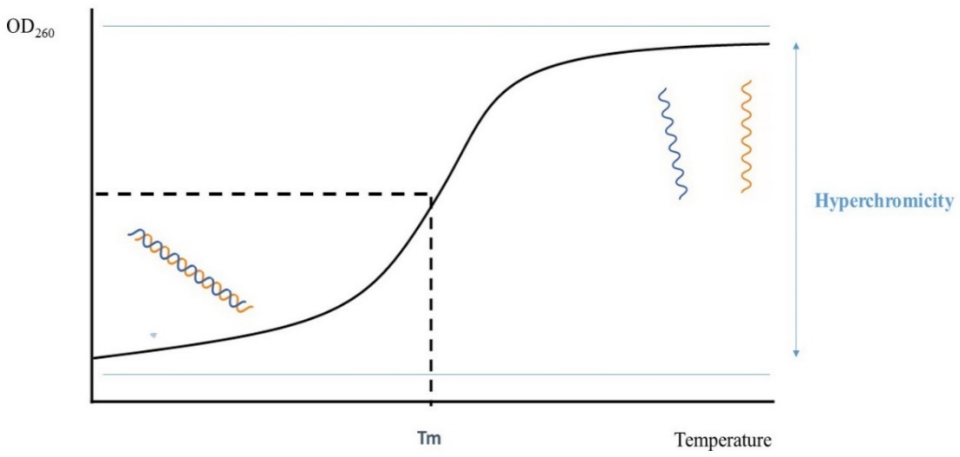

Figure 2.6. Representation of a typical melting curve. The absorbance at 260 nm is recorded while the temperature is increased

DNA light absorption is due to the aromatic purine and pyrimidine rings of the DNA bases around 260 nm [48]. The absorption of light for ssDNA is higher than dsDNA due to π-stacking of bases in the double helix, this phenomenon is called hyperchromicity [44]. Different models exist to theoretically calculate the melting temperature. The nearest neighbour method is commonly used, as it take into consideration the enthalpy for the formation of a base pair as well as stacking effects of neighbouring bases [49]. Many online website, which used different theoretical models, are also available to obtain melting temperature for specific oligonucleotides (e.g. OligoCalc, OligoAnalyser).

Solid-phase synthesis allows designed and customised oligonucleotides to be obtained [50]. In order to increased DNA stability, a large range of modification is available to functionalised DNA with anchors (e.g. thiol, amine), fluorescent dyes or moieties for additional chemical reactions [51-55].

2.3.2 Stability improvement for gold-DNA nanoparticle assemblies

The oligonucleotides used in the next chapters have been specially designed and modified to be employed in self-assemblies' experiments.

It has been shown that thiol groups have high affinity for gold [56]. Therefore the functionalisation of gold nanoparticles by thiolated oligonucleotides is found in a various range of applications and especially in programmable self-assemblies [57]. The 5'end of most of the DNA used in this work were functionalised with a single thiol group (see **Figure 2.7A**). Nevertheless, for AuNPs growing experiments in **Chapter 5** extra anchoring onto the DNA surface was needed. The 5' ends of DNA strands Bcc and Ccc (see **Table 3.1** for sequences) were therefore modified with a three thiol anchor previously developed in the literature (see **Figure 2.7B**) [58].

.

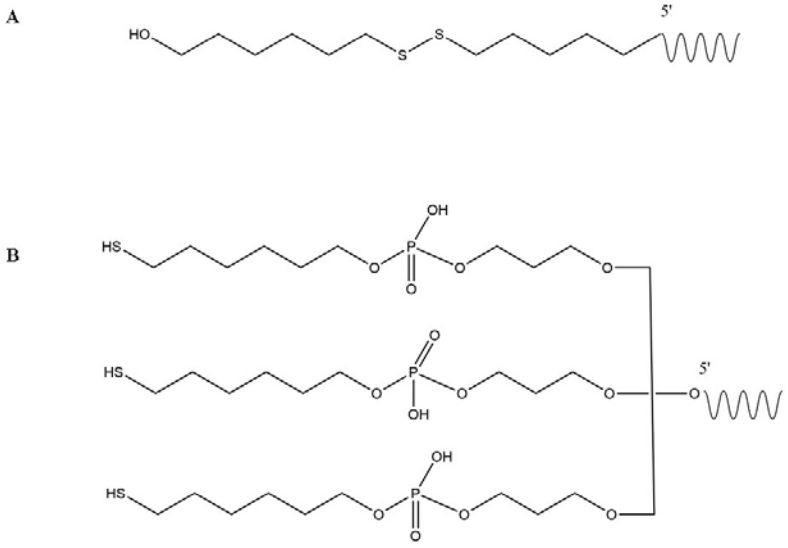

Figure 2.7. Details of chemical modifications of 5'end on DNA used with **A)** single thiol anchor and **B)** triple thiol anchor

To obtain more stable DNA-AuNP assemblies particular attention must be given to the DNA scaffold. As discussed in **section 2.3.1** DNA duplexes are sensitive to their environment and can easily degrade. To overcome this issue chemical groups can be added to the DNA strands to permit an inter-strands ligation [59]. In this work DNA strands have been modified with two moieties, dibenzocyclooctyne (DIBO) and azide, to take advantages of the copper free click chemistry previously developed in the group (see **Figure 2.8**) [53].

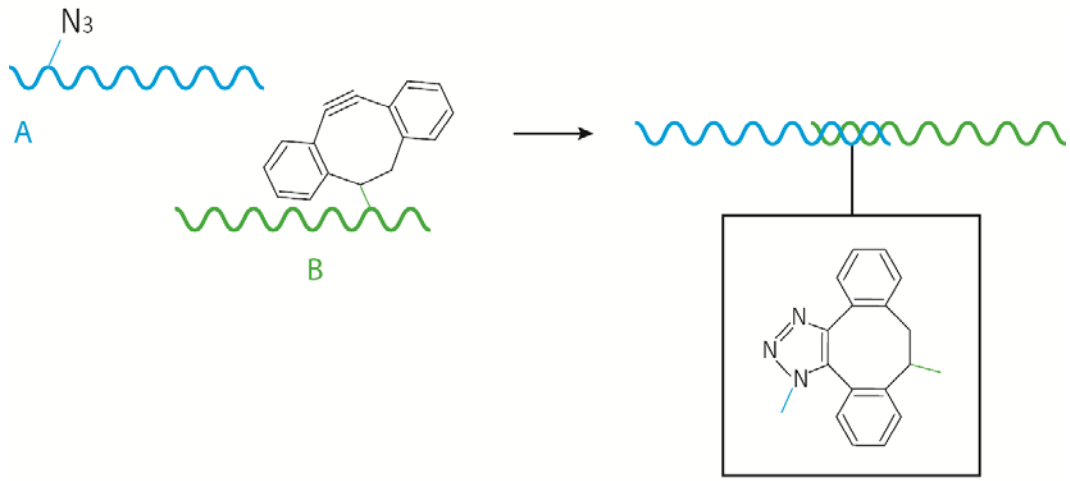

Figure 2.8. Representation of the modifications and click ligation for DNA strands Bcc and Ccc (see **Table 3.1** for sequences).

When the DNA strands are in close proximity, an instantaneous cycloaddition occurs and results in a highly stable triazole moiety. This lead to a high yield of stable DNA duplexes [53]. To go even further in the control of assemblies a reversible link can also be created using the cyno-vinyl carbazole recently introduced [55].

The success of hybridisation and ligation are analysed using polyacrylamide gel electrophoresis (PAGE), where DNA migrates differently depending on its size and charge.

2.4 Synthesis of DNA-AuNP self-assemblies

Two set of designed DNA strands have been used in this thesis. The first one was made of three DNA strands (1, 2, 3 see **Table 3.1** for sequences) and was used to form dimer assemblies. The second set was composed of four DNA strands (A to D and Bcc and Ccc see **Table 3.1** for sequences). Theses strands were design to adopt a tetrahedral shape in solution (see **Figure 2.9**) [60].

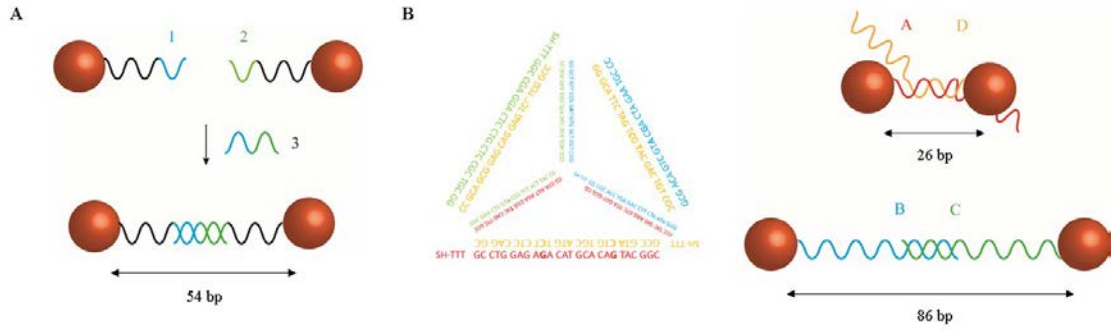

Figure 2.9. Representation of the design of the two DNA sets used in this thesis. **A)** Three strands system and **B)** Four strands system

As seen in **Section 2.2.1**, post synthesis gold nanoparticles of various sizes were stabilised via weak electrostatic repulsions using either citrate or borohydride anions [61]. To increase their stability towards centrifugation and salt aggregation a ligand exchange with the bulky phosphine ligand Bis(p-sulfonatophenyl)phenyl phosphine dehydrate dipotassium salt (BSPP) is widely used [62]. BSPP allows the particles to be reversibly aggregated using salt facilitating the purification and concentration of gold nanoparticles. Moreover ligand exchange between BSPP and thiolated molecules is permitted.

Stability of gold nanoparticles could also be increased by covering their surface with a dense shell of DNA taking advantage of the thiol gold affinity. To do so a technique called ‘salt-ageing’ has been developed [63]. It consists of a slow increase of salt concentration over time to screen the repulsive forces between gold nanoparticle surface and DNA backbone and increase the DNA coverage. This technique is efficient but time consuming (over a day), recently a pH assisted method has been develop and allows the dense DNA functionalisation of AuNPs within 10 minutes [64]. A similar process has been develop to coat CTAB functionalised particles with a DNA shell [65].

2.4.1 Synthesis of small particles assemblies

Due to the programmability of oligonucleotides, DNA-AuNP building blocks are of high interest for the formation of nanoparticles self-assemblies. After showing the possibility to use thiolated DNA as linker between AuNPs in 1996, Alivisatos group demonstrated for the first time the use of agarose gel electrophoresis to purified conjugated DNA-AuNPs in 2000 [66]. Even if DNA and Au are mixed in an equimolar ratio a distribution of number of DNA per particles will occurs. For assemblies purposes it is important to be able to control the number of DNA present at the surface. In agarose gel electrophoresis DNA-AuNP conjugates are separated depending on their charge and size. In 2007, Pellegrino et al. showed that in the case of AuNPs the size factor is dominant [67]. The key of a successful conjugates separation using electrophoresis is to have a good ratio between particles and DNA size. If the use of agarose gel electrophoresis is straightforward for separation of smaller particles with long DNA strands it becomes more difficult for larger particles with shorter DNA. High pressure liquid chromatography (HPLC) can be used to separate such building blocks

nevertheless it is an expensive technique [68]. In this thesis an alternative using agarose gel electrophoresis was investigated (see **Section 2.4.2**).

2.4.2 Synthesis of large particles (>30 nm) assemblies

As discussed in **Section 2.4.1**, the most commonly used approach to separate DNA-AuNP mono or diconjugates from unconjugated AuNPs is agarose gel electrophoresis. However, a current limitation of this approach is the inability to separate large AuNPs (>30 nm) with a discrete number of short DNA strands attached [68]. Large AuNPs modified with short oligonucleotides represent the perfect building blocks to enhance plasmonic interactions in assemblies; therefore they are of high interest [69].

To overcome this difficulty the concept of temporarily increasing the electrophoretic mobility of the conjugates by hybridisation of a large DNA strand to the short one on the particles surface is found in the literature [66, 69, 70]. In this thesis, a new universal strategy to isolate discrete large DNA-AuNP conjugates through agarose gel was envisaged (see **Figure 2.10**).

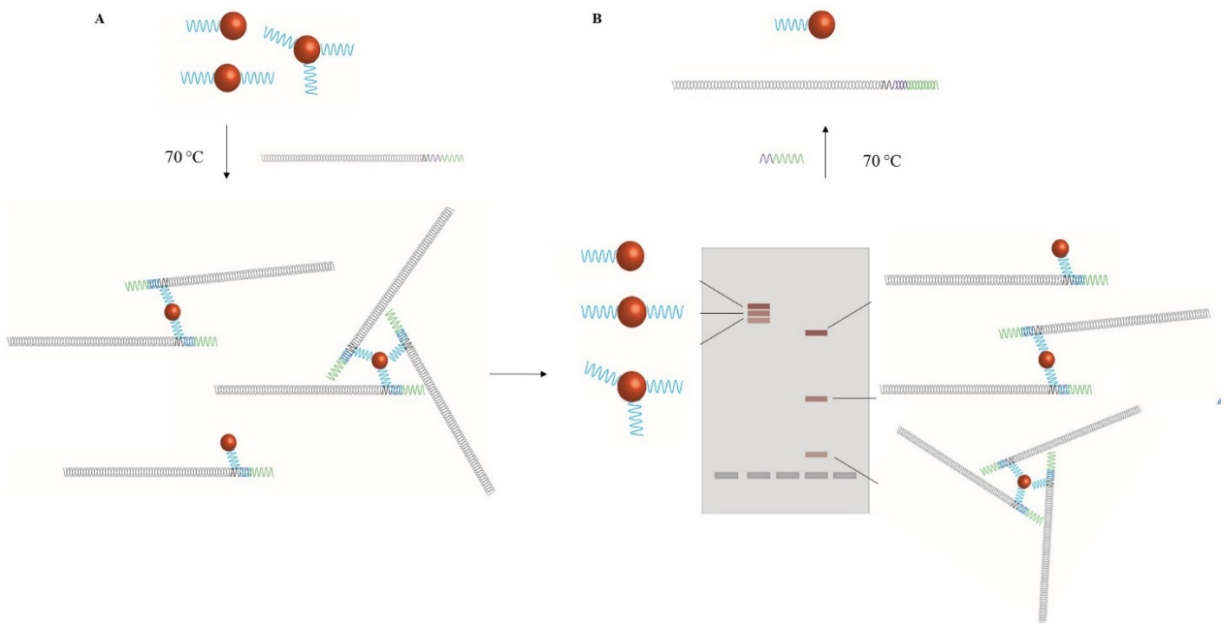

Figure 2.10. Description of the new DNA-AuNPs monoconjugates separation for large particles **A)** Hybridisation of DNA duplexes to DNA-AuNP conjugates and **B)** Purification and peel-off of the duplexes for DNA-AuNP monoconjugates

A long random DNA duplex (541 base pair (bp)) including a specific single-stranded overhang (45 bp) was synthesised by polymerase chain reaction (PCR). In the context of this work, the overhang was designed to partially hybridise to any of the strands of the four DNA strands system (DNA A to D, see **Table 3.1** for sequences). The large size of the duplex hybridised to the DNA-AuNPs results in a great difference in DNA length/size to AuNP size. As discussed previously, a large size difference between AuNPs and DNA is key to achieving successful electrophoretic separation of mono, di and triconjugates (see **Figure 2.10B**).[67] The long DNA extension can then be peeled off using a single DNA strand with full complementarity to the overhang, exposing the short conjugated DNA (see **Figure 2.10B**).

Nowadays artificially designed oligonucleotides can be easily synthesised using solid-phase synthesis [71-73]. Nevertheless, this method cannot be easily employed to obtain strands > 200 bases. In fact due to side reactions the number of errors accumulates

with the length of the oligonucleotide [74, 75]. Therefore this approach was not suitable for the synthesis of the long DNA required for this part of the project. In this approach nine randomly designed short oligonucleotides (see **Table 3.2** for sequences) were mixed with Phire enzyme and the appropriate forward and reverse primers. This mixture was subsequently used in PCR and yielded the desired duplex in a 'one-pot' reaction. This new approach is universal as the only thing to change to adapt it to any DNA-AuNP conjugate system is to redesign the reverse primer that will form the overhang.

After being functionalised with the desired number of DNA small and large particles can be introduced into the formation of self-assemblies using the intrinsic properties of DNA (see **Section 2.3**).

2.5 DNA metallisation

The programmable structures of oligonucleotides became of high interest in nanoelectronics for the design of nanocircuits. Unfortunately, the conductivity properties of DNA at a large scale are poor [76]. The idea of metallisation, which consists of the deposition of metal (silver, gold, palladium, platinum or cupper) on a DNA template by reducing DNA-complexed metal salts, could permit to solve this issue [77]. In 1998, Braun et al. were the first to create a conductive silver wire using DNA metallisation [78]. Since, numerous protocols were developed and sequence-selective DNA metallisation became a new challenge [79]. Most of the protocols occur in three step. The process starts with the activation where metal ions bind to DNA. In the case of gold or silver the positive ions are attracted to the negatively charged backbone of the DNA. In the second step a reducing agent is used and forms seeds incorporated in the

DNA structure. Finally, more reducing agent and metal ions are added to permit the growth of the metal around the DNA (see **Figure 2.11**) [80].

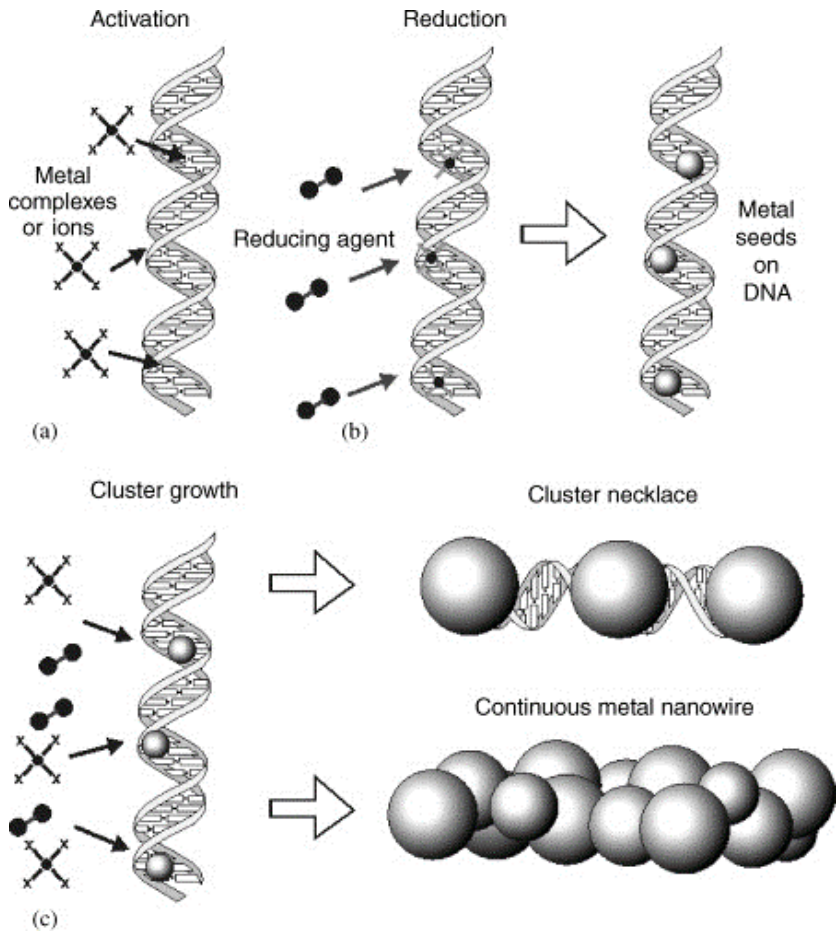

Figure 2.11. Representation of the DNA metallization three steps process with **A)** activation **B)** reduction and **C)** growth. From [80].

This concept of DNA metallisation can also be applied to the formation of anisotropic particles or programmed nanostructures. Ma et al., recently reported the synthesis of design branched particles using DNA metallisation [81]. By metallising dsDNA (1 to 5 DNA) attach to the surface of small single spherical AuNPs, they synthesised branched gold nanoparticles with a discrete number of branches.

2.6 References

1. Eustis, S. and M.A. El-Sayed, *Why gold nanoparticles are more precious than pretty gold: Noble metal surface plasmon resonance and its enhancement of the radiative and nonradiative properties of nanocrystals of different shapes.* Chemical Society Reviews, 2006. **35**(3): p. 209-217.

2. Huang, X. and M.A. El-Sayed, *Gold nanoparticles: Optical properties and implementations in cancer diagnosis and photothermal therapy*. Journal of Advanced Research, 2010. **1**(1): p. 13-28.

3. Faraday, M., *X. The Bakerian Lecture. —Experimental relations of gold (and other metals) to light.* Philosophical Transactions of the Royal Society of London, 1857. **147**: p. 145-181.

4. Amendola, V., et al., *Surface plasmon resonance in gold nanoparticles: a review*. Journal of Physics-Condensed Matter, 2017. **29**(20).

5. Tomaszewska, E., et al., *Detection Limits of DLS and UV-Vis Spectroscopy in Characterization of Polydisperse Nanoparticles Colloids.* Journal of Nanomaterials, 2013. **2013**: p. 10.

6. van Dijk, M.A., et al., *Absorption and scattering microscopy of single metal nanoparticles.* Physical Chemistry Chemical Physics, 2006. **8**(30): p. 3486-3495.

7. Navarro, J.R.G. and M.H.V. Werts, *Resonant light scattering spectroscopy of gold, silver and gold-silver alloy nanoparticles and optical detection in microfluidic channels.* Analyst, 2013. **138**(2): p. 583-592.

8. Loumaigne, M., et al., *Optical extinction and scattering cross sections of plasmonic nanoparticle dimers in aqueous suspension.* Nanoscale, 2016. **8**(12): p. 6555-6570.

9. Deželić, G. and J.P. Kratohvil, *Determination of size of small particles by light scattering. experiments on ludox colloidal silica.* Kolloid-Zeitschrift, 1960. **173**(1): p. 38-48.

10. Draine, B.T. and P.J. Flatau, *Discrete-Dipole Approximation For Scattering Calculations.* Journal of the Optical Society of America A, 1994. **11**(4): p. 1491-1499.

11. Lange, H., et al., *Tunable Plasmon Coupling in Distance-Controlled Gold Nanoparticles.* Langmuir, 2012. **28**(24): p. 8862-8866.

12. Cha, H., J.H. Yoon, and S. Yoon, *Probing Quantum Plasmon Coupling Using Gold Nanoparticle Dimers with Tunable Interparticle Distances Down to the Subnanometer Range.* ACS Nano, 2014. **8**(8): p. 8554-8563.

13. Kohli, I., et al., *Interaction and diffusion of gold nanoparticles in bovine serum albumin solutions.* Applied Physics Letters, 2013. **102**(20): p. 203705.

14. Cho, E.C., Q. Zhang, and Y. Xia, *The effect of sedimentation and diffusion on cellular uptake of gold nanoparticles.* Nature nanotechnology, 2011. **6**(6): p. 385-391.

15. Wong, K., et al., *Diffusion of gold nanoparticles in toluene and water as seen by dynamic light scattering.* Journal of Nanoparticle Research, 2015. **17**(3): p. 153.

16. Werts, M.H.V., et al., *Quantitative full-colour transmitted light microscopy and dyes for concentration mapping and measurement of diffusion coefficients in microfluidic architectures.* Lab on a Chip, 2012. **12**(4): p. 808-820.

17. Choban, E.R., et al., *Microfluidic fuel cell based on laminar flow.* Journal of Power Sources, 2004. **128**(1): p. 54-60.

18. Giri, B., *1 - Introduction to Microfluidics*, in *Laboratory Methods in Microfluidics*. 2017, Elsevier. p. 1-7.

19. Balaji, P.S., et al., *Fluorescence Correlation Spectroscopy of Gold Nanoparticles.* Spectroscopy Letters, 2012. **45**(1): p. 22-28.

20. Perrin, J., *Mouvement brownien et molécules.* J. Phys. Theor. Appl., 1910. **9**(1): p. 5-39.

21. Haw, M.D., *Colloidal suspensions, Brownian motion, molecular reality: a short history.* Journal of Physics: Condensed Matter, 2002. **14**(33): p. 7769.

22. Sharma, V., K. Park, and M. Srinivasarao, *Shape separation of gold nanorods using centrifugation.* Proceedings of the National Academy of Sciences, 2009. **106**(13): p. 4981-4985.

23. Scarabelli, L., et al., *Monodisperse Gold Nanotriangles: Size Control, Large-Scale Self-Assembly, and Performance in Surface-Enhanced Raman Scattering.* ACS Nano, 2014. **8**(6): p. 5833-5842.

24. Zook, J.M., et al., *Measuring Agglomerate Size Distribution and Dependence of Localized Surface Plasmon Resonance Absorbance on Gold Nanoparticle Agglomerate Size Using Analytical Ultracentrifugation.* ACS Nano, 2011. **5**(10): p. 8070-8079.

25. Carney, R.P., et al., *Determination of nanoparticle size distribution together with density or molecular weight by 2D analytical ultracentrifugation.* Nature Communications, 2011. **2**: p. 335.

26. Demeler, B., et al., *Characterization of Size, Anisotropy, and Density Heterogeneity of Nanoparticles by Sedimentation Velocity.* Analytical Chemistry, 2014. **86**(15): p. 7688-7695.

27. Alexander, C.M., J.C. Dabrowiak, and J. Goodisman, *Gravitational sedimentation of gold nanoparticles.* Journal of Colloid and Interface Science, 2013. **396**: p. 53-62.

28. Mason, M. and W. Weaver, *The Settling of Small Particles in a Fluid.* Physical Review, 1924. **23**(3): p. 412-426.

29. Turkevich, J., P.C. Stevenson, and J. Hillier, *A study of the nucleation and growth processes in the synthesis of colloidal gold.* Discussions of the Faraday Society, 1951. **11**: p. 55-75.

30. Turkevich, J., P.C. Stevenson, and J. Hillier, *The Formation of Colloidal Gold.* The Journal of Physical Chemistry, 1953. **57**(7): p. 670-673.

31. Frens, G., *Controlled Nucleation for Regulation of Particle-Size in Monodisperse Gold Suspensions.* Nature-Physical Science, 1973. **241**(105): p. 20-22.

32. Xia, H., et al., *Synthesis of Monodisperse Quasi-Spherical Gold Nanoparticles in Water via Silver(I)-Assisted Citrate Reduction.* Langmuir, 2010. **26**(5): p. 3585-3589.

33. Ziegler, C. and A. Eychmüller, *Seeded Growth Synthesis of Uniform Gold Nanoparticles with Diameters of 15−300 nm.* The Journal of Physical Chemistry C, 2011. **115**(11): p. 4502-4506.

34. Jana, N.R., L. Gearheart, and C.J. Murphy, *Evidence for Seed-Mediated Nucleation in the Chemical Reduction of Gold Salts to Gold Nanoparticles.* Chemistry of Materials, 2001. **13**(7): p. 2313-2322.

35. Bastus, N.G., J. Comenge, and V. Puntes, *Kinetically Controlled Seeded Growth Synthesis of Citrate-Stabilized Gold Nanoparticles of up to 200 nm: Size Focusing versus Ostwald Ripening.* Langmuir, 2011. **27**(17): p. 11098-11105.

36. Piella, J., N.G. Bastus, and V. Puntes, *Size-Controlled Synthesis of Sub-10-nanometer Citrate-Stabilized Gold Nanoparticles and Related Optical Properties.* Chemistry of Materials, 2016. **28**(4): p. 1066-1075.

37. Bastús, N.G., et al., *Synthesis of Highly Monodisperse Citrate-Stabilized Silver Nanoparticles of up to 200 nm: Kinetic Control and Catalytic Properties.* Chemistry of Materials, 2014. **26**(9): p. 2836-2846.

38. Brust, M., et al., *Synthesis of thiol-derivatised gold nanoparticles in a two-phase Liquid-Liquid system.* Journal of the Chemical Society, Chemical Communications, 1994(7): p. 801-802.

39. Deraedt, C., et al., *Sodium borohydride stabilizes very active gold nanoparticle catalysts.* Chemical Communications, 2014. **50**(91): p. 14194-14196.

40. Tréguer-Delapierre, M., et al., *Synthesis of non-spherical gold nanoparticles.* Gold Bulletin, 2008. **41**(2): p. 195-207.

41. Grzelczak, M., et al., *Shape control in gold nanoparticle synthesis.* Chemical Society Reviews, 2008. **37**(9): p. 1783-1791.

42. Personick, M.L. and C.A. Mirkin, *Making Sense of the Mayhem behind Shape Control in the Synthesis of Gold Nanoparticles.* Journal of the American Chemical Society, 2013. **135**(49): p. 18238-18247.

43. Day, H.A., et al., *Controlling the three-dimensional morphology of nanocrystals.* Crystengcomm, 2010. **12**(12): p. 4312-4316.

44. Blackburn, G.M. and R.S.o. Chemistry, *Nucleic Acids in Chemistry and Biology*. 2006: RSC Pub.

45. Watson, J.D. and F.H. Crick, *Molecular structure of nucleic acids; a structure for deoxyribose nucleic acid.* Nature, 1953. **171**(4356): p. 737-8.

46. Thundat, T., D.P. Allison, and R.J. Warmack, *Stretched DNA structures observed with atomic force microscopy.* Nucleic Acids Research, 1994. **22**(20): p. 4224-4228.

47. Morfin, I., et al., *Adsorption of Divalent Cations on DNA.* Biophysical Journal, 2004. **87**(4): p. 2897-2904.

48. Clark, L.B. and I. Tinoco, *Correlations in the Ultraviolet Spectra of the Purine and Pyrimidine Bases1*. Journal of the American Chemical Society, 1965. **87**(1): p. 11-15.

49. Tataurov, A.V., Y. You, and R. Owczarzy, *Predicting ultraviolet spectrum of single stranded and double stranded deoxyribonucleic acids.* Biophysical Chemistry, 2008. **133**(1-3): p. 66-70.

50. Qiu, J.Q., A.H. El-Sagheer, and T. Brown, *Solid phase click ligation for the synthesis of very long oligonucleotides.* Chemical Communications, 2013. **49**(62): p. 6959-6961.

51. Theisen, P., et al., *Fluorescent dye phosphoramidite labelling of oligonucleotides.* Tetrahedron Letters, 1992. **33**(35): p. 5033-5036.

52. Proudnikov, D. and A. Mirzabekov, *Chemical Methods of DNA and RNA Fluorescent Labeling.* Nucleic Acids Research, 1996. **24**(22): p. 4535-4542.

53. Heuer-Jungemann, A., et al., *Copper-free click chemistry as an emerging tool for the programmed ligation of DNA-functionalised gold nanoparticles.* Nanoscale, 2013. **5**(16): p. 7209-7212.

54. Sandström, P., M. Boncheva, and B. Åkerman, *Nonspecific and Thiol-Specific Binding of DNA to Gold Nanoparticles.* Langmuir, 2003. **19**(18): p. 7537-7543.

55. Harimech, P.K., et al., *Reversible Ligation of Programmed DNA-Gold Nanoparticle Assemblies.* Journal of the American Chemical Society, 2015. **137**(29): p. 9242-9245.

56. Hakkinen, H., *The gold-sulfur interface at the nanoscale.* Nature Chemistry, 2012. **4**(6): p. 443-455.

57. Barrow, S.J., et al., *DNA-directed self-assembly and optical properties of discrete 1D, 2D and 3D plasmonic structures.* Nano Today, 2013. **8**(2): p. 138-167.

58. Li, Z., et al., *Multiple thiol-anchor capped DNA–gold nanoparticle conjugates.* Nucleic Acids Research, 2002. **30**(7): p. 1558-1562.

59. Kočalka, P., A.H. El-Sagheer, and T. Brown, *Rapid and Efficient DNA Strand Cross-Linking by Click Chemistry.* ChemBioChem, 2008. **9**(8): p. 1280-1285.

60. Mastroianni, A.J., S.A. Claridge, and A.P. Alivisatos, *Pyramidal and Chiral Groupings of Gold Nanocrystals Assembled Using DNA Scaffolds.* Journal of the American Chemical Society, 2009. **131**(24): p. 8455-8459.

61. Dumur, F., et al., *Controlled spontaneous generation of gold nanoparticles assisted by dual reducing and capping agents.* Gold Bulletin, 2011. **44**(2): p. 119-137.

62. Schmid, G. and A. Lehnert, *The Complexation of Gold Colloids.* Angewandte Chemie-International Edition, 1989. **28**(6): p. 780-781.

63. Hurst, S.J., A.K.R. Lytton-Jean, and C.A. Mirkin, *Maximizing DNA loading on a range of gold nanoparticle sizes.* Analytical Chemistry, 2006. **78**(24): p. 8313-8318.

64. Zhang, X., M.R. Servos, and J.W. Liu, *Instantaneous and Quantitative Functionalization of Gold Nanoparticles with Thiolated DNA Using a pH-Assisted and Surfactant-Free Route.* Journal of the American Chemical Society, 2012. **134**(17): p. 7266-7269.

65. Shi, D.W., et al., *A facile and efficient method to modify gold nanorods with thiolated DNA at a low pH value.* Chemical Communications, 2013. **49**(25): p. 2533-2535.

66. Zanchet, D., et al., *Electrophoretic isolation of discrete Au nanocrystal/DNA conjugates.* Nano Letters, 2001. **1**(1): p. 32-35.

67. Pellegrino, T., et al., *Gel electrophoresis of gold-DNA nanoconjugates.* Journal of Biomedicine and Biotechnology, 2007.

68. Claridge, S.A., et al., *Isolation of discrete nanoparticle - DNA conjugates for plasmonic applications.* Nano Letters, 2008. **8**(4): p. 1202-1206.

69. Busson, M.P., et al., *Optical and Topological Characterization of Gold Nanoparticle Dimers Linked by a Single DNA Double Strand.* Nano Letters, 2011. **11**(11): p. 5060-5065.

70. Akiyama, Y., et al., *Modulation of Interparticle Distance in Discrete Gold Nanoparticle Dimers and Trimers by DNA Single-Base Pairing.* Small, 2015. **11**(26): p. 3153-3161.

71. Pon, R.T., N. Usman, and K.K. Ogilvie, *Derivatization of controlled pore glass-beads for solid-phase oligonucleotide synthesis.* Biotechniques, 1988. **6**(8): p. 768-775.

72. Damha, M.J., P.A. Giannaris, and S.V. Zabarylo, *An improved procedure for derivatization of controlled-pore glass-beads for solid-phase oligonucleotide synthesis.* Nucleic Acids Research, 1990. **18**(13): p. 3813-3821.

73. Caruthers, M.H., *Gene synthesis machines - dna chemistry and its uses.* Science, 1985. **230**(4723): p. 281-285.

74. Qiu, J., A.H. El-Sagheer, and T. Brown, *Solid phase click ligation for the synthesis of very long oligonucleotides.* Chemical Communications, 2013. **49**(62): p. 6959-6961.

75. Beaucage, S.L. and R.P. Iyer, *Advances in the Synthesis of Oligonucleotides by the Phosphoramidite Approach.* Tetrahedron, 1992. **48**(12): p. 2223-2311.

76. Swami, A.S., N. Brun, and D. Langevin, *Phase Transfer of Gold Metallized DNA.* Journal of Cluster Science, 2009. **20**(2): p. 281-290.

77. Eidelshtein, G., et al., *Synthesis and Properties of Novel Silver-Containing DNA Molecules.* Advanced Materials, 2016. **28**(24): p. 4839-4844.

78. Braun, E., et al., *DNA-templated assembly and electrode attachment of a conducting silver wire.* Nature, 1998. **391**(6669): p. 775-778.

79. Filoramo, A., *DNA Metallization Processes and Nanoelectronics.* Nanopackaging: From Nanomaterials to the Atomic Scale, 2015: p. 17-32.

80. Richter, J., *Metallization of DNA.* Physica E: Low-dimensional Systems and Nanostructures, 2003. **16**(2): p. 157-173.

81. Ma, X., et al., *Gold nanocrystals with DNA-directed morphologies.* Nature Communications, 2016. **7**.

Chapter 3. Experimental procedures

This chapter includes all the experimental methods and techniques used in this thesis. Synthetic protocols for gold nanoparticle-DNA assemblies are presented in **Sections 3.1-3.4**, while characterisation techniques for designed oligonucleotides, gold nanoparticles and their assemblies are found in **Section 3.5**.

3.1 Synthesis of spherical gold nanoparticles

Spherical gold nanoparticles of various size were synthesised using wet chemical synthesis protocols. Approaches for smaller particles (4.5 and 12.1 nm) are presented in **Sections 3.1.1** and **3.1.2**, bigger particles (>30 nm) are detailed in **Section 3.1.3** and 5.7 nm gold nanoparticle seeds are developed in **Section 3.1.4**.

3.1.1 Synthesis of 4.5 ± 0.4 nm spherical gold nanoparticles

Small 4.5 ± 0.4 nm spherical gold nanoparticles were synthesised using an established published protocol (see **Section 2.2.1** for theoretical background) [1]. In detail, a solution made of sodium tetrachloroaurate (375 µL, 100 mM) and potassium carbonate (500 µL, 0.2 M) in 4 ºC Milli-Q water (100 mL) was stirred in an ice bath. Once the mixture was homogenous, a freshly prepared aqueous solution of sodium

borohydride (0.5 mg/ml) was added in 5 x 1 ml aliquots with vigorous stirring. The colour of the solution changed from dark purple to orange-red, indicating the formation of small AuNPs [2]. After stirring for 5 additional minutes, the solution was subject to centrifugation at 9,300 x g (Eppendorf 5417R used for all centrifugations) for 10 minutes. Larger nanoparticles were excluded by only collecting the supernatant so obtaining a narrow size distribution. In order to increase particles stability, a ligand exchange between citrate and BSPP was then performed by incubating the particles with 15 mg of BSPP (see **Figure 3.1**) [3]. After overnight stirring, sodium chloride (NaCl) was added to aggregate the particles. Aggregation was confirmed by a colour change from reddish orange to light purple [4-6]. The aggregated particles were subject to centrifugation at 25,000 x g for 20 minutes at 6 °C and re-suspended in Milli-Q water (3 ml). Particles were characterised using transmission electron microscopy (TEM) and extinction spectroscopy (see **Section 3.5**) and stored at 4 ºC before further use in protocols described in **Sections 3.2.1** and **3.3**.

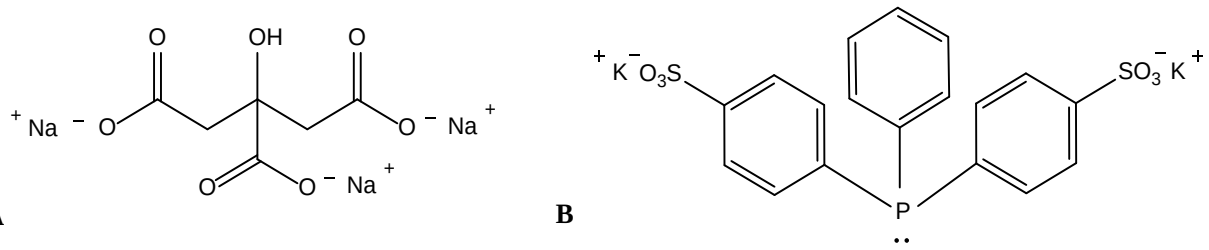

A **B**

Figure 3.1. Chemical structures of **A)** trisodium citrate and **B)** BSPP

3.1.2 Synthesis of 12.1 ± 0.3 nm spherical gold nanoparticles

Spherical gold nanoparticles of 12.1 ± 0.3 nm were synthesised using the well-established Turkevich method modified later by Frens et al. [7, 8] (see **Section 2.2.1** for theoretical background). In detail, a solution of sodium tetrachloroaurate (100 ml, 1 mM) was brought to 100 °C with mild stirring. Once boiling, a warm solution of trisodium citrate (5 ml, 2% wt/V) was added with vigorous stirring. A colour change occurred from yellow through to colourless to dark purple and finally to deep red [9]. Once the red colour was obtained, the boiling and the stirring were maintained for 15 additional minutes before allowing the reaction mixture to cool down to room temperature. The stability of the particles was increased by incubating them with BSPP (15 mg) [3]. After overnight stirring, NaCl was added to aggregate the particles. Aggregation was confirmed by a colour change from blood red to dark blue [4-6]. The aggregated particles were then subject to centrifugation at 25,000 x g for 30 min at 25 °C and re-suspended in Milli-Q water (3 ml). Particles were characterised using TEM and extinction spectroscopy (see **Section 3.5**) and stored at 4 ºC before further used in protocols described in **Sections 3.2.1, 3.3 and 3.4.**

3.1.3 Synthesis of larger (>30 nm) spherical gold nanoparticles

Spherical gold nanoparticles larger than 30 nm diameter were synthesised according to a recently published seeded-growth method developed by Puntes and co-workers [10]. First 10 nm AuNPs seeds were synthesised by adding a gold salt solution

(1 ml, 25 mM) into a boiling solution of trisodium citrate (150 ml, 2.2 mM). The solution slowly turned bright pink. After 10 minutes the temperature was reduced to 90 °C. Gold salt solution was added (1 ml, 25 mM) and left to react for 30 minutes; this was repeated twice to achieve the first growth step (AuG_0). The solution was then diluted by withdrawing 55 ml and replacing this with an equal volume of an aqueous solution of sodium citrate (55 ml, 2.2 mM). When the temperature came back to 90°C, this growth step was repeated until the desired particle size was obtained (AuG_1 to AuG_6, 18 to 54 nm respectively). Particles were stabilised using BSPP. After overnight incubation, particles were subject to centrifugation at 2,300 x g for 20 minutes. Characterisation using TEM and extinction spectroscopy were carried out as per **Section 3.5**; samples were kept in the fridge before being used in **Section 3.2.2**.

3.1.4 Synthesis of 5.7 ± 0.2 nm gold nanoparticle seeds

Spherical gold nanoparticle seeds of narrow size distribution (5.7 ± 0.2 nm) were synthesised using a recently published protocol [11]. In detail, an aqueous solution made of sodium citrate (150 ml, 2.2 mM), Tannic acid (100 µL, 2.5 mM) and potassium carbonate (1 ml, 150 mM) was stirred and heated to 70 ºC. A solution of sodium tetrachloroaurate (1 ml, 25 mM) was then injected and the reaction was left to react for 5 minutes. Subsequently, 55 ml of the reaction mixture was extracted and replaced by a fresh solution of sodium citrate (55 ml, 2.2 mM). When the reaction reheated to 70 ºC, more sodium tetrachloroaurate (0.5 ml, 25 mM) was injected and the reaction was left for 10 minutes; this last step was repeated once. The solution was cooled down to room temperature and 15 mg of BSPP was added to stabilise the particles. After stirring

overnight, the particles were aggregated using NaCl and subject to centrifugation at 25,000 x g for 20 minutes. The supernatant was removed and the pellet was redispersed in Milli-Q water. These particles were used as single nanoparticle seeds in **Section 3.4.1**. Furthermore, these seeds were assembled into dimers using DNA strands Bcc and Ccc (see **Table 3.1** for sequences and **Section 3.3.2** for protocol) to be used in seeded-growth experiments (see **Section 3.4**).

3.2 Oligonucleotide modification of spherical gold nanoparticles

Spherical AuNPs of different sizes were functionalised with designed thiol terminated oligonucleotides for self-assembly purposes. The procedure for oligonucleotide modification of smaller particles is given in **Section 3.2.1,** while the modification of larger particles is described in **Section 3.2.2**. All oligonucleotides were synthesised at the University of Oxford by Dr Afaf El-Sagheer in the group of Prof. Tom Brown (see **Chapter 2** for background information).

3.2.1 Modification of smaller particles (4.5 ± 0.4 and 12.1 ± 0.3 nm) with oligonucleotides

The “discrete” or “dense shell” surface modifications of small gold nanoparticles with thiol terminated oligonucleotides were performed using modified published protocols [12-15] (see **Sections 3.2.1.1** and **3.2.1.2**).

3.2.1.1 Discrete modification of nanoparticles with oligonucleotides

A published protocol was modified to synthesise 4.5 ± 0.4 and 12.1 ± 0.3 nm spherical gold nanoparticles, bearing exactly only one DNA strand, also called DNA monoconjugates [12]. Modifications were made to improve the monoconjugates yield and included changes in buffer and incubation time compare to the original protocol. In detail, 4.5 (1000 pmol) or 12.1 nm (500 pmol) BSPP coated gold nanoparticles (see **Sections 3.1.1 and 3.1.2**) were redispersed in attachment buffer (20 mM phosphate, 5 mM NaCl, pH=7.2). An equimolar amount of thiolated oligonucleotides (Strands 1, 2, A, B, C, D, Bcc or Ccc (see **Table 3.1** for DNA sequences and **Figure 3.3** for their modifications)) and a solution of BSSP (10 µl, 1 mg/20µl) were added and the reaction mixture was shaken for 1 hour. The BSPP solution was used to deprotect the thiolated DNA strands by reducing the disulfide bond into its reactive thiol form [16] (see **Figure 3.2**). As no HPLC instrument was available, DNA monoconjugates were purified using agarose gel electrophoresis (see **Section 3.5.1.2**). DNA monoconjugate concentrations were determined using the UV-Visible extinction spectra (see **Section 3.5.3.1**); and

functionalised particles were stored at 4 ºC before being used in further protocols (see **Sections 3.3 and 3.5**).

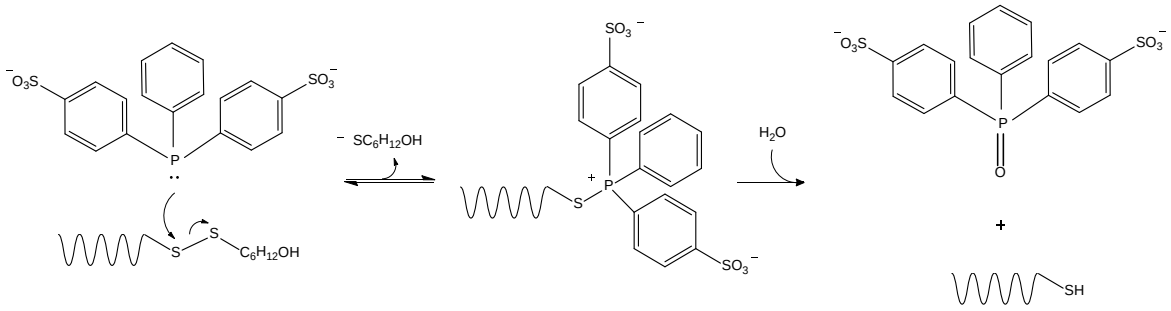

Figure 3.2. Mechanism of the disulfide bond reduction by BSPP

Table 3.1. DNA sequences used for gold nanoparticles functionalisation. Modifications X_1 and X_2 are shown in **Figure 3.3**

Abbreviations	DNA sequences and modifications
Three Strands system	
1	5' – ($C_6H_{12}S$)AAAAAAAACGAGTGCTAAGGATCCGAA**X_1**
2	3' – ($C_6H_{12}S$)AAAAAAAAGCTTACCTATAGACGTCACTT**X_2**
3	5' – CGAATGGATATCTGCAGTGAATTCGGATCCTTAGCACTCG
Four Strands system	
A	5' – ($C_6H_{12}S$)TTTGCCTGGAGATACATGCACATTACGGCTTTCCCTATTAG AAGGTCTCAGGTGCGCGTTTCGGTAAGTAGACGGGACCAGTTCGCC
B	5' – ($C_6H_{12}S$)TTTCGCGCACCTGAGACCTTCTAATAGGGTTTGCGACAGTC GTTCAACTAGAATGCCCTTTGGGCTGTTCCGGGTGTGGCTCGTCGG
C	5' – ($C_6H_{12}S$)TTTGGCCGAGGACTCCTGCTCCGCTGCGGTTTGGCGAACTG GTCCCGTCTACTTACCGTTTCCGACGAGCCACACCCGGAACAGCCC
D	5' – ($C_6H_{12}S$)TTTGCCGTAATGTGCATGTATCTCCAGGCTTTCCGCAGCGG AGCAGGAGTCCTCGGCCTTTGGGCATTCTAGTTGAACGACTGTCGC
Bcc	5' – ($C_6H_{12}S$)TTTCGCGCACCTGAGACCTTCTAATAGGGTTTGCGACAGTC GACGACTAGAATGCCCTTTGGGCTGTTCCGG**X_1**GTGGCTCGTCGG
Ccc	5' – ($C_6H_{12}S$)TTTGGCCGAGGACTCCTGCTCCGCTGCGGTTTGGCGAACTG GACCGTCTACTTACCGTTTCCGACGAGCCAC**X_2**CCGGAACAGCCC
Other	
S	5' – ($C_6H_{12}S$)AAACGGGCTTTTTTTTTTTTTTTTTTTTTTTTTTTT

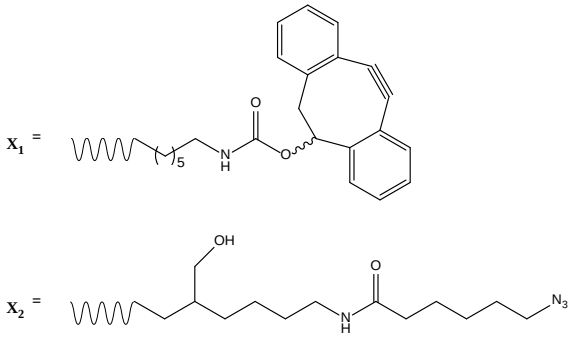

Figure 3.3. Chemical modifications on designed DNA sequences with $\mathbf{X_1}$: DIBO, $\mathbf{X_2}$: Azide

3.2.1.2 Surface modification of nanoparticles with a dense shell of oligonucleotides

The coverage of gold nanoparticles with a dense shell of DNA has been achieved in three different ways for three different experiments (see **Sections 3.4** and **3.5**).

First, in order to study the influence of the ligands on the gold nanoparticles sedimentation process (see **Section 3.5.5**), larger particles (see **Section 3.1.3**) were coated with a dense shell of DNA strands using a slow "salt ageing" method [13]. AuG_0 or AuG_1 (35 and 47 nm) (1 ml, 10 nM) were incubated overnight with thiol modified DNA strand A (1 nmol) (see **Table 3.**1 for sequence). Solutions of phosphate buffer (0.1 M, pH 7.4), sodium dodecyl sulphate (SDS) (10%) and BSPP (10 µl, 1 mg/20 µl) were added to the AuNPs to obtain final concentrations of 0.01 M phosphate and 1 % SDS, respectively. To increase the salt concentration of the reaction mixture to 0.1 M, six additions of a NaCl solution (2 M) were performed over a period of 6 h. After another 12h of incubation the excess DNA was removed *via* centrifugation at 2,300 x g for 10 minutes and the DNA coated particles were redispersed in Milli-Q water. After

spectroscopic characterisation (see **Section 3.5.3**), particles were stored in the fridge before being used in further experiments (see **Section 3.5.5**).

Second, in order to purify grown gold nanoparticles (see **Sections 3.4.1.1** and **3.4.1.2**), the CTAB layer present around them was replaced by a shell of short DNA strands using a modified published protocol [14]. In detail, 5 nmol of the short DNA, S, (see **Table 3.1** for sequence) was deprotected by incubating it with a BSPP solution (50 µl, 1 mg/ 20 µl) for one hour. A buffer made of 5 x Tris borate ethylenediaminetetraacetic acid (TBE) buffer (1 ml), SDS (50 µl, 10% wt/V), NaCl (750 µl, 2M) and Milli-Q water (3.7 ml) was freshly prepared. The pH of the buffer was adjusted to 3 with concentrated hydrochloric acid. Thiolated DNA and gold nanoparticles in a 750:1 molar ratio were added to 1 ml of the buffer. The mixture was shaken for 10 minutes before being subject to centrifugation, twice at 1500 x g for 15 minutes. DNA:AuNPs, incubation time and centrifugation parameters were optimised for the type of particles functionalised in this protocol. Particles were then redispersed in Milli-Q water before being purified using agarose gel electrophoresis (see **Section 3.4.1.3**).

Finally, for further use in DNA metallisation protocol, the surface of 5.7 or 12.1 nm BSPP gold nanoparticles (see **Sections 3.1.4** and **3.1.2**) was covered with a dense shell of short DNA using a published protocol [15]. In detail, 1 nmol of the short DNA strand S (see **Table 3.1** for sequence) was incubated for an hour with a solution of BSPP (10 µl, 1 mg / 20 µl) to break the disulphide bond and form a reactive thiol group. The deprotected DNA was then added to 1 pmol of AuNPs alongside citrate buffer (20 µl, 10 mM) and Milli-Q water to obtain a final volume of 870 µl. The mixture was allowed to shake for 3 minutes before addition of an aqueous solution of NaCl (180 µl, 2 M). After five further minutes of shaking the solution was subject to centrifugation at 2,300 x g for 10 minutes, after which, the supernatant was removed and the particles

redispersed in Milli-Q water. This was repeated once the particles were subsequently used in DNA metallisation protocols (see **Section 3.4.2**).

3.2.2 Modification of larger particles (>30 nm) with oligonucleotides

3.2.2.1 Synthesis of large DNA duplexes (541 bp)

As larger particle DNA monoconjugates cannot be easily purified using agarose gel electrophoresis, a protocol to synthesise long DNA duplexes by PCR was established (see **Section 2.4.2** for theoretical background) [17-19]. In detail, for one PCR reaction (10 µL) a master mix made of DNA free water (4 µL), 5x Phire Buffer (2 µL), magnesium chloride ($MgCl_2$) (0.6 µL), deoxynucleotide triphosphates (dNTPs) (0.2 µL, 0.2 mM), forward and reverse primers (1 µL, 0.2 µM) (Fp and RpA to D, see **Table 3.2** for sequences and **Figure 3.4** for their modification) was prepared in a laminar flow cabinet. Then the Phire Hot Start II DNA polymerase (0.2µl) and the mix of the 9 oligos (1 µl, 0.2 µM) (see **Table 3.2** for sequences) were added to the master mix. In order to follow the PCR in real time a SYBR Green solution (0.6 µl) was also incorporated into the mix [20]. The PCR program consisted of 50 cycles of 5 seconds at 98 °C, 5 seconds at 55 °C and 15 seconds at 72 °C. The fragment of interest was then purified by agarose gel electrophoresis (see **Section 3.5.1.2**) using the extraction kit Wizard® SV Gel and PCR clean-up system from Promega. The DNA duplexes were kept dissolved in Milli-Q water at -20ºC before being used in further protocol (see **Section 3.2.2.2**).

Table 3.2. DNA sequences used for synthesis of long DNA duplexes and synthesis of large DNA monoconjugates. Modification Y is shown in **Figure 3.4**

Abbreviations	DNA sequences and modifications
Forward and Reverse Primers	
Fp	5' – GGAGAGGGTGAAGGT
RpA	5' – GGCTACAGGTAGGACGGCGAACTGACACCG**Y**TCTTTCGAAAGGGCAGAT
RpB	5' – GGCTACAGGTAGGACGGCGAACTGACACCG**Y**TCTTTCGAAAGGGCAGAT
RpC	5' – GGCTACAGGTAGGACGGGCTGTTCCGGGT**Y**TCTTTCGAAAGGGCAGAT
RpD	5' – GGCTACAGGTAGGACGCGACAGTCGTTCAC**Y**TCTTTCGAAAGGGCAGAT
Oligonucleotides	
1	5' – GGAGAGGGTGAAGGTGATGCAACATACGGAAAACTTACCCTTAAATTTATTTGCA CTACTGGAAAACTACCTGTTCCATGGCCAACACTTGTCACTACTTTAACTTA
2	5' – GGTGTTCAATGCTTTTCAAGATACCCAGATCACATGAAACGGCATGACTTTTTCAA GAGTGCCATGCCCGAAGGTTATGTACAGGAAAGAACTATATTTTTCAAAGA
3	5' – GACGGCAACTACAAGACACGTTGCTGAAGTCAAGTTTGAAGGTGATACCCTTGTT AATAGAATCGAGTTAAAAGGTATTGATTTTAAAGAAGATGGAAACATT
4	5' – CTTGGACACAAATTGGAATACAACTATAACTCACACAATGTATACATCATGGCAGA CAAACAAAAGAATGGAATCAAAGTTAACTTCAAAATTAGACACAACATTGAAGA
5	5' – GGAAGCGTTCAACTAGCAGACCATTATCAACAAATACTCCAATTGGCGATGGCCC TGTCCTTTTACCAGACAACCATTACCTGTCCACACAATCTGCCCTTTCGAAAGA
6	5' – GGCACTCTTGAAAAAGTCATGCCGTTTCATGTGATCTGGGTATCTTGAAAAGCAT TGAACACCATAAGTTAAAGTAGTGACAAGTGTTGGCCATGGAACAGGTAGT
7	5' – AACAAGGGTATCACCTTCAAACTTGACTTCAGCACGTGTCTTGTAGTTCCCGTCA TCTTTGAAAAATATAGTTCTTTCCTGTACATAACCTTCGGGCA
8	5' – GCCATGATGTATACATTGTGTGAGTTATAGTTGTATTCCAATTTGTGTCCAAGAATG TTTCCATCTTCTTTAAAATCAATACCTTTTAACTCGATTCTAT
9	5' – GGAGTATTTTGTTGATAATGGTCTGCTAGTTGAACGCTTCCATCTTCAATGTTGTG TCTAATTTTGAAGTTAACTTTGATTCCATTCTTTTGTTTGTC
Peel off strands	
PoA	5' – CGGTGTCAGTTCGCCGTCCTACCTGTAGCC
PoB	5' – GGTGTGGCTCGTCGGGTCCTACCTGTAGCC
PoC	5' – ACCCGGAACAGCCCGTCCTACCTGTAGCC
PoD	5' – GTGAACGACTGTCGCGTCCTACCTGTAGCC

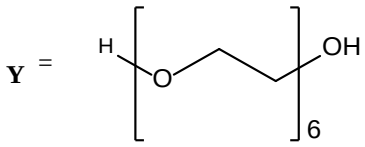

Figure 3.4. Chemical structure of the Heg spacer used in DNA strands RpA, RpB, RpC and RpD

3.2.2.2 Purification of gold-DNA nanoparticle monoconjugates

The protocol used for the purification of large gold-DNA nanoparticle monoconjugates was developed in the context of this work and is described in **Figure 3.5**.

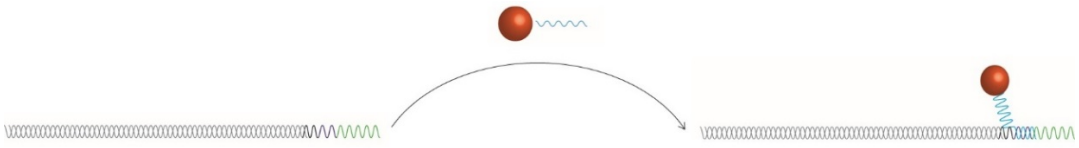

Figure 3.5. Schematic illustration of the monoconjugates synthesis for larger particles

DNA monoconjugates of 13 nm (for preliminary experiments) or larger spherical gold nanoparticles (1 pmol) were synthesised (see **Section 3.2.1.1**) but not purified through agarose electrophoresis. They were then subject to centrifugation at 25,000 or 2,300 x g respectively for 10 minutes and redispersed in hybridisation buffer (6 mM phosphate, 80 mM NaCl, pH=7.2). A five-fold excess of long DNA duplexes (5 pmol) was then added and the reaction was heated to 70ºC, with subsequent cooling down to room temperature. Particles were then subject to centrifugation and redispersed in attachment buffer (20 mM phosphate, 5 mM NaCl); purification was carried out by agarose gel electrophoresis (see **Section 3.5.1.2**).

3.3 Synthesis of spherical gold-DNA nanoparticle assemblies using DNA hybridisation

Dimers assemblies of gold nanoparticles were synthesised using the previously described building blocks (see **Sections 3.1** and **3.2**). Protocols using either modified (clicking moieties) or unmodified (no clicking moieties) DNA strands, are described in **Section 3.3.1.**

3.3.1 Synthesis of dimers using a three DNA strands system

Dimer assemblies, were synthesised using a published protocol [21]. BSPP coated AuNPs of 4.5 or 12.1 nm in Milli-Q water were precipitated using NaCl and then were subject to centrifugation for 20 minutes at 25,000 x g. The supernatant was removed and phosphate buffer was added (20 mM phosphate, 5 mM NaCl). DNA strands 1 or 2 (see **Table 3.1** for sequences) were added to separate nanoparticle batches to achieve a ratio of DNA: particles of 3:1. A solution of BSSP (10 µL, 1 mg/20µL) was added and the reaction mixture was shaken for 1 hour. The AuNPs were then subject to centrifugation for 15 minutes at 25,000 x g and redispersed in hybridisation buffer (6 mM phosphate, 80 mM NaCl). DNA strand 3 (4.45 µl, 0.56 µM) was then added to create the dimers. The hybridisation step was realised by heating up the solution to 70 °C and leaving it to slowly and gradually cool down to room temperature. The particles were purified by agarose gel electrophoresis (1.75 % agarose gel in 0.5 x TBE, 1 h at 90 V. See **Section 3.5.1.2**). The dimers were redissolved in Milli-Q water and characterised

using agarose gel electrophoresis, TEM and spectroscopy (see **Sections 3.5.1.2, 3.5.2, 3.5.3** and **3.5.5**).

3.3.2 Synthesis of dimers using a four strands system

Dimers assemblies formed using a system of four DNA strands were synthesised using a published protocol [22]. In detail, equimolar amounts of selected DNA monoconjugates (A and D, B and C or Bcc and Ccc (see **Section 3.2.1.1** for protocol and **Table 3.1** for sequences)) were mixed together in hybridisation buffer (6 mM phosphate, 80 mM NaCl). The particles were then heated up to 70 ºC and left to cool slowly to room temperature. Dimers were then purified using agarose gel electrophoresis (see **Section 3.5.1.2**). In the case of DNA strands modified for click chemistry (Bcc and Ccc), denaturing conditions were applied to the solution before purification to ensure that any unclicked assembly fell apart. Formamide was added (1/2 of the final volume) to particles, which were heated up to 70 ºC for 10 minutes before being cooled in an ice bath and loaded on the agarose gel [23, 24]. Resulting dimers were all redispersed in Milli-Q water and kept in the fridge before further utilisation (see **Sections 3.4** and **3.5**).

3.4 Synthesis of DNA-gold nanoparticle assemblies using seeded growth

Synthesis of single or dimer DNA-gold nanoparticle assemblies using seeded growth method was developed. In **Section 3.4.1** protocols for the synthesis of large spherical or anisotropic dimers are described while in **Section 3.4.2** DNA metallisation protocols are being developed.

3.4.1 Synthesis of large spherical or anisotropic nanoparticle dimers

3.4.1.1 Synthesis of single or dimer large spherical gold nanoparticles

A published protocol originally used to produce gold nanorods was modified to synthesise large spherical gold nanoparticles, using the previously synthesised nanoparticle seeds as templates (see **Section 3.1.4**) [25]. In detail, a reaction mixture made of Milli-Q water (1 ml), CTAB (1.25 ml, 0.2 M) and sodium tetrachloroaurate (250 µl, 5 mM) was gently left to stir at 40 ºC for 5 minutes. Silver nitrate originally added for synthesis of gold nanorods was not incorporated. Freshly prepared L-ascorbic acid (17.5 µl, 80 mM) was injected whilst stirring vigorously. After 30 seconds, 1.25 pmol of seeds (single or dimer nanoparticles) was added and the stirring was stopped after 5 seconds; the solution turned light pink immediately. The solution was left

undisturbed for 15 minutes in order to allow the particles to grow. The purification step for these particles is described in **Section 3.4.1.3**.

3.4.1.2 Synthesis of single or dimer anisotropic gold nanoparticles

A protocol previously developed in the group has been adapted to synthesise anisotropic particles using previously synthesised seeds (see **Section 3.1.4**) [26]. A reaction mixture made of CTAB (1.425 ml, 0.2 M), sodium tetrachloroaurate (200 µl, 5 mM) and silver nitrate (41 µl, 5 mM) was gently left to stir at 40 ºC for 5 minutes. The solution was vigorously stirred and 0.8 pmol of seeds (singles or dimers) were introduced in the reaction. After 5 seconds, freshly prepared L-ascorbic acid (16 µl, 160 mM) was added; the solution turned blue slowly. The solution was left to age for 15 minutes in order to allow the particles to grow. The purification step for these particles is described in **Section 3.4.1.3**.

3.4.1.3 Purification of grown single or dimer gold nanoparticles

CTAB coated gold nanoparticles do not run through agarose gel electrophoresis [27]. In order to purify the previously grown particles (see **Sections 3.4.1.1** and **3.4.1.2**), the CTAB shell was replaced by a shell of DNA using the protocol described in **Section 3.2.1.2**. Particles were then purified through agarose gel electrophoresis (see **Section 3.5.1.2**) and, after being redispersed in Milli-Q water, kept in the fridge. They were characterised using the techniques described in **Section 3.5**.

3.4.2 DNA metallisation

A published DNA metallisation protocol was applied to gold nanoparticles (250 µl, 0.5 pmol) previously coated with a shell of DNA S (see **Section 3.2.1.2**) [28]. They were incubated with hydroxylamine (100 µl, 1 mM) and sodium tetrachloroaurate (57 µl, 0.75 µM) for 15 minutes using a shaker. A change in colour from clear to greyish was observed after one minute. The solution was then subject to centrifugation twice at 25,000 x g for 10 minutes. Samples characterisation was carried out (see **Section 3.5**) and metallised assemblies were kept in the fridge.

3.5 Characterisation of designed oligonucleotides, gold nanoparticles and their assemblies

Many techniques were employed for the characterisation of designed oligonucleotides, gold nanoparticles and their self-assemblies. Protocols for gel electrophoresis, transmission electron microscopy, spectroscopy techniques, measurement of diffusion and sedimentation are described from **Sections 3.5.1** to **3.5.5.**

3.5.1 Gel electrophoresis techniques

3.5.1.1 Native and denaturing polyacrylamide gel electrophoresis

Native 8 % polyacrylamide gels were prepared by mixing acrylamide monomer solution (10.5 mL, 40% wt/V), TBE buffer (14 mL, 5x) and Milli-Q water (45.5 mL). The polymerisation was then initiated by adding N, N, N',N'-tetramethylethylenediamine (56 µL) as a catalyst and amine persulfate (560 µL, 10 % wt/V) as an initiator. In the case of the denaturing 8 % polyacrylamide gel, urea (29.4 g, 8 M) was mixed with an acrylamide monomer solution (14 mL, 40% wt/V), TBE buffer (14 mL, 5 x) and Milli-Q water (up to 70 mL). The polymerisation was then initiated by adding N,N,N',N'-tetramethylethylenediamine (45 µL) as a catalyst and amine persulfate (450 µl, 10 % wt/V) as an initiator. In both cases the gels were quickly syringed between two glass plates and a comb was inserted to create wells. After 1 hour of polymerisation, the gel was placed in a bath of 1 x TBE running buffer, the comb was removed and the wells were flushed. Electrodes of the PROTEAN II xi Cell from Bio-Rad were connected and the gel was prerun at 10 W for 1 h to fill the gel matrix with TBE buffer. Sample preparations were carried out by mixing an equimolar ratio of the desired DNA strands in buffer (10µL, 10mM Tris: 5mM $MgCl_2$) in a final volume of 50 µl. The hybridisation was conducted by heating up the mixture for 5 minutes at 95 °C and letting it cool down slowly to room temperature. When using denaturing conditions after hybridisation, samples were mixed with a solution of formamide (1/2 of the final volume) and heated up to 85 ºC for 10 minutes before being chilled in an ice bath; the formamide allows the denaturation of the DNA strands by lowering their melting temperature [23]. A solution of ficoll, high-mass polysaccharide (1/3 of the final

volume, 15% in 3 x TBE), was added to increase the density of the samples. Samples were loaded and the gel was run at 20 W for 2 h 30 minutes. The polyacrylamide gel was then stained using Diamond™ Nucleic acid dye (10 µL in 200 mL) for 10 minutes. The gel was rinsed with Milli-Q water and imaged using the Gel Doc EZ system from Bio-Rad.

3.5.1.2 Agarose gel electrophoresis

Purification of DNA monoconjugates and their self-assemblies were carried out using a published protocol [18]. Agarose gels were prepared by dissolving the appropriate amount of agarose (0.75 to 3 % wt/V) in 0.5 x TBE buffer. After melting using microwave heating, the gel was cast into the gel caster and combs were inserted in order to form wells. After an hour, the gel was transferred to the electrophoresis chamber previously filled with 0.5 x TBE buffer. A solution of Ficoll (15 % in 3 x TBE) was added to the samples to increase their density and prevent floating [29]. After being loaded, the gel was subject to electrophoresis at 100 V for 30 to 60 minutes. Expected bands were cut from the gel and, after being further cut into small pieces, particles were diffused from the gel in Milli-Q water overnight with gentle shaking. Particles were then filtered using a 0.2 µm syringe filter to remove any unwanted agarose pieces and subject to centrifugation at the appropriated speed before being redispersed in a selecting media (Milli-Q, attachment buffer or hybridisation buffer).

3.5.2 Transmission electron microscopy

Visualisation of gold nanoparticles and their assemblies was performed using a transmission electron microscope (Hitachi H7000 TEM, bias voltage: 75kV). All sample preparation involved deposition and evaporation of a specimen droplet on a Formvar/Carbon Film 400 Mesh Copper grid. Size distribution histograms were created using Origin software, after analysis of the corresponding images using Image J software.

3.5.3 Optical Spectroscopy

3.5.3.1 Extinction spectroscopy

Two spectrophotometers were used to characterise gold nanoparticles and their assemblies. At the laboratory in Southampton, extinction spectra were collected using a small volume quartz cuvette (1 cm optical path length) on a UV – 2600 Shimadzu spectrophotometer over the range 400 to 800 nm.

At the laboratory in Rennes extinction light spectra were collected using an optical fibre-based system (Ocean Optics, USA) incorporating a USB4000-VIS-IR charge coupled device (CCD) spectrometer and a LS-1 tungsten halogen light source (6.5 W, 3100 K). Milli-Q water was used as a reference. Each spectrum was taken with an integration time of 3.8 ms and an average of 500 scans. All spectrum saved were plotted using Veusz software.

Gold nanoparticle concentrations were determined using their optical density maxima and the Beer-Lambert law (see **Equation 3.1**).

$$C = \frac{\mathrm{OD}}{\varepsilon . \mathrm{l}}$$

Equation 3.1. Beer-Lambert Law for calculation of colloidal gold nanoparticle concentrations. C: Concentration (mol/L), OD: Maximal Optical Density, l: path length of light (cm) and ε: extinction coefficient (L.mol-1.cm-1) obtained from [30]

3.5.3.2 Oligonucleotide UV melting curves

The melting temperatures for all DNA strand systems were determined using UV melting curves. Equimolar amounts of DNA for every existing combination (see **Table 3.1** for sequences) were mixed in Tris buffer (10 mM Tris, 100 mM NaCl and 7.5 mM $MgCl_2$) [31]. Using a Cary Series UV-Vis spectrophotometer (Agilent Technologies), the OD at 260 nm was monitored whilst temperature cycles were applied to the sample. In detail, DNA mixtures were heated up quickly to 90 ºC (10 ºC/minute). Then they were subject to 3 cycles of slow cooling to 25ºC followed by slow heating to 90ºC (1 ºC/minute). Melting temperatures were determined using the obtained plots of OD_{260nm} versus temperature (ºC) (see **Section 2.3.1** for theoretical background).

3.5.3.3 Resonant light scattering spectroscopy

At the Rennes laboratory, resonant light scattering measurements were performed at room temperature using an optical fibre-based system (Ocean Optics, USA) incorporating the QE65000 back-thinned CCD spectrometer and the LS-1 tungsten halogen light source. The procedure for performing these RLS measurements has been described in the literature [32, 33]. Ludox was used as a reference and was first subject to centrifugation at 9700 x g for 1 hour, the supernatant was then taken and diluted 200 times with a NaCl solution (0.05 M). All samples were diluted in Milli-Q water to achieve an optical density under 0.05. The dark spectrum was made of Milli-Q water and each spectrum was taken with an integration time of 10 seconds and an average of 5 scans. The raw data were processed using the Python programming language and data were plotted using the Veusz software.

3.5.4 Measurement of diffusion coefficient using microfluidic systems

3.5.4.1 Microfluidic system fabrication

All fabrication processes of microfluidic systems were carried out in the clean room at ENS Rennes. In detail, two layers of Eternal Resine were laminated (114 ºC) onto a microscope glass wafer to obtain the desired channels height (150 µm). Photolithography was then realised using the mask of the selected microfluidic system (see **Figure 3.6**).

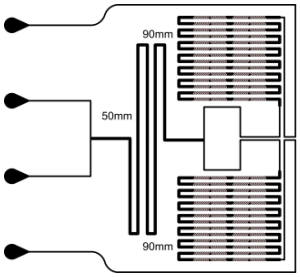

Figure 3.6. Mask used for the photolithography of the Microsystem

The microfluidic system cast shape was revealed in an aqueous solution of potassium carbonate (1% wt/V) for 3 minutes and the reaction was stopped in hard water (350 ppm calcium carbonate). The polydimethyl siloxan (PDMS) solution was then prepared by mixing a cross-linker agent sensitive to UV light with the PDMS solution at a weight ratio of 1:10. The solution was put under vacuum to remove all the air bubbles. After drying the cast, the PDMS was poured in the mould and let to cross-link at 70 °C overnight. After removing the microsystem from the mould, input and exit holes were drilled and the system was cleaned with Milli-Q water. A microscope glass slide was cleaned using a low air pressure plasma cleaner (Harrick) for 30 minutes. For final plasma bonding of the PDMS onto the glass slide, the PDMS slab and the glass slide were exposed to the low-pressure air plasma for 70 seconds and immediately assembled together.

3.5.4.2 Determination of diffusion coefficient

The microfluidic measurement of diffusion coefficient is based on the microfluidic 'H-filter' [34]. The previously described microfluidic method for measuring diffusion coefficients was modified to include a spectroscopic flow cell (SMA-Z-10

Ultem, FIAlab Instruments, Seattle WA, USA) which was used to measure the optical extinction spectrum using the fiber-coupled spectrometer cited in **Section 3.5.3.1** [35]. The long (1 cm) path length of the flow cells enables precise measurement of OD, even at low concentrations (see **Figure 5.13**).

The overall concentration of the injected nanoparticle solution (OD_{TOT}) was measured by stopping the injection of the pure solvent, causing only the pure nanoparticle solution to exit at both exits and traverse the flow cell. On the other hand, when injecting only pure solvent, the baseline for the extinction measurement was recorded.

The experimental flow rates were chosen such that the measured ξ was in the range 0.1- 0.7. For each sample, several determinations of D were carried out, at various flow rates over several days, giving access to the statistical uncertainty on the diffusion coefficient. The temperature was close to 298K, but fluctuated somewhat (± 2 K) during measurement.

The microsystem used had an interaction channel of height 140 µm, width 200 µm and length 50 mm. The precise microfluidic circuit is shown in **Chapter 5**. Prior to each experiment the system was washed with Milli-Q water (200 µL) at a flow rate of 4 µL/min. Milli-Q water (Entry A) and the sample studied (Entry B) were introduced in the microsystem using two syringes (d= 2.5 mm) mounted on individual syringe pumps. The system was left to stabilise for one hour at the flow rate selected for each experiment (typically between 1 x 2 µl/min and 10 x 2 µl/min).

3.5.5 Sedimentation process using digital photography

Mechanical and thermal perturbations were avoided by carrying out the experiments in a undisturbed laboratory fridge at 277 K. Images were taken using a digitalcamera (Nikon Coolpix P7800, Nikon Corp., Japan) providing the output of unprocessed ('RAW') image data, where the individual pixel values are proportional to the detected light intensity. Typically, four samples were photographed in a single picture. A black area was also included to serve as the source for background subtraction.

The 'RAW' image data were read by ImageJ software. The three colour channels of the images were separated and treated individually as monochrome intensity images. Intensity gradient profiles for all samples in each image of the time series were extracted by horizontal averaging over a rectangular area (typically, the visible optical window of the cells). The pixel values of the black area were averaged for background subtraction. The digital intensity profiles were then further treated numerically usingthe Python programming language with scientific extensions. The final corrected optical density is obtained using a Beer-Lambert-Bouguer formulation.

For the study of the sedimentation of gold nanospheres standard aqueous solutions of colloidal gold from commercial sources (BBI Solutions, UK, and Sigma-Aldrich, France) and samples synthesised and characterised according to literature procedures were used (see **Sections 3.1 to 3.3**). All colloids were stabilised with negatively charged carboxylate ligands. The samples were diluted with pure water where necessary. Typical optical densities at the extinction maximum were

in the range 0.3-1. Under these dilute conditions, the ligands do not influence the sedimentation behaviour of the particles. Also, the only solvent parameters of relevance for sedimentation are the viscosity and the density, and these are very close to those for pure water at low concentrations of stabilising ligand.

3.6 References

1. Zhang, T., et al., *A new strategy improves assembly efficiency of DNA mono-modified gold nanoparticles.* Chemical Communications, 2011. **47**(20): p. 5774-5776.
2. Yeh, Y.C., B. Creran, and V.M. Rotello, *Gold nanoparticles: preparation, properties, and applications in bionanotechnology.* Nanoscale, 2012. **4**(6): p. 1871-1880.
3. Schmid, G. and A. Lehnert, *The Complexation of Gold Colloids.* Angewandte Chemie-International Edition, 1989. **28**(6): p. 780-781.
4. Mirkin, C.A., et al., *A DNA-based method for rationally assembling nanoparticles into macroscopic materials.* Nature, 1996. **382**(6592): p. 607-609.
5. Shipway, A.N., et al., *Investigations into the electrostatically induced aggregation of Au nanoparticles.* Langmuir, 2000. **16**(23): p. 8789-8795.
6. Liu, J.W. and Y. Lu, *Accelerated color change of gold nanoparticles assembled by DNAzymes for simple and fast colorimetric Pb2+ detection.* Journal of the American Chemical Society, 2004. **126**(39): p. 12298-12305.
7. Turkevich, J., P.C. Stevenson, and J. Hillier, *The Formation of Colloidal Gold.* The Journal of Physical Chemistry, 1953. **57**(7): p. 670-673.
8. Frens, G., *Controlled Nucleation for Regulation of Particle-Size in Monodisperse Gold Suspensions.* Nature-Physical Science, 1973. **241**(105): p. 20-22.
9. Turkevich, J., P.C. Stevenson, and J. Hillier, *A study of the nucleation and growth processes in the synthesis of colloidal gold.* Discussions of the Faraday Society, 1951. **11**: p. 55-75.
10. Bastus, N.G., J. Comenge, and V. Puntes, *Kinetically Controlled Seeded Growth Synthesis of Citrate-Stabilized Gold Nanoparticles of up to 200 nm: Size Focusing versus Ostwald Ripening.* Langmuir, 2011. **27**(17): p. 11098-11105.
11. Piella, J., N.G. Bastus, and V. Puntes, *Size-Controlled Synthesis of Sub-10-nanometer Citrate-Stabilized Gold Nanoparticles and Related Optical Properties.* Chemistry of Materials, 2016. **28**(4): p. 1066-1075.
12. Claridge, S.A., et al., *Enzymatic ligation creates discrete multinanoparticle building blocks for self-assembly.* Journal of the American Chemical Society, 2008. **130**(29): p. 9598-9605.

13. Hurst, S.J., A.K.R. Lytton-Jean, and C.A. Mirkin, *Maximizing DNA loading on a range of gold nanoparticle sizes.* Analytical Chemistry, 2006. **78**(24): p. 8313-8318.

14. Shi, D.W., et al., *A facile and efficient method to modify gold nanorods with thiolated DNA at a low pH value.* Chemical Communications, 2013. **49**(25): p. 2533-2535.

15. Zhang, X., M.R. Servos, and J.W. Liu, *Instantaneous and Quantitative Functionalization of Gold Nanoparticles with Thiolated DNA Using a pH-Assisted and Surfactant-Free Route.* Journal of the American Chemical Society, 2012. **134**(17): p. 7266-7269.

16. Reinhard, B.M., et al., *Use of plasmon coupling to reveal the dynamics of DNA bending and cleavage by single EcoRV restriction enzymes.* Proceedings of the National Academy of Sciences of the United States of America, 2007. **104**(8): p. 2667-2672.

17. Claridge, S.A., et al., *Isolation of discrete nanoparticle - DNA conjugates for plasmonic applications.* Nano Letters, 2008. **8**(4): p. 1202-1206.

18. Zanchet, D., et al., *Electrophoretic Isolation of Discrete Au Nanocrystal/DNA Conjugates.* Nano Letters, 2001. **1**(1): p. 32-35.

19. Borovok, N., E. Gillon, and A. Kotlyar, *Synthesis and Assembly of Conjugates Bearing Specific Numbers of DNA Strands per Gold Nanoparticle.* Bioconjugate Chemistry, 2012. **23**(5): p. 916-922.

20. Zipper, H., et al., *Investigations on DNA intercalation and surface binding by SYBR Green I, its structure determination and methodological implications.* Nucleic Acids Research, 2004. **32**(12): p. e103-e103.

21. Heuer-Jungemann, A., et al., *Copper-free click chemistry as an emerging tool for the programmed ligation of DNA-functionalised gold nanoparticles.* Nanoscale, 2013. **5**(16): p. 7209-7212.

22. Harimech, P.K., et al., *Reversible Ligation of Programmed DNA-Gold Nanoparticle Assemblies.* Journal of the American Chemical Society, 2015. **137**(29): p. 9242-9245.

23. Blake, R.D. and S.G. Delcourt, *Thermodynamic effects of formamide on DNA stability.* Nucleic Acids Research, 1996. **24**(11): p. 2095-2103.

24. Fuchs, J., et al., *Effects of formamide on the thermal stability of DNA duplexes on biochips.* Analytical Biochemistry, 2010. **397**(1): p. 132-134.

25. Nikoobakht, B. and M.A. El-Sayed, *Preparation and growth mechanism of gold nanorods (NRs) using seed-mediated growth method.* Chemistry of Materials, 2003. **15**(10): p. 1957-1962.

26. Day, H.A., et al., *Controlling the three-dimensional morphology of nanocrystals.* Crystengcomm, 2010. **12**(12): p. 4312-4316.

27. Patra, H.K., D. GuhaSarkar, and A.K. Dasgupta, *Multimodal electrophoresis of gold nanoparticles: A real time approach.* Analytica Chimica Acta, 2009. **649**(1): p. 128-134.

28. Ma, X., et al., *Gold nanocrystals with DNA-directed morphologies.* Nature Communications, 2016. **7**.

29. Claridge, S.A., et al., *Directed assembly of discrete gold nanoparticle groupings using branched DNA scaffolds.* Chemistry of Materials, 2005. **17**(7): p. 1628-1635.

30. Haiss, W., et al., *Determination of size and concentration of gold nanoparticles from UV-Vis spectra.* Analytical Chemistry, 2007. **79**(11): p. 4215-4221.

31. Springer, T., et al., *Shielding effect of monovalent and divalent cations on solid-phase DNA hybridization: surface plasmon resonance biosensor study.* Nucleic Acids Research, 2010. **38**(20): p. 7343-7351.

32. Navarro, J.R.G. and M.H.V. Werts, *Resonant light scattering spectroscopy of gold, silver and gold-silver alloy nanoparticles and optical detection in microfluidic channels.* Analyst, 2013. **138**(2): p. 583-592.

33. Loumaigne, M., et al., *Optical extinction and scattering cross sections of plasmonic nanoparticle dimers in aqueous suspension.* Nanoscale, 2016. **8**(12): p. 6555-6570.

34. Brody, J.P. and P. Yager, *Diffusion-based extraction in a microfabricated device.* Sensors and Actuators a-Physical, 1997. **58**(1): p. 13-18.

35. Werts, M.H.V., et al., *Quantitative full-colour transmitted light microscopy and dyes for concentration mapping and measurement of diffusion coefficients in microfluidic architectures.* Lab on a Chip, 2012. **12**(4): p. 808-820.

Chapter 4. Synthesis and characterisation of DNA-gold nanoparticle assemblies

The capability of bringing together colloidal metal nanoparticles into programmed 2D or 3D structures has enabled the assembly of novel nanomaterials with unique physical and chemical properties [1]. Great effort has been made to design novel strategies to control the organisation of nanomaterials. The use of DNA as a scaffold to link inorganic nanoparticles into complex assemblies has been investigated widely [2, 3].

In the following chapters DNA-gold nanoparticle assemblies are used as seeds for growing larger particles ('seeded growth' protocols, see **Chapter 6**) and their physicochemical properties are investigated (see **Chapter 5**). For these purposes it is essential for the synthesised assemblies to be pure and stable in aqueous media. Stability and ease-of-purification, can be obtained by functionalising the nanoparticles using stabilising ligands and well-designed oligonucleotides (see **Chapter 2** for background information).

Firstly, this chapter explains the synthesis and characterisation of different sizes of spherical gold nanoparticles (4.5 nm in **Section 4.1.1**, 12.1 nm in **Section 4.1.2** and larger than 30 nm in **section 4.1.3**) using well known published procedures (see **Chapter 2** for background information and **Chapter 3** for experimental procedures). Secondly, the characterisation of the designed oligonucleotides (see **Section 4.2**) and their use in functionalisation of previously synthesised gold nanoparticles is discussed

(see **Section 4.3**). Lastly, the formation of DNA-gold nanoparticles assemblies is shown (see **Section 4.4**).

4.1 Synthesis of spherical gold nanoparticles

Spherical gold nanoparticles of various sizes can be synthesised using wet chemistry. In particular the final particle size can be tuned through the use of weak, mild or strong reducing agents (see **Section 2.2** for background information) [4].

4.1.1 Synthesis of 4.5 ± 0.4 nm gold nanoparticles

Spherical gold nanoparticles of 4.5 ± 0.4 nm were synthesised using a previously published protocol. This protocol used the rapid reduction of gold (Au^{3+}) salts by the strong reducing agent sodium borohydride at low temperature (see **Sections 2.2.1 and 3.1.1** for background information and experimental procedure) [5]. To ensure higher stability of the colloidal particles during the purification process, a ligand exchange between borohydride and BSPP was performed (see background information in **Section 2.4**) [6]. A TEM image, representative of the synthesised particles, is shown in **Figure 4.1A**. Using TEM images of three independent syntheses, a size analysis has been performed on 400 particles and a corresponding histogram was obtained (see **Figure 4.1B).** The average size of the particles was 4.5 ± 0.4 nm.

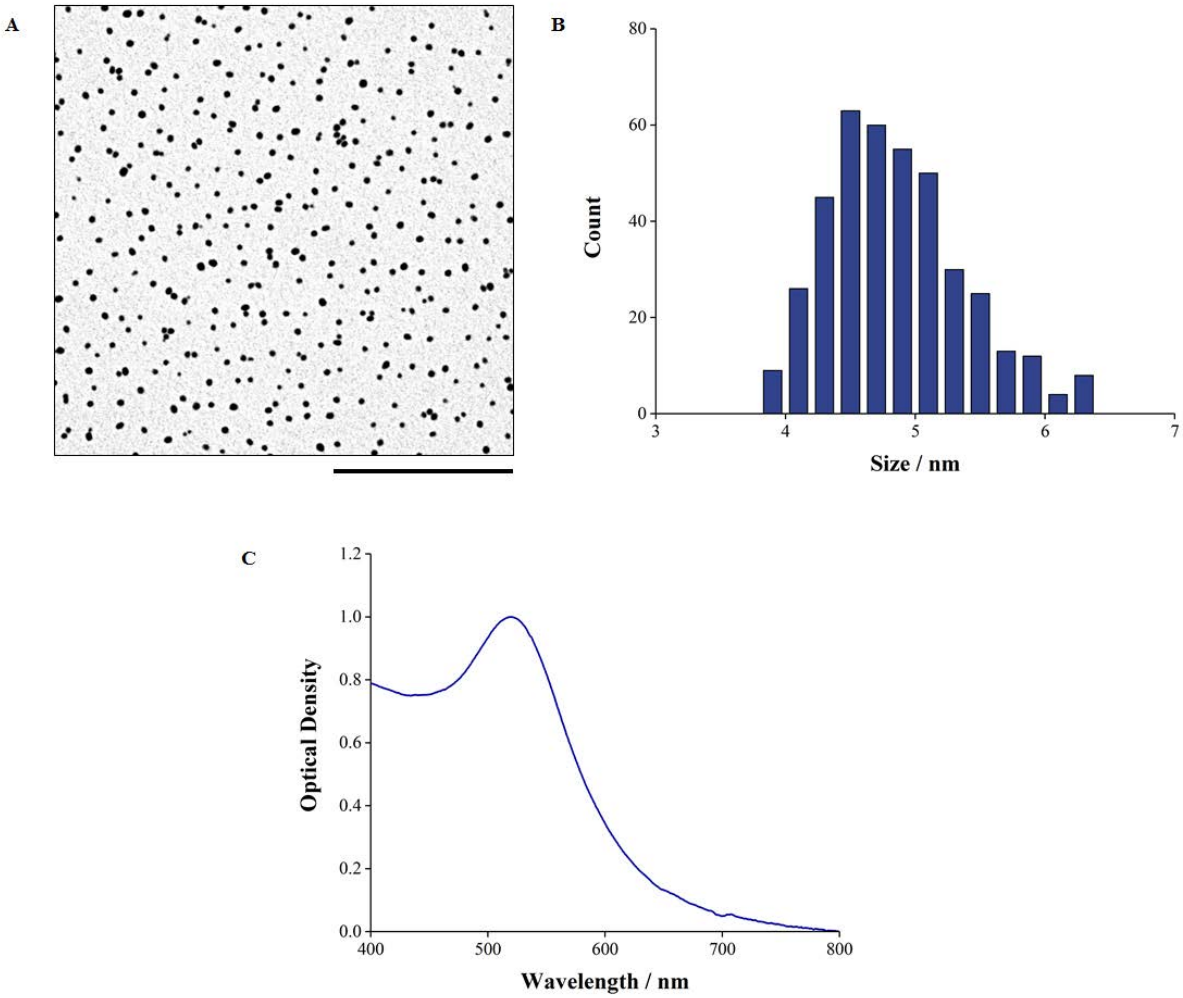

Figure 4.1. Characterisation of 4.5 ± 0.4 nm spherical gold nanoparticles **A)** Transmission electron microscopy image. Scale bar is 200 nm. **B)** Size distribution histogram. **C)** Normalised extinction spectrum

The particular optical properties exhibited by gold nanoparticles (see **Section 2.1.1** for theoretical background) can also be used to characterise them after synthesis. Extinction spectroscopy constitutes an ideal tool to visualise the LSPR peak and judge the stability and the narrowness of the size distribution of the freshly synthesised sample. As shown in **Figure 4.1C,** the extinction spectrum of 4.5 ± 0.4 nm particles displays a relatively narrow LSPR peak with a maximum at 518 nm, characteristic for 5 nm gold nanoparticles with a narrow size distribution [7].

4.1.2 Synthesis of 12.1 ± 0.3 nm gold nanoparticles

Spherical gold nanoparticles of 12.1 ± 0.3 nm were synthesised using the well-established Turkevich method (see **Section 2.2.1** for background information) [8]. In contrast to borohydride, citrate is a mild reducing agent and is used at high temperature (100 ºC). Citrate has a dual role in this specific synthesis as it is also used as a stabilising agent. The colloid stability was further increased by ligand exchange between citrate and BSPP [9]. **Figure 4.2A** shows a representative TEM micrograph of the particles. By analysing 400 particles from three different syntheses, a size distribution histogram was plotted (see **Figure 4.2.B**); the average size of the particles was 12.1 ± 0.3 nm.

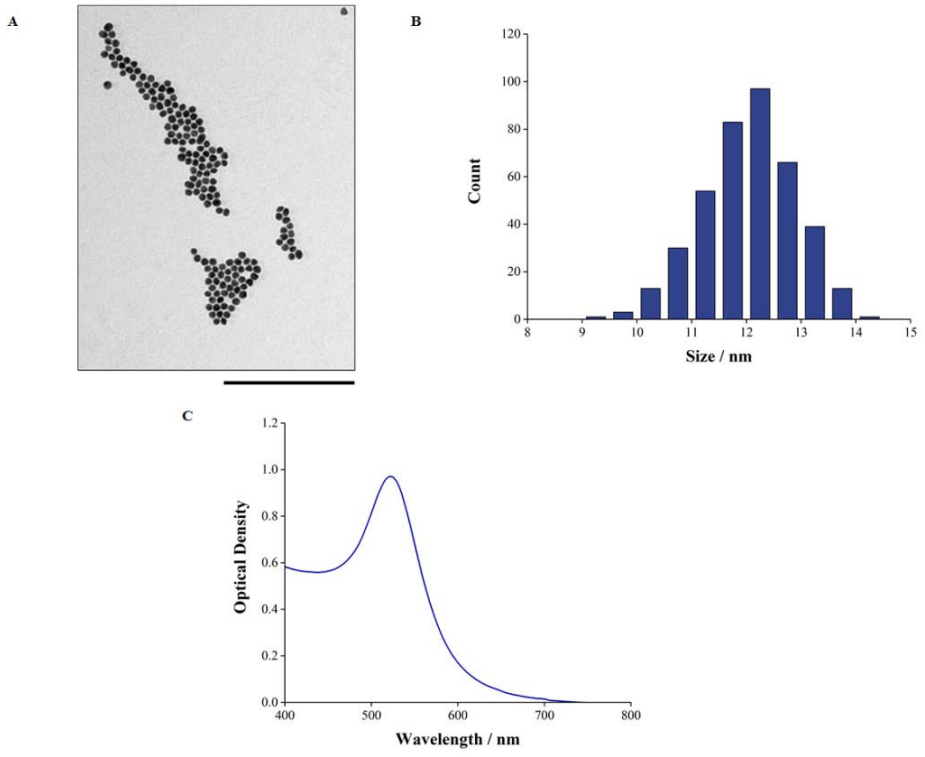

Figure 4.2. Characterisation of 12.1 ± 0.3 nm spherical gold nanoparticles **A)** Transmission electron microscopy image. Scale bar is 200 nm. **B)** Size distribution histogram. **C)** Normalised Extinction spectrum

The extinction spectrum (see **Figure 4.2C**) shows a sharp LSPR peak at 522 nm characteristic of stable 12 nm spherical gold nanoparticles [7].

4.1.3 Synthesis of large gold nanoparticles (> 30 nm)

In order to obtain larger spherical gold nanoparticles with a narrow size distribution, a recently published protocol was used [10]. This synthesis was based on the use of a seeded growth method (see **Section 2.2.1** for background information). In this method the nucleation and growth processes are separated into two steps by using small particles (seeds) as a nucleation point. This technique is employed to obtain a narrower size distribution. In this protocol, each growth step corresponds to a generation of particles. This synthesis gives the possibility to grow citrate stabilised particles up to 178 nm (Generation 14). For the purpose of this work, only generations 0 and 1 (G_0 and G_1) have been produced. Representative TEM images of both generations can be visualised in **Figure 4.3A and C**. 400 and 45 particles for generation 0 and generation 1, were analysed, respectively. This was done for three different experiments and histograms of size distributions were plotted (see **Figure 4.3B and D**). The particles produced from generation 0 were 31.3 ± 0.4 nm and 47.4 ± 0.6 nm from generation 1.

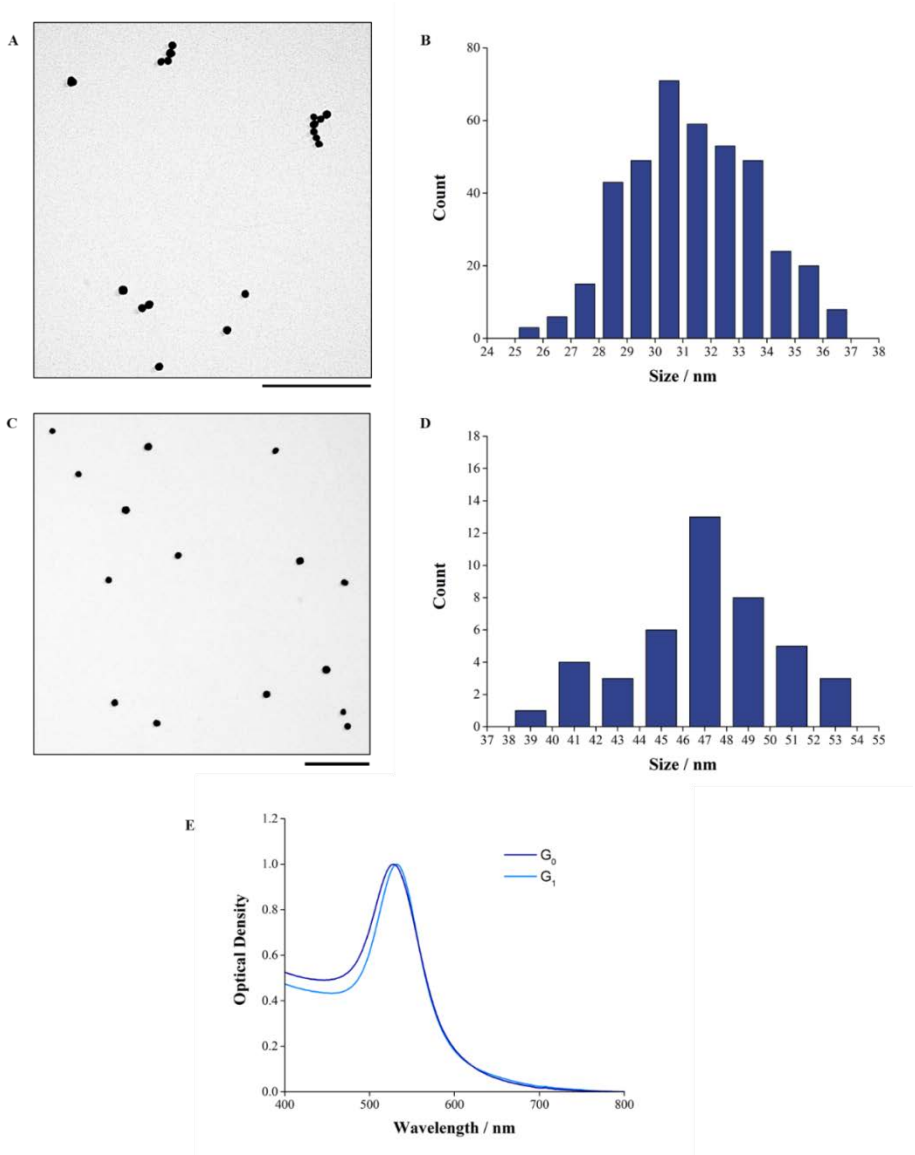

Figure 4.3. Characterisation of G_0 and G_1 spherical gold nanoparticles **A)** Transmission electron microscopy image of G_0 particles. Scale bar is 200 nm. **B)** Size distribution histogram of G_0 NPs. **C)** Transmission electron microscopy image of G_1 particles. Scale bar is 200 nm. D) Size distribution histogram of G_1 NPs. **E)** Normalised extinction spectrum of G_0 and G_1 particles

As particles grow, their optical properties change. As expected, on **Figure 4.3E** the LSPR peak is red shifted between G_0 and G_1 particles with a maximum peak at 528 and 532 nm, respectively. Both peaks are sharp, and do not show any shoulder around 570 nm, characteristic of stable samples [7].

4.2 Oligonucleotides as scaffolds for nanoparticle self-assemblies

In order to create DNA-AuNP assemblies for utilisation, either as seeds in **Chapter 6** or for analysis of their physicochemical properties in **Chapter 5,** specifically designed oligonucleotides were used (see sequences in **Section 3.2.1.1** and strand systems in **Section 2.4**). To increase the stability of assemblies, the oligonucleotides were altered with chemical groups to allow inter strand ligation (see **Section 2.3.2** for background information). To create the desired assemblies, it is essential to ensure that the DNA hybridises and ligates in the specific manner it has been designed for (see **Section 2.4** for background information). Prior to attachment to the spherical gold nanoparticles of various sizes, a complete characterisation of the oligonucleotides for hybridisation and ligation was performed using extinction spectroscopy (see **section 4.2.1**), UV melting analysis (see **Section 4.2.2**) and polyacrylamide gel electrophoresis (see **Section 4.2.3**).

Among the oligonucleotides used in this work, strands 1 to 3 and A to D (see **Section 3.2.1.1** for sequences) were already characterised using UV melting and polyacrylamide gel electrophoresis by previous PhD students (Dr. Amelie Heuer-Jungeman and Dr. Pascal Harimech). Therefore, these DNA strands were used without further characterisation. Their UV melting data were used to determine the melting temperatures of the DNA strands cited above; and were also confirmed using the OligoAnalyser program. Their polyacrylamide gel analysis confirmed hybridisation and ligation of the DNA strands.

4.2.1 Extinction spectroscopy of designed oligonucleotides

Obtaining a high yield of particles functionalised with a single DNA strand is a key step in the formation of DNA-AuNP assemblies. Thus, the ratio between DNA strands and particles has to be accurately controlled during the formation of DNA-AuNP building blocks. Oligonucleotide concentrations can be easily determined using UV-Visible spectroscopy, due to the characteristic absorbance in the ultraviolet region between 250 and 280 nm of the aromatic heterocycle of the purine and pyrimidine bases (see **Section 2.3.1** for background information) [11]. As an example, **Figure 4.4** shows the extinction spectrum of the oligonucleotide S (see **Section 3.2.1.1** for sequence).

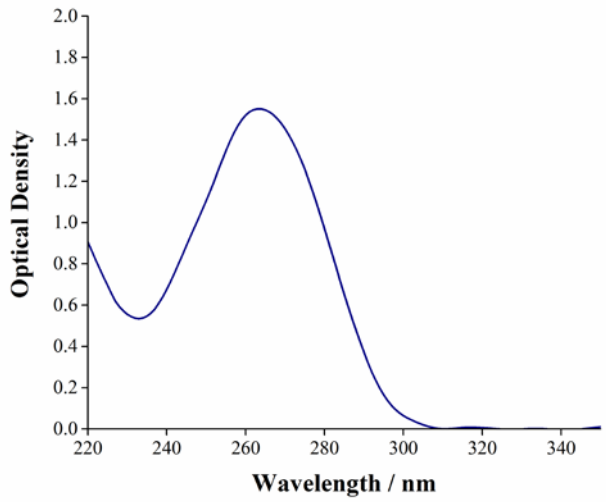

Figure 4.4. Ultraviolet region of the extinction spectrum of the oligonucleotide S

In above example, the spectrum shows a maximal optical density of 1.55 at 263 nm after 100 x dilution of the sample. The extinction coefficient of this specific DNA was calculated using the nearest neighbour method (see **Section 2.3.1** for background information) and found to be 316700 $M^{-1}.cm^{-1}$ [12]. By incorporating these values in the

Beer- Lambert law equation (see **Equation 3.1**), the concentration of the oligonucleotide was determined to be 489 μM. This principle was applied to all DNA strands to determine their precise concentration before using them to functionalise gold nanoparticles.

4.2.2 UV melting curves

The distinctive ultraviolet absorption band of oligonucleotides can also be used to follow the duplex formation of complementary single stranded DNA using UV-Visible spectroscopy. The light absorption of DNA duplexes is lower than single stranded DNA due to π-stacking of bases in the double helix: this phenomenon is called hyperchromicity [13]. By applying a temperature gradient to a DNA solution, DNA duplexes are denatured into single stranded DNA (see **Section 2.3.1** for background information). During UV melting analysis, the optical density of the solution is recorded at 260 nm and gives a distinctive sigmoidal shaped DNA melting curve. Melting temperatures extracted from these curves are important for the formation of DNA-AuNP assemblies (see **Section 2.4** for background information). UV melting experiments were performed on the DNA strands Bcc and Ccc (86 bp), which were designed for use in seeding growth method synthesis and incorporated DIBO and azide modifications (see **Chapter 6**). **Figure 4.5** presents the average melting curve recorded at the DNA maximal absorption (260 nm) over three temperature cycles between 25 and 90 °C (see **Section 3.5.3.2** for experimental details).

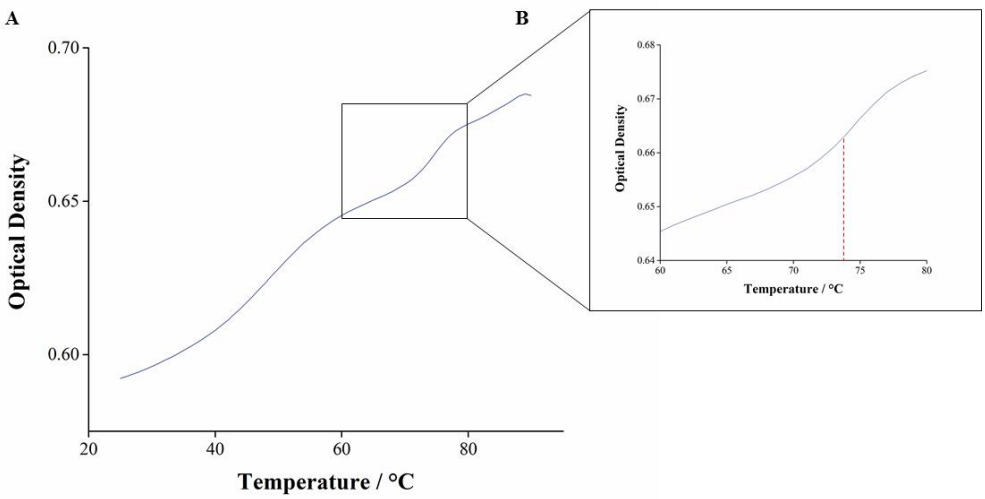

Figure 4.5. Average melting curve recorded at 260 nm over three temperature cycles between 25 and 90 °C for oligonucleotides Bcc and Ccc

As seen on **Figure 4.5B,** which shows a zoom in of the hypochromicity, the melting temperature of strands Bcc and Ccc in the buffer used in the hybridisation experiment was 74 °C. This value is in accordance with the theoretical melting temperature of the 26 bp complementary DNA of 73.2 °C, given by the OligoAnalyser program. As the value was in a reasonable range for hybridisation experiments it was further employed for DNA hybridisation when synthesising DNA-AuNP assemblies (see **Section 4.4**). In addition, an increase of the optical density was observed between 30 and 60 °C. After analysis of both strands using OligoAnalyser, this phenomenon was attributed to the dehybridisation of secondary structures (hairpins), created by small self-complementarities (2 to 6 bp). Due to the length of the strands, these small self-complementarities are hard to avoid when designing long oligonucleotides [14]. Nevertheless, it is important to note that these self-complementarities have low melting temperatures and do not affect the hybridisation between the two complementary strands.

4.2.3 Polyacrylamide gel electrophoresis analysis

After determining the oligonucleotide concentrations and their stability using UV-Visible spectroscopy, their hybridisation and ligation abilities were confirmed using polyacrylamide gel electrophoresis. With this technique, oligonucleotides are separated through a polymer matrix accordingly to their size [13]. In order to confirm the covalent bonding of the DNA strands by click chemistry, denaturing conditions were used by addition of formamide to denature the DNA double helix before running the samples through the polyacrylamide matrix (see **Section 2.3.2** for background information) [15].

Figure 4.6 presents native and denaturing polyacrylamide gels to characterise respectively the hybridisation and the ligation of strands Bcc and Ccc.

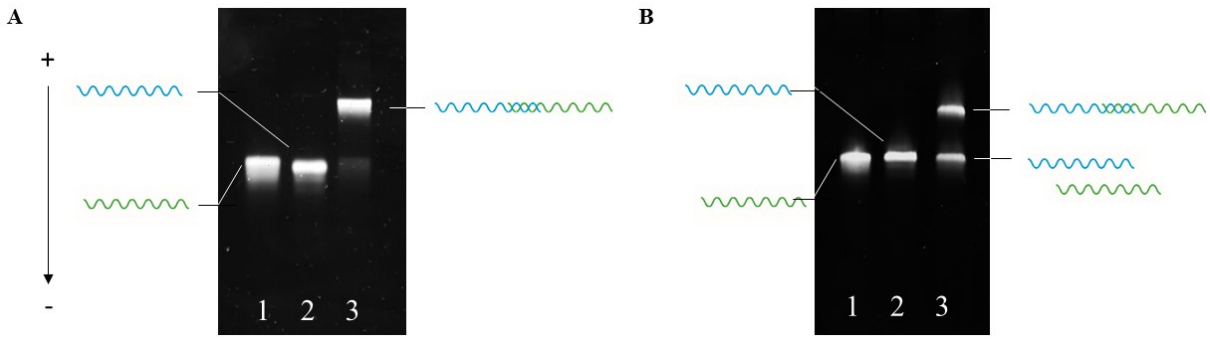

Figure 4.6. A) Native and **B)** Denaturing polyacrylamide gel (8%) for oligonucleotides Bcc and Ccc. In both gel lane 1 is ssDNA Bcc (86 bp), lane 2 is ssDNA Ccc (86 bp) and lane 3 is dsDNA Bcc-Ccc

In each gel, lanes 1 and 2 display a single band, characteristic of pure ssDNA (Bcc for lanes 1 and Ccc for lanes 2). In the native gel (see **Figure 4.6A**), lane 3 shows a bright band of hybridised DNA at the top of the gel, compared with the lower bands

of ssDNA in lanes 1 and 2. A faint band of ssDNA is seen in lane 3 which shows that ssDNA Bcc and Ccc are hybridised with a yield of almost 100 %. The faint band is attributed to a slight difference in concentration of the two ssDNA before their hybridisation.

In the denaturing gel (see **Figure 4.6B**), lane 3 exhibits two distinctive bands. The top band is attributed to clicked dsDNA Bcc-Ccc and the bottom band is attributed to a mix of ssDNA Bcc and Ccc which has dehybridised in the denaturing conditions due to failure of the clicking reaction between some of the DNA strands. The intensity of the two bands was determined using Image J software and showed that a yield of 53 % was achieved using the clicking chemistry of the ssDNA Bcc and Ccc. The first paper published about the use of copper free click chemistry applied to DNA ligation and gold nanoparticles assemblies in our group showed a ligation yield of 92% [16]. The lower yield obtained here can be justified in two ways. Firstly, the position of the clicking groups are different. In this previous work the clicking groups are found at the end of the DNA. Comparatively, the strands in this present study are attached in the middle of the sequences where some steric interactions may play a role and prevent the ligation reaction from happening. Secondly, the DNA used here are more complex as they are longer (86 bp compared to 27 bp) and contain a three thiol anchor at their 5’ end. Thus, it may be possible that during the synthesis process some of the DNA strands were not functionalised with the ligation moieties. Nevertheless, the yield obtained here is still good and DNA-AuNP assemblies formed using these DNA strands were later purified using agarose gel electrophoresis, before being introduced into seeding growth method synthesis (see **Chapter 6**) and characterised using spectroscopy (see **Chapter 5**).

4.3 Functionalisation of gold nanoparticles with designed oligonucleotides

After being characterised, gold nanoparticles and oligonucleotides were mixed together in order to synthesise DNA-AuNP building blocks; these were later employed to form DNA-AuNP assemblies. The attachment of DNA to AuNPs was achieved via the well-established sulfur-gold (S-Au) chemistry. It has been reported that the S-Au bond is almost as strong as an Au-Au bond and thus creates stable DNA-AuNP building blocks [17]. In order to obtain a high yield of the expected self-assemblies, it is crucial to control the number of DNA strands attached to the NP surface. It has been shown that, even if AuNPs and DNA are mixed in a stoichiometric ratio, different conjugate species (mono, di or tri) are formed [18]. Separation of these different species, therefore, is key. Different separation techniques including anion exchange, HPLC, size exclusion chromatography and agarose gel electrophoresis can be used to do this. Of the aforementioned techniques, agarose gel electrophoresis is most commonly employed for purification of DNA-AuNP conjugates [19]. With this technique, molecules are separated according to their size and charge. Pellegrino et al. showed that, in the case of DNA-AuNP conjugates, the determining factor controlling changes in electrophoretic mobility is the size of the conjugates [20]. Thus, it is critical to have a significant size difference between the DNA strand and the AuNP in order to be able to separate mono, di and triconjugates.

Moreover, the addition of a DNA shell on the particle surface can be used to increase stability and has previously allowed the use of particles in different applications [21]. In the case of this thesis it has been used during metallisation experiments to avoid

template DNA sticking onto the particle surface due to repulsion forces (see **Section 2.5** for background details).

The conjugation of small particles with oligonucleotides is presented in **Section 4.3.1** while the DNA conjugation of larger particles is developed in **Section 4.3.2**.

4.3.1 Modification of smaller particles (4.5 ± 0.4 and 12.1 ± 0.3 nm) with oligonucleotides

The modification of small gold nanoparticles with either a specific number or a dense shell of oligonucleotides is achieved using well-established and straightforward protocols (see **Section 3.2.1** for experimental procedure) [22, 23]. In **Section 4.3.1.1,** discrete modifications of 4.5 ± 0.4 and 12.1 ± 0.3 nm gold nanoparticles were undertaken using either short (DNA 1 or 2, see **Section 3.2.1.1** for sequences) or long DNA strands (DNA A to D or DNA Bcc and Ccc). These DNA-coated particles were later used for synthesis of self-assemblies (see **Section 4.4**). **Section 4.3.1.2** shows the functionalisation of 4.5 ± 0.4 and 12.1 ± 0.3 nm gold nanoparticles with a dense shell, produced using DNA strand S (See **Section 3.2.1.1** for sequence). These functionalised particles were later used in DNA metallisation experiments (see **Chapter 6**).

4.3.1.1 Discrete modification with oligonucleotides

Spherical gold nanoparticles of 4.5 ± 0.4 and 12.1 ± 0.3 nm were mixed with an equimolar ratio of thiolated oligonucleotides in order to form DNA-AuNP conjugates

via S-Au bonds (see **Section 3.2.1.1** for experimental details). Depending on the application, particles of 4.5 ± 0.4 and 12.1 ± 0.3 nm were conjugated to short DNA (1 or 2, 27 or 29 bp) or long DNA (A to D or Bcc and Ccc, 86 bp) (see **Section 3.2.1.1** for sequences). **Figure 4.7** shows the typical separation of DNA-AuNP conjugates using agarose gel electrophoresis for 4.5 ± 0.4 (see **Figure 4.7A**) and 12.1 ± 0.3 (see **Figure 4.7B**) AuNPs.

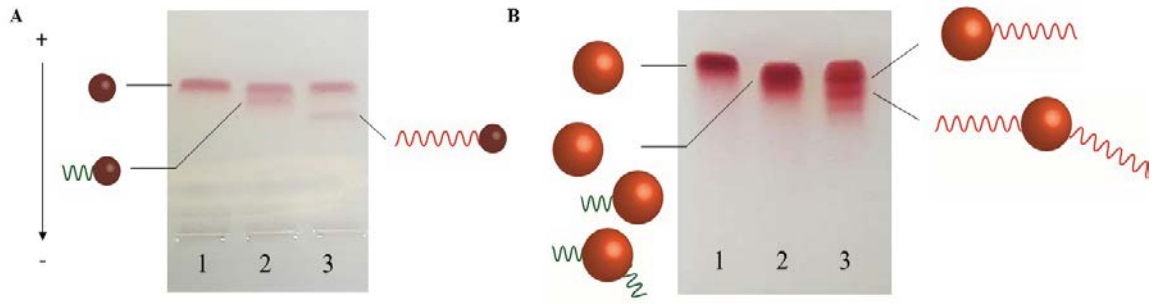

Figure 4.7. Agarose gel purification of DNA-AuNP conjugates for **A)** 4.5 ± 0.4 and **B)** 12.1 ± 0.3 nm. Lanes 1 contain BSPP particles, lanes 2 contain conjugates using short DNA strand 2 and lanes 3 contain conjugates using the long DNA strand A

As observed in the agarose gels, for both sizes of particles, a clearer separation between the conjugates is obtained when the longer DNA strand is employed (lanes 3, 86 bp). As stated previously, the separation of conjugates in an agarose gel is mainly due to the size difference; the size ratio between DNA length and gold core has to be higher than 5 for a good separation to be achieved [24]. Gold nanoparticles of 12.1 ± 0.3 nm modified with the short DNA 2 (29 bp) do not have this characteristic (ratio ≈ 2). That is why no separation could be observed in lane 2 of **Figure 4.7B**. In this case, monoconjugates were not purified using agarose gel electrophoresis but directly used in self-assembly syntheses.

Bands containing spherical gold nanoparticles of 4.5 ± 0.4 and 12.1 ± 0.3 nm, which bear one short or long DNA strand were extracted from the gel and further used for the formation of programmed assemblies (see **section 4.4**). Furthermore, their optical properties were studied in detail using UV-Visible and resonant light scattering spectroscopy (see **Chapter 5**).

4.3.1.2 Dense shell modification with oligonucleotides

DNA-AuNP monoconjugates of small particles (4.5 ± 0.4 and 12.1 ± 0.3 nm) were covered with a shell of short DNA strand S (see **Section 3.2.1.1** for sequence) for further use in DNA metallisation protocols (see **Chapter 6**) [25]. The DNA shell was used to avoid interaction with the longer DNA strand present at the surface of the DNA-AuNP monoconjugates (see **Section 2.5** for background details). In order to verify the attachment of a large amount of DNA onto the gold core, BSPP coated particles were coated with a DNA shell and analysed using agarose gel electrophoresis (see **Figure 4.8A and B**).

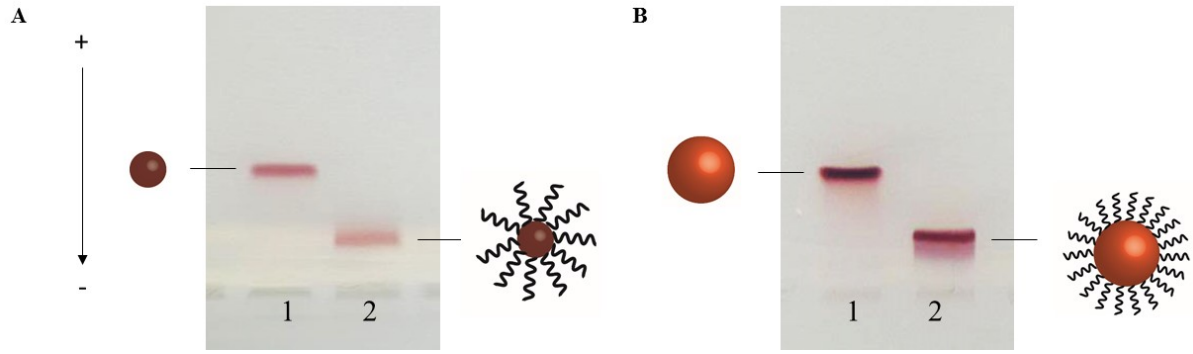

Figure 4.8. Characterisation of 4.5 and 12.1 nm AuNPs bearing a dense DNA shell. Agarose gel of BSPP (lanes 1) and DNA covered (lanes 2) **A)** for 4.5 and **B)** 12.1 nm AuNPs

As stated at the beginning of **Section 4.3**, with DNA-AuNP conjugates, the determining factor for changes in electrophoretic mobility is the size of the conjugates [20]. In both gels (see **Figure 4.8A and B**), particles functionalised by a dense shell of DNA (lanes 2) exhibit a lower electrophoretic mobility than BSPP-coated particles (lanes 1). This difference is due to the increased size caused by the presence of numerous DNA strands at the particles surfaces. This gel, therefore, validates that the DNA successfully attached onto the particles surfaces. In contrast to many applications, such as bio-sensing, it was not necessary to determine the exact DNA loading per nanoparticle [21, 26]. DNA-AuNP monoconjugates from small particles of 4.5 ± 0.4 and 12.1 ± 0.3 nm functionalised with a dense shell of DNA were subsequently used in DNA metallisation protocols (see **Section 6.6**).

4.3.2 Modification of larger particles (>30 nm) with oligonucleotides

Large AuNPs (>30 nm) modified with short oligonucleotides represent the perfect building blocks for assemblies with plasmonic applications due to their higher scattering properties [19]. As discussed in the introduction of **Section 4.3**, the most commonly used approach to separate DNA-AuNP monoconjugates from other conjugates is agarose gel electrophoresis [19]. A current limitation of gel electrophoresis is the inability to separate these large AuNPs with a discrete number of short DNA strands attached [24]. Nevertheless, to overcome this limitation, a new strategy to isolate discrete large DNA-AuNP conjugates was envisaged (see **Section 2.4.2** for background information). Briefly, this method consists of hybridising a long DNA duplex (541 bp) to the DNA strand of large gold nanoparticle conjugates. This temporarily increases the size ratio between DNA length and gold core as the duplex can subsequently be removed due to the presence of a specifically designed “overhang” sequence.

4.3.2.1 Synthesis of long DNA duplex

The experiments presented in this section were carried out in collaboration with Dr. Nittaya Gale working in ATD Bio, Southampton.

Current methods to synthesise artificial oligonucleotides, for example solid-phase synthesis, are only effective to obtain pure DNA strands up to 100 bases [27]. In this section, a method using polymerase chain reaction was developed to produce a long

randomly designed DNA duplex (541 bp) including a specific single-stranded "overhang" (45 bp) (see **Figure 4.9**).

Figure 4.9. Design of the long DNA duplex (541 bp) synthesised by PCR. **A)** 541 bp random DNA duplex **B)** Heg spacer **C)** complementary part to DNA strand onto AuNP surface (DNA A to D) and **D)** random part of the overhang. The parts B, C and D constitutes the 45 bp overhang of the duplex. In this work the overhang correspond to the reverse primer introduce in the PCR

The overhang was designed to partially hybridise with either of the four oligonucleotides designed to form a tetrahedral assembly (see **Section 3.2.1.1** for sequences). Briefly, PCR was undertaken by mixing an equimolar amount of nine oligonucleotides of approximately 100 bp length with Phire enzyme and appropriate forward and reverse primers (see **Section 3.2.2.1** for sequences).

In order to make sure the overhang fixed onto the DNA duplex, two reactions were conducted in parallel. One was carried out with a basic primer without an overhang (18 bases) and the second one with the overhang primer (47 bases). Agarose gel electrophoresis was utilised to analyse the PCR amplicon. **Figure 4.10A** shows a representative picture of a relevant agarose gel.

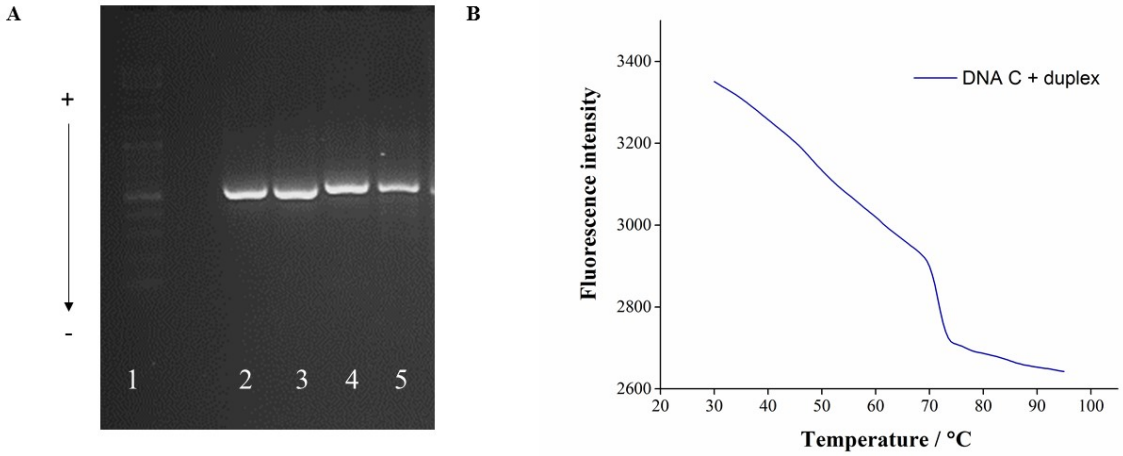

Figure 4.10. **A)** Agarose gel stained with EtBr for analysis of the PCR involving different primers. Lane 1: Ladder, lane 2 and 3: PCR with the basic primer, lane 4 and 5: PCR with the overhang primer. **B)** Melting curve measured for hybridisation of the DNA duplex with its complementary strand C

A ladder (a commercial mixture of DNA fragments of known lengths) was placed in lane 1 and used as a reference. Lanes 2 and 3 show the PCR amplicon produced when using the basic primer. Lanes 4 and 5 show the PCR amplicon obtained when the overhang primer was used. In both cases one single clear band was observed per lane. This is showing that the reaction lead to products with high purity. When comparing with the ladder in lane 1, it can be observed that in both reactions a DNA duplex of more than 500 bp was obtained. A slight difference in electrophoretic mobility between the two different reactions (lanes 2/3 and lanes 4/5) is also noticeable; the duplex containing the overhang primer was slightly delayed. This can be attributed to the additional size caused by the overhang (29 bp). The analysis using agarose gel electrophoresis indicates that the desired DNA duplex, incorporating the 30 base overhang, was successfully synthesised using the ‘one-pot’ PCR.

Fluorescence melting analysis was then used to follow and characterise the hybridisation of the DNA duplex with one of the specific thiolated DNA strands (Strand

C, see **Section 3.2.1.1** for sequences and experimental procedures). For this melting curve, SybrGreen, a fluorescent dye, was introduced along with the two DNA strands. The fluorescence was measured with increasing temperatures. SybrGreen fluorescence is known to be much more intense when intercalated within dsDNA [28], compared to the free dye in solution. When increasing the temperature, the dsDNA dehybridises and thus SybrGreen is released into the solution. Upon release, the fluorescence intensity of SybrGreen decreases. **Figure 4.10B** shows the melting curve measured for hybridisation of the DNA duplex with its complementary strand C. Two characteristic sigmoidal shapes can be observed along the curve. The first shift in fluorescence was seen at 50°C and was attributed to the dehybridisation of C with the overhang of the duplex. The higher and more pronounced shift at 72°C was attributed to the dehybridisation of the duplex. These results were in accordance with theoretical values given by the OligoCalc program. This analysis indicates the successful hybridisation of the thiolated oligonucleotide C to the overhang-containing DNA duplex. The DNA duplex was subsequently bound with AuNPs for DNA-AuNP conjugate separation experiments.

4.3.2.2 Purification of DNA-AuNP monoconjugates

The strategy adopted to functionalise DNA-AuNP conjugates with a long DNA duplex consisted of creating normal conjugates (see **Section 4.3.1.1**) and hybridising the long DNA duplex with the short thiolated DNA strand (DNA A to D, see **Section 3.2.1.1** for sequences).

Initial experiments to determine the effectiveness of this new approach were undertaken using 12.1 ± 0.3 nm AuNPs, due to their ease of synthesis. **Figure 4.11**

shows the agarose gel obtained after 20 minutes of electrophoresis (see **Section 3.2.2.2** for experimental procedures).

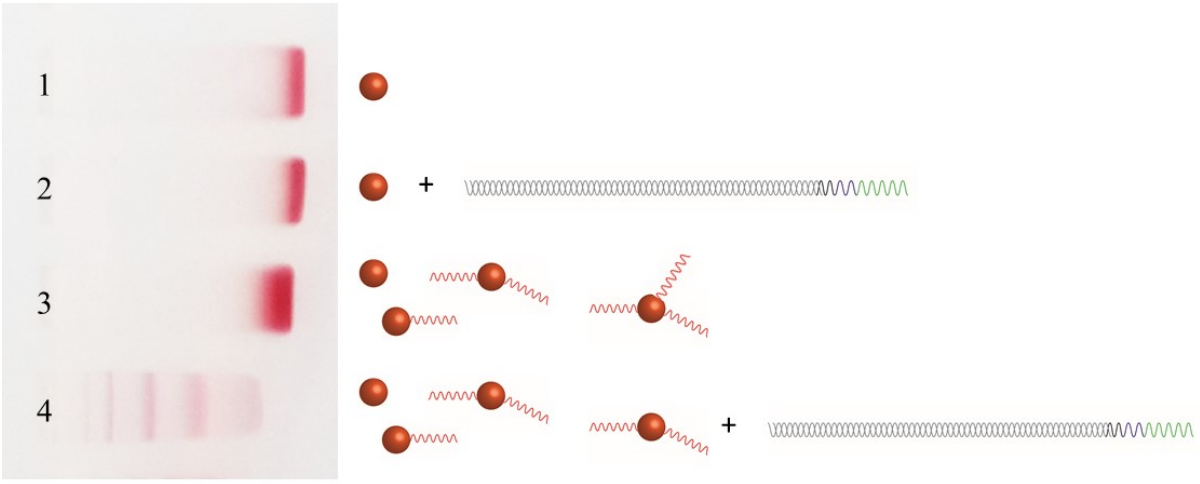

Figure 4.11. Agarose gel showing separation of the 12.1 ± 0.3 nm conjugates using the new DNA strategy. Lane 1: BSPP-coated NPs, lane 2: BSPP-coated NPs incubated with 10x DNA duplex, lane 3: Classic conjugates separation, lane 4: Separation of conjugates using the DNA duplex strategy

In lane 1, BSPP-coated particles were used as a reference. In lane 2, the incubation of the DNA duplex with BSPP coated particles did not influence their mobility. This result was expect as no thiol anchor was incorporated in the DNA and electrostatic repulsion between the negatively surface of the particles and the negative backbone of the DNA duplex should occur. Lane 3 contains the results of a classical conjugates separation. As seen in this figure, the separation of the bands is not efficient, highlighting the requirement of the DNA duplex strategy. Unlike in earlier experiments (see **Figure 4.7B),** in **Figure 4.11**, no bands were seen as the electrophoresis ran for a shorter time (20 instead of 60 minutes). Finally, lane 4 shows the results for the use of the DNA duplex strategy and displays four bands. The band with the highest electrophoretic mobility contained BSPP-coated AuNPs. This band is delayed compared to lane 1 as samples were run in a different buffer. The second band shows

monoconjugates hybridised to the long duplex. The third shows diconjugates hybridised to two duplexes. Finally, the fourth band which had a low electrophoretic mobility shows the presence of triconjugates hybridised with three duplexes. This preliminary experiment proves the success of the new DNA duplex strategy for a quick and effective separation of conjugates using 12.1 ± 0.3 nm particles. It also permits the establishment of the appropriate experimental conditions for an efficient DNA-AuNP conjugates separation, for example the excess of the DNA duplexes needed in order to achieve complete hybridisation of all strands (see **Section 3.2.2.2** for experimental details).

Furthermore, the same experiment was performed with large particles, G_0 (31.3 ± 0.4 nm). **Figure 4.12** shows an agarose gel electrophoresis characterising the formation of large DNA-AuNP monoconjugates.

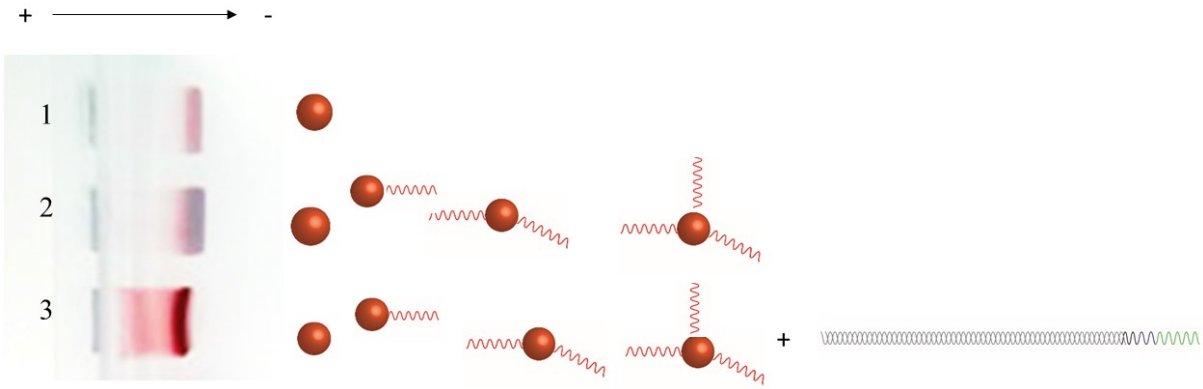

Figure 4.12. Agarose gel showing separation of the 31.3 ± 0.4 nm conjugates using the new DNA strategy. Lane 1: BSPP-coated NPs, lane 2: Classic conjugates separation, lane 3: Separation of conjugates using the DNA duplex strategy

Lane 1 shows G_0 AuNPs coated with BSPP as a reference. Lane 2, shows the result of DNA conjugation to G_0 AuNPs. As expected no band separation was observed. Finally, lane 3 shows the use of the long DNA duplex strategy for separation of DNA-

AuNP conjugates. The band appeared to have run slightly slower than lanes 1 and 2. Unfortunately no band separation was observed. The delay was attributed to a dispersion buffer difference between samples. Separation of larger DNA-AuNP conjugates using the duplex strategy was unsuccessful. Due to the use of larger particles and to ensure their stability, the experiment conditions used in the preliminary results were altered. The salt concentration for the hybridisation step of the long DNA duplex had to be reduce from 80 to 20mM. Higher salt concentration resulted in particles aggregation. These conditions did not permit the attachment of the DNA duplex. In order to tackle the stability problem experiments were carried on using G_0 particles cover with a DNA shell (Strand S, see **Section 3.2.1.1** for sequence). It was then possible to carry out experiments with a salt concentration of 80 mM as for the 12.1 ± 0.3 nm AuNPs. Unfortunately no improvement of the separation of the conjugates was observed. The DNA shell added for particles stabilisation might increase steric hindrance and block the hybridisation of the overhang. The reason of the failure to adapt the duplex strategy to larger particles is still under investigation. Nevertheless, dimers of large particles were synthesised by mixing conjugates without purification (see **Section 4.4.3**.).

4.4 Formation of gold-DNA nanoparticle assemblies

Several research groups have already demonstrated that gold nanoparticle dimers, trimers or even tetrahedron can be assembled *via* DNA hybridisation using DNA-AuNP building blocks [29, 30]. In the next section DNA-AuNP conjugates were employed to synthesise dimers and trimers using different AuNP sizes.

4.4.1 Formation of 4.5 ± 0.4 nm AuNP dimers and trimers

Dimer and trimer assemblies were synthesised using the 4.5 ± 0.4 nm DNA-AuNP monoconjugates purified by agarose gel electrophoresis (see **Section 4.3.1.1** and **Section 3.2.1.1** for experimental procedures). DNA-AuNP self-assemblies were separated from other reaction products using agarose gel electrophoresis, taking advantage of the same separation principle used for DNA-AuNP monoconjugates purification (see **Figure 4.13A**).

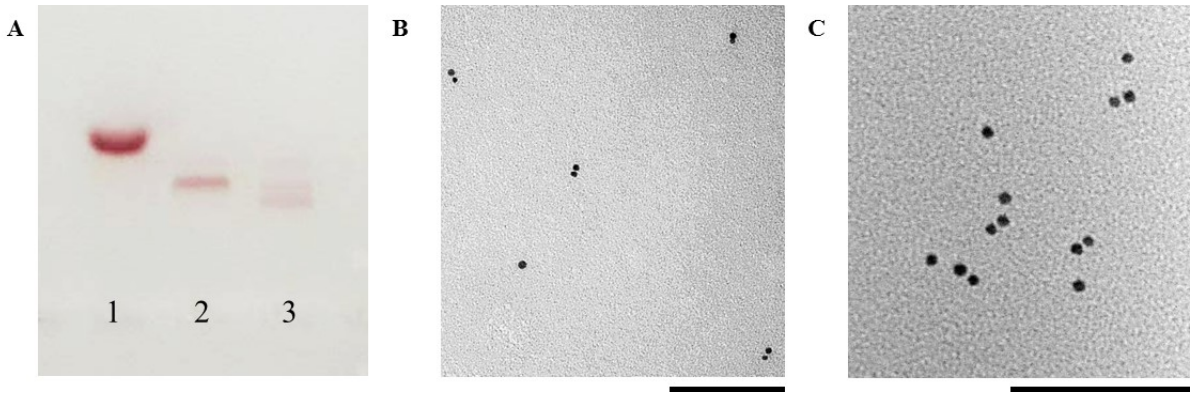

Figure 4.13. Characterisation of 4.5 ± 0.4 nm AuNP dimers and trimers **A)** agarose gel electrophoresis. Lane 1, BSPP coated AuNPs, lane 2, DNA-AuNP dimers and lane 3, DNA –AuNP trimers. TEM pictures of **B)** 4.5 ± 0.4 nm AuNP dimers and **C)** 4.5 ± 0.4 nm AuNP trimers

In the gel, lane 1 displays BSPP-AuNPs as a reference. Dimer and trimer assemblies were run in lanes 2 and 3, respectively. As discussed earlier, for the separation of DNA-AuNP conjugates in agarose gel electrophoresis, the mobility is mainly driven by the size of the assemblies. The results presented in the above gel

confirmed the formation of dimer and trimer structures as the electrophoretic mobility was reduced when the size of the assemblies increased.

After extraction of the assemblies from each band, TEM analysis was employed to visualise the DNA-AuNP dimers and trimers (see **Figure 4.13B and C**). The TEM micrographs display dimers (see **Figure 4.13B**) and trimers (see **Figure 4.13C**). The DNA strand system which forms the dimer assemblies separates the two particles by 87 bases. Since 10 bp is equivalent to 3.4 nm (for dsDNA), AuNP dimers should be theoretically separated by a maximum of ~ 9 nm [31]. However, the TEM image shows dimeric AuNPs in close proximity. This observation is the result of the capillary drying forces and Van der Waals nanoparticle attractions which occur during drying of the TEM grid [32]. Due to low concentration of trimer assembly samples only dimer samples were subsequently studied using optical spectroscopic techniques (see **Chapter 5**).

4.4.2 Formation of 12.1 ± 0.3 nm AuNP dimers and trimers

By hybridising the 12.1 ± 0.3 nm DNA-AuNP monoconjugates purified by agarose gel electrophoresis (see **Section 4.3.1.1**), dimers and trimers were successfully synthesised (see **Section 3.3**. for experimental procedures). These were separated from other reaction products by agarose gel electrophoresis using the same separation principle used for DNA-AuNP monoconjugates (see **Figure 4.14A**).

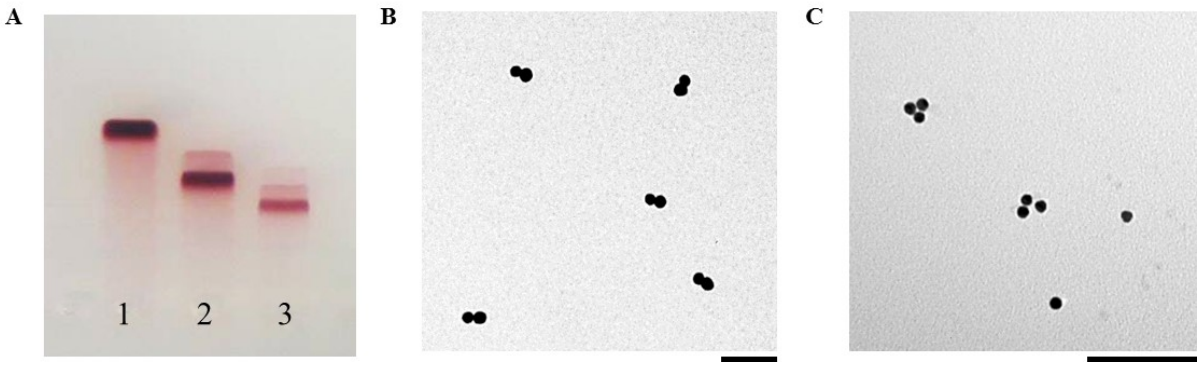

Figure 4.14. Characterisation of 12.1 ± 0.3 nm AuNP dimers and trimers **A)** agarose gel electrophoresis. Lane 1, BSPP coated AuNPs, lane 2, DNA-AuNP dimers and lane 3, DNA –AuNP trimers. TEM pictures of **B)** 12.1 ± 0.3 nm AuNP dimers and **C)** 12.1 ± 0.3 nm AuNP trimers

In lane 1 of the gel, BSPP-coated AuNPs were run as a reference. Products of the dimers reaction were run in lane 2 and trimers reaction in lane 3. Lane 1 displays a single clear band, characteristic of monodispersed BSPP-coated gold nanoparticles. In lane 2, the faint higher gel mobility band corresponds to unreacted DNA-AuNP monoconjugates. The second dense band corresponds to the dimer products. In lane 3, the higher faint band is attributed to dimer products and the second clearer one to trimer products. Similarly to dimer and trimer structures formed using 4.5 ± 0.4 nm particles, the formation of 12.1 ± 0.3 nm dimers and trimers was confirmed by a decrease in electrophoretic mobility.

DNA-AuNP dimers and trimers were subsequently characterised using TEM (see **Figure 4.14B and C**). The TEM micrographs display dimers (see **Figure 4.14B**) and trimers (see **Figure 4.14C**). As stated in the previous paragraph, the observed interparticle distances most likely do not reflect the interparticle distance in solution. Only dimer assemblies properties were then analysed using optical spectroscopy (see **Chapter 5**).

4.4.3 Formation of >30nm AuNP dimers

DNA-AuNPs monoconjugates of 31.3 ± 0.4 nm could not be obtained using the newly developed DNA duplex strategy (see **Section 4.3.2**). Unpurified conjugates were hybridised to successfully synthesised dimers (see **Section 3.3**. for experimental procedures). Dimer assemblies were purified using agarose gel electrophoresis (see **Figure 4.15A**).

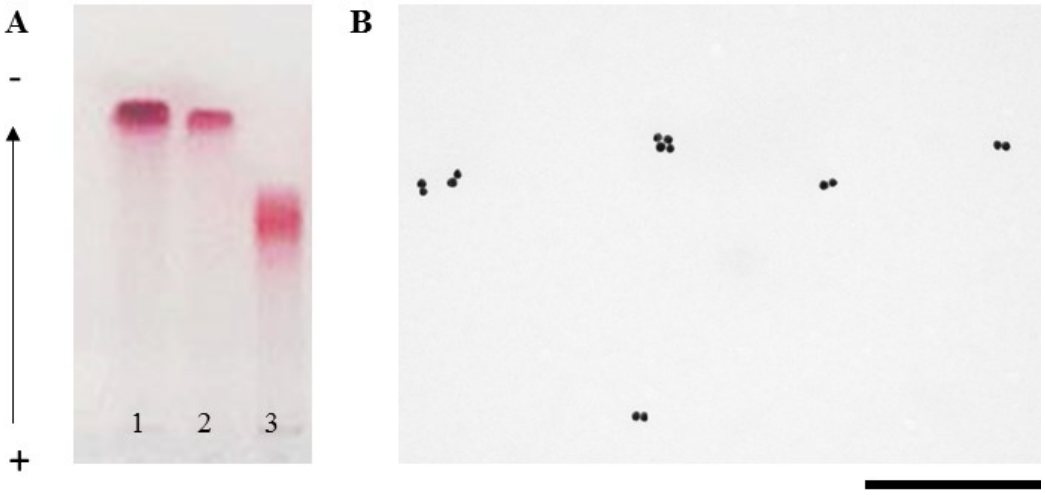

Figure 4.15. Characterisation of 31.3 ± 0.4 nm AuNP dimers **A)** by agarose gel electrophoresis and **B)** TEM pictures. Scale bar is 500 nm

BSPP-coated G_0 AuNPs and unpurified DNA-AuNP conjugates were run as references in lanes 1 and 2 of the gel. The dimer assemblies were run in lane 3. Compared to the references the band in lane 3 displayed a reduced electrophoretic mobility. This is a proof of the successful synthesis of 31.3 ± 0.4 nm DNA-AuNP dimers. The assemblies were then characterised using TEM (see **Figure 4.15B**). The

TEM images showed the presence of dimer assemblies. As stated previously the interparticle distance on the grid is not reflecting the reality in solution. Spectroscopy was used to characterise further the samples (see **Chapter 5**).

In this chapter, AuNPs from 5 to 50 nm with narrow size distribution were synthesised via different chemical syntheses and characterised using TEM and UV-Vis spectroscopy. Synthetic designed DNA used as scaffolds for DNA-AuNP assemblies were characterised with spectroscopy and gel electrophoresis. Smaller particles (< 30 nm) were functionalised with a discrete number or a dense shell of DNA. A new approach to functionalised larger particles with a discrete number of DNA was investigated but unfortunately did not permit to obtain satisfying results. Finally DNA-AuNP dimers of different sizes were synthesised *via* DNA hybridisation and are further studied in **Chapter 5**.

4.5 References

1. Wang, L., et al., *Dynamic Nanoparticle Assemblies.* Accounts of Chemical Research, 2012. **45**(11): p. 1916-1926.
2. Samanta, A. and I.L. Medintz, *Nanoparticles and DNA - a powerful and growing functional combination in bionanotechnology.* Nanoscale, 2016. **8**(17): p. 9037-9095.
3. Rogers, W.B., W.M. Shih, and V.N. Manoharan, *Using DNA to program the self-assembly of colloidal nanoparticles and microparticles.* Nature Reviews Materials, 2016. **1**(3).
4. Perrault, S.D. and W.C.W. Chan, *Synthesis and Surface Modification of Highly Monodispersed, Spherical Gold Nanoparticles of 50-200 nm.* Journal of the American Chemical Society, 2009. **131**(47): p. 17042-+.
5. Zhang, T., et al., *A new strategy improves assembly efficiency of DNA mono-modified gold nanoparticles.* Chemical Communications, 2011. **47**(20): p. 5774-5776.
6. Sharma, J., et al., *Toward reliable gold nanoparticle patterning on self-assembled DNA nanoscaffold.* Journal of the American Chemical Society, 2008. **130**(25): p. 7820-+.
7. Haiss, W., et al., *Determination of size and concentration of gold nanoparticles from UV-Vis spectra.* Analytical Chemistry, 2007. **79**(11): p. 4215-4221.
8. Turkevich, J., P.C. Stevenson, and J. Hillier, *The Formation of Colloidal Gold.* The Journal of Physical Chemistry, 1953. **57**(7): p. 670-673.
9. Schmid, G. and A. Lehnert, *The Complexation of Gold Colloids.* Angewandte Chemie-International Edition, 1989. **28**(6): p. 780-781.
10. Bastus, N.G., J. Comenge, and V. Puntes, *Kinetically Controlled Seeded Growth Synthesis of Citrate-Stabilized Gold Nanoparticles of up to 200 nm: Size Focusing versus Ostwald Ripening.* Langmuir, 2011. **27**(17): p. 11098-11105.
11. Clark, L.B. and I. Tinoco, *Correlations in the Ultraviolet Spectra of the Purine and Pyrimidine Bases1*. Journal of the American Chemical Society, 1965. **87**(1): p. 11-15.
12. Tataurov, A.V., Y. You, and R. Owczarzy, *Predicting ultraviolet spectrum of single stranded and double stranded deoxyribonucleic acids.* Biophysical Chemistry, 2008. **133**(1-3): p. 66-70.
13. Blackburn, G.M. and R.S.o. Chemistry, *Nucleic Acids in Chemistry and Biology*. 2006: RSC Pub.

14. Schreck, J.S., et al., *DNA hairpins destabilize duplexes primarily by promoting melting rather than by inhibiting hybridization.* Nucleic Acids Research, 2015. **43**(13): p. 6181-6190.

15. Blake, R.D. and S.G. Delcourt, *Thermodynamic effects of formamide on DNA stability.* Nucleic Acids Research, 1996. **24**(11): p. 2095-2103.

16. Heuer-Jungemann, A., et al., *Copper-free click chemistry as an emerging tool for the programmed ligation of DNA-functionalised gold nanoparticles.* Nanoscale, 2013. **5**(16): p. 7209-7212.

17. Hakkinen, H., *The gold-sulfur interface at the nanoscale*. Nature Chemistry, 2012. **4**(6): p. 443-455.

18. Zanchet, D., et al., *Electrophoretic Isolation of Discrete Au Nanocrystal/DNA Conjugates.* Nano Letters, 2001. **1**(1): p. 32-35.

19. Claridge, S.A., et al., *Isolation of discrete nanoparticle - DNA conjugates for plasmonic applications.* Nano Letters, 2008. **8**(4): p. 1202-1206.

20. Pellegrino, T., et al., *Gel electrophoresis of gold-DNA nanoconjugates.* Journal of Biomedicine and Biotechnology, 2007.

21. Hurst, S.J., A.K.R. Lytton-Jean, and C.A. Mirkin, *Maximizing DNA loading on a range of gold nanoparticle sizes.* Analytical Chemistry, 2006. **78**(24): p. 8313-8318.

22. Claridge, S.A., et al., *Enzymatic ligation creates discrete multinanoparticle building blocks for self-assembly.* Journal of the American Chemical Society, 2008. **130**(29): p. 9598-9605.

23. Zhang, X., M.R. Servos, and J.W. Liu, *Instantaneous and Quantitative Functionalization of Gold Nanoparticles with Thiolated DNA Using a pH-Assisted and Surfactant-Free Route*. Journal of the American Chemical Society, 2012. **134**(17): p. 7266-7269.

24. Busson, M.P., et al., *Optical and Topological Characterization of Gold Nanoparticle Dimers Linked by a Single DNA Double Strand.* Nano Letters, 2011. **11**(11): p. 5060-5065.

25. Ma, X., et al., *Gold nanocrystals with DNA-directed morphologies.* Nature Communications, 2016. **7**.

26. Giljohann, D.A., et al., *Oligonucleotide Loading Determines Cellular Uptake of DNA-Modified Gold Nanoparticles.* Nano Letters, 2007. **7**(12): p. 3818-3821.

27. Qiu, J.Q., A.H. El-Sagheer, and T. Brown, *Solid phase click ligation for the synthesis of very long oligonucleotides.* Chemical Communications, 2013. **49**(62): p. 6959-6961.

28. Zipper, H., et al., *Investigations on DNA intercalation and surface binding by SYBR Green I, its structure determination and methodological implications.* Nucleic Acids Research, 2004. **32**(12): p. e103-e103.

29. Harimech, P.K., et al., *Reversible Ligation of Programmed DNA-Gold Nanoparticle Assemblies.* Journal of the American Chemical Society, 2015. **137**(29): p. 9242-9245.

30. Mastroianni, A.J., S.A. Claridge, and A.P. Alivisatos, *Pyramidal and Chiral Groupings of Gold Nanocrystals Assembled Using DNA Scaffolds.* Journal of the American Chemical Society, 2009. **131**(24): p. 8455-8459.

31. Thundat, T., D.P. Allison, and R.J. Warmack, *Stretched DNA structures observed with atomic force microscopy.* Nucleic Acids Research, 1994. **22**(20): p. 4224-4228.

32. Barrow, S.J., et al., *Surface Plasmon Resonances in Strongly Coupled Gold Nanosphere Chains from Monomer to Hexamer.* Nano Letters, 2011. **11**(10): p. 4180-4187.

Chapter 5. Study of optical and diffusion properties of DNA-AuNP assemblies

Plasmonic gold nanoparticles exhibit specific optical and hydrodynamic properties depending on their size, shape and arrangement [1]. Thus, their assemblies could be described as 'plasmonic molecules' with adjustable responses correlated to their unique structures [2, 3].

DNA-AuNP assemblies have been extensively studied as sensors or plasmonic rulers using absorbance or scattering spectroscopy [4, 5]. However, a key disadvantage of these spectroscopic methods is that they cannot effectively detect the interactions between the nanoparticles, when either the interparticle distance is too large or when the particles are too small in size. On the other hand, sedimentation and diffusion are important aspects of the behaviour of colloidal nanoparticles in solution and merit attention during the synthesis, characterisation and application of nanoparticles and their assemblies. To be able to manipulate AuNPs and their DNA linked assemblies it is important to study and understand their physicochemical properties in detail.

Firstly, this chapter investigates the optical properties of different sizes of particles using UV-Vis, RLS and photon time-of-flight spectroscopies (PTOFS) (see **Section 5.1**). Secondly, using microfluidics, the diffusion properties of 12.1 nm AuNPs and their assemblies were studied (see **Section 5.2**). Finally, the sedimentation process of different gold nanoparticle samples was followed and analysed using digital photography (see **Section 5.3**).

5.1 Investigation of AuNP and DNA-AuNPs optical properties

Part of the work presented in this section was published in: Johanna Midelet, Anne Débarre, Afaf H. El-Sagheer, Tom Brown, Antonios G. Kanaras, Martinus H.V. Werts. "Spectroscopic and hydrodynamic characterisation of DNA-linked gold nanoparticle dimers in solution using two-photon photoluminescence".*ChemPhysChem*. 2018, 19, 1-11.

As gold nanoparticles are plasmonic particles their absorption and scattering properties are particularly efficient [6]. As stated previously these properties are also tuneable by changing particles size, shape and arrangement. Therefore it is important to be able to monitor these variations. UV-visible spectroscopy is widely used to estimate size and to determine the concentration of free non-interacting spherical AuNPs (see **Sections 3.5.3 and 5.1.1**) [7]. Large spherical (> 30 nm) and non-spherical particles (including assemblies) exhibit strong scattering properties [8]. Therefore the use of resonant light scattering spectroscopy as a complement, permits further characterisation of these kind of particles (see **Section 5.1.2**). Furthermore, the optical and hydrodynamic behavior of nanoparticles and their assemblies could be monitored, with single particle sensitivity, using two-photon photoluminescence fluctuation correlation spectroscopy (TPPL-FCS) (see **Section 5.1.3**).

5.1.1 UV-Visible spectroscopy

5.1.1.1 Small single and DNA assembled 4.5 and 12.1 nm gold nanoparticles

Extinction spectra of the spherical BSPP-AuNPs of 4.5 ± 0.4 nm diameter and of the corresponding AuNP-DNA monoconjugates as well as the dimers form were recorded (see **Figure 5.1**).

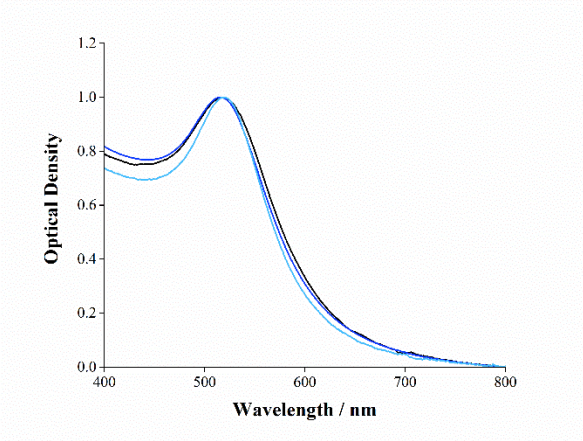

Figure 5.1. Normalised extinction spectra of the 4.5 nm BSPP-AuNPs (Black line), DNA-AuNP monoconjugates (Dark blue line) and DNA-AuNP dimers (Light blue line)

The shape and λ_{max} (516 nm) of the spectra did not change when the DNA was added to the surface of the AuNPs (black and dark blue lines). A small redshift of 3 nm of the λ_{max} was observed for the DNA-AuNP dimers. This result was expected as the particles were very small and the distance between them was large. Thus, they would be seen as individual particles by the spectrometer. As the variation is quite small and the overall shape of the spectrum stayed the same, it did not definitely confirm the presence

of dimers in solution. Scattering spectroscopy was further employed to see if the sensitivity could be improved to differentiate dimers from single particles (see **Section 5.1.2**).

Then experiments were carried out on various well-characterised 12.1 ± 0.3 nm AuNP-DNA monoconjugates and their corresponding linked AuNP dimers, previously synthesised in **Chapter 4**. Two types of dimers were analysed, the 'short-link' dimer AD and 'long-link' dimer BC with 26 and 146 bp interparticle distances, respectively (see **Figure 5.2**).

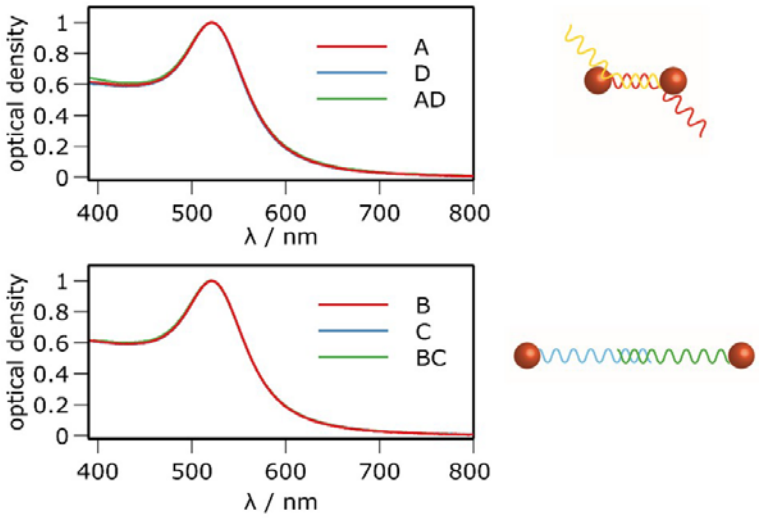

Figure 5.2. Normalised extinction spectra of 12.1 ± 0.3 nm ssDNA-gold nanoparticle monoconjugates and their resulting DNA-linked dimers in aqueous solution, A) short-link dimer AD; B) long-link dimer BC

The linear optical extinction spectra of the 12.1 ± 0.3 nm ssDNA-AuNP monoconjugates and the DNA-linked AuNP dimers were similar in shape, displaying the well-known plasmonic resonance near 520 nm for 12 nm AuNP. The short-link dimer AD and long-link dimer BC did not show any significant alteration of the plasmon resonance band compared with the monomers. This was illustrated by the position of the extinction maximum, which was consistently found at 521 nm.

From the similarity of the extinction spectra between monomers and dimers, it was inferred that there were no significant plasmonic interactions between the constituent gold nanospheres in the dimer. The absence of significant plasmonic interaction indicated that the interparticle distance in both types of dimers (AD and BC) was too large for such an interaction to occur. It has been demonstrated that such a plasmonic interaction critically depends on the interparticle gap and also on the nanoparticle diameters. Jain et al. found that the fractional wavelength shift $\Delta\lambda/\lambda_0$ of the plasmon band in homodimers depends on the particle diameter d and the surface-to-surface gap s (see **Equation 5.1**) [9].

$$\frac{\Delta\lambda}{\lambda_0} \approx 0.18 \exp\left(\frac{-(\frac{s}{d})}{0.23}\right)$$

Equation 5.1. Fractional wavelength shift $\Delta\lambda/\lambda_0$ of the plasmon band in homodimers with d, particle diameter and s, surface-to-surface gap

In this study 12 nm diameter gold nanospheres were used. Using the above formula, it was estimated that interparticle gaps beyond 6 nm lead to undetectable plasmonic interactions. This calculation confirmed the observations made as the interparticle distance in dimers AD and BC were around 9 and 50 nm respectively.

5.1.1.2 Large <30 nm single and DNA assembled gold nanoparticles

The optical extinction spectra of larger than 30 nm particles G_0 (31.3 ± 0.4 nm) and G_1 (47.4 ± 0.6 nm) were recorded. All spectra were normalised to OD 1 for

comparison between G_0 BSPP coated, DNA monoconjugates and DNA shell or G1 BSPP coated, DNA monoconjugates, DNA shell and DNA dimers (see **Figure 5.3**).

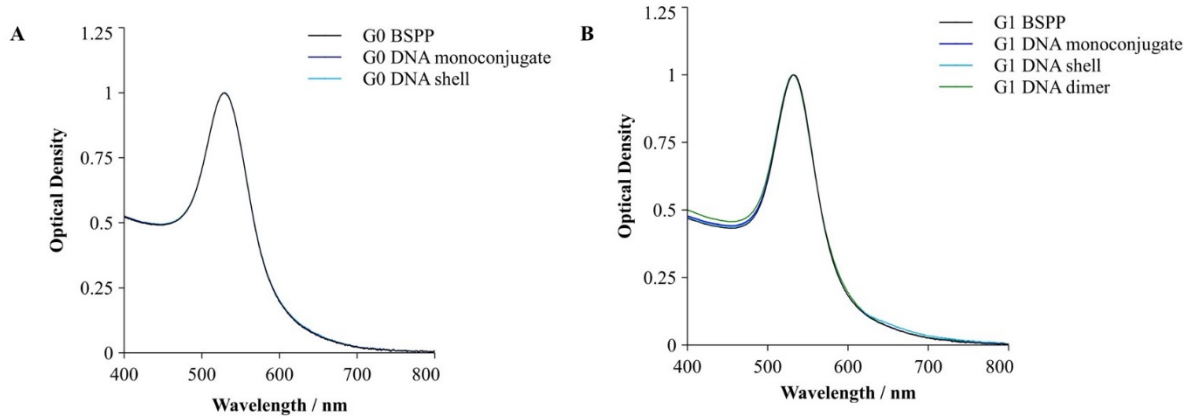

Figure 5.3. Normalised extinction spectra of **A)** G_0 AuNPs and DNA-AuNPs and **B)** G_1 AuNPs, DNA AuNPs and DNA-AuNP dimers

For the G_0 (31.3 ± 0.4 nm) particles, attachment of a discrete number or a dense shell of ssDNA had no impact on the optical extinction response. The λ_{max} were found consistently at 529 nm and the overall shape was not altered. Results were similar for the optical extinction response of the G_1 (47.4 ± 0.6 nm) particles, except that the λ_{max} were found consistently at 533 nm. The same samples were analysed using RLS spectroscopy in order to see if the sensitivity of this method was better (see **Section 5.1.2**).

5.1.2 RLS spectroscopy

In addition to light extinction, AuNPs and DNA-AuNP assemblies display light scattering properties, depending on their shape, size, and core material. Light scattering

provides further information on the plasmonic properties of the objects. As described previously in the literature, a corrected light scattering spectrum of a nanoparticle solution can be obtained in a conventional right-angle fluorimeter configuration using white light as the illumination source (see **Section 2.1** for background information) [10].

5.1.2.1 Small 4.5 and 12.1 nm single and DNA assembled gold nanoparticles

The exercise of measuring the light scattering from small 4.5 nm AuNP suspensions was interesting as it gave a clear idea of the lower limits of RLS spectroscopy. Therefore, scattering spectra of 4.5 nm AuNPs were recorded (see **Figure 5.4**).

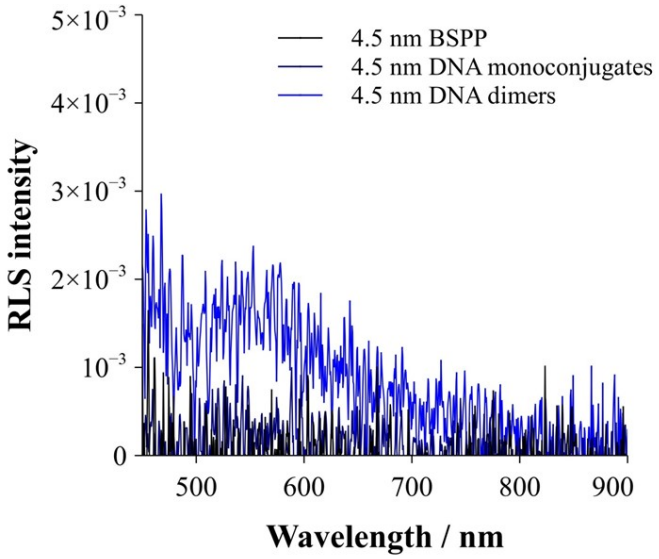

Figure 5.4. Normalised RLS spectrum of the 4.5 nm AuNPs and DNA-AuNP samples

The extremely weak scattering spectra of 4.5 ± 0.4 nm AuNPs do not show the clear plasmon-related scattering resonance. For the dimers sample there seems to be a signature near 500-600 nm. However, this may be due to extremely small quantities of aggregates. As expected, the light scattering spectra from 4.5 ± 0.4 nm AuNPs and their assemblies were too weak and too unstructured to draw any solid conclusions: thus 4.5 ± 0.4 nm AuNPs were too small to yield a useful light scattering signature.

The QENLS spectra of the purified 12.1 ± 0.3 nm ssDNA-AuNP monoconjugates and DNA-linked dimers in pure water were recorded (see **Figure 5.5**).

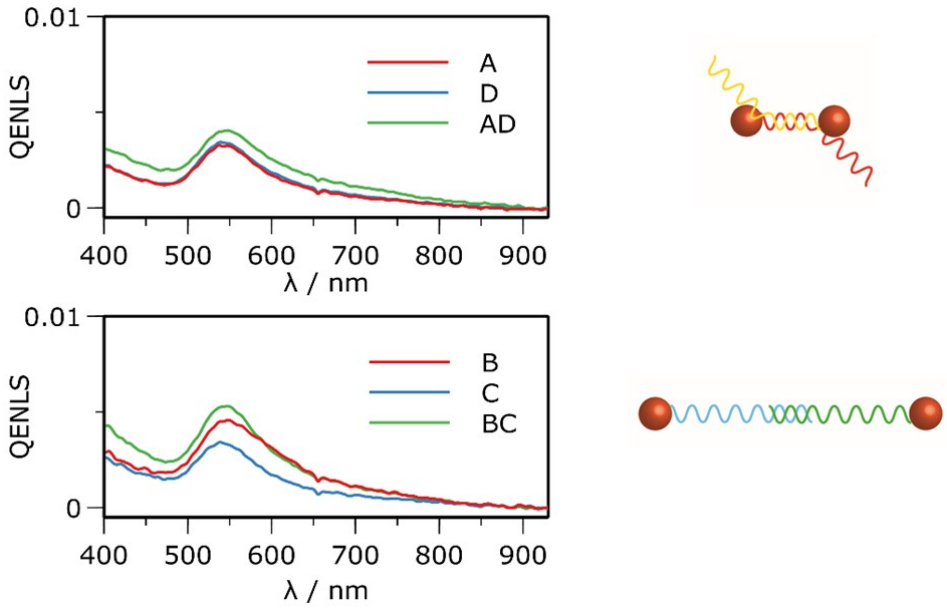

Figure 5.5. Quantum-efficiency normalised light scattering spectra of ssDNA-AuNP monoconjugates and their corresponding DNA-linked dimers in aqueous solution. **A)** AD dimer; **B)** BC dimer

The scattering efficiency of all samples were low, below 1%, as expected for 'plasmonically small' gold nanoparticles [10]. While the scattering by the nanoparticles

was weak, it could still be discerned from the light scattering spectrum by the plasmon-resonant band near 540 nm. These spectra were obtained from diluted solutions in cuvettes using a bright white light source and were not spectra from single-particles. The measurement of this weak scattering is relatively sensitive to even minor quantities of scattering impurities and tiny air bubbles. Care was thus taken to avoid these, by careful filtration and also by letting the samples rest and equilibrate before measurement.

The experimental scattering efficiencies at the scattering maximum were between 3 and 5 x 10^{-3}. A simple, idealised calculation using Mie theory on isolated 12 nm diameter perfect gold nanospheres in water (refractive index of 1.3) (see **Figure 5.6**) yielded 2 x 10^{-3}; this was close to the experimental values. The experimental values were marginally higher than the theoretical values, due to the particle size distribution. Deviations from spherical shape and local refractive index effects were due to the ligand shell. These were not taken into account in the simple theoretical model. This comparison further confirmed the relevance of the QENLS spectrum for the characterisation of plasmonic nanostructures in solution.

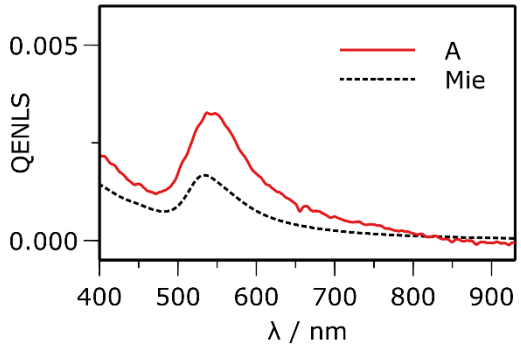

Figure 5.6. QENLS spectrum calculated using Mie theory and idealised 12 nm gold nanospheres in pure water (dotted line), comparison with experimental QENLS spectrum for monomeric "A" DNA-modified AuNPs (solid red line)

There was very little difference in the light scattering by the DNA-linked AuNP dimers compared with the ssDNA-AuNPs monoconjugates (see **Figure 5.5**). Similarly to the extinction spectra, the scattering spectra did not show any distinct features, indicating strong plasmonic interaction between the nanoparticles in these dimer structures. The DNA linkers created had interparticle distances which were too large for such plasmonic interactions to occur. As discussed above, plasmonic interactions critically depend on the interparticle distance and the plasmonic properties of the particles.

5.1.2.2 Large >30 nm single and DNA assembled gold nanoparticles

Finally, scattering measurements were performed on larger particles (>30 nm). Scattering spectra of previously synthesised G_0 (31.3 ± 0.4 nm) and G_1 (47.4 ± 0.6 nm) particles and their assemblies were compared (see **Figure 5.7**).

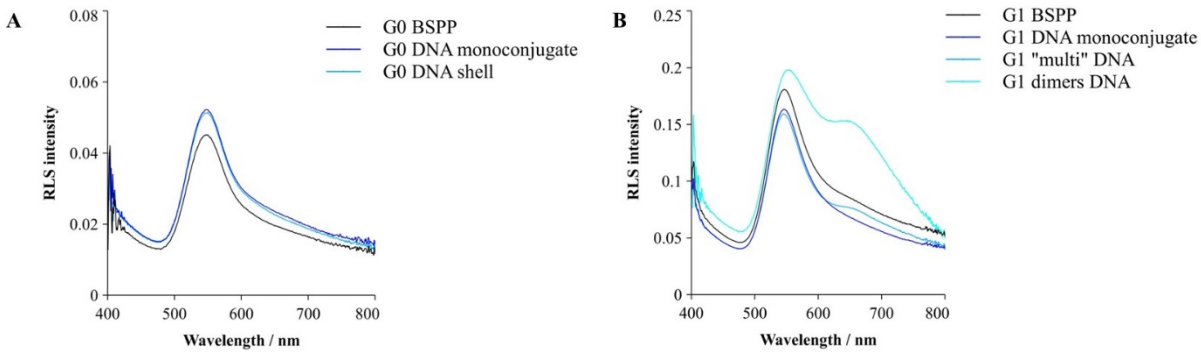

Figure 5.7. Normalised RLS spectra of **A)** G_0 AuNPs and DNA-AuNPs and **B)** G_1 AuNPs, DNA AuNPs and DNA-AuNP dimers

As observed in **Figure 5.7A**, no variation of the optical scattering properties occurred when functionalising G_0 AuNPs with one or a shell of ssDNA. The λ_{max} of the

spectra were consistently at 546 nm. Spectra of G_1 BSPP-AuNPs, DNA-AuNP monoconjugates and DNA-AuNP dense DNA shells were extremely similar in shape and all exhibited a λ_{max} at 547 nm. The spectrum of G1 DNA shell particles also exhibited a small shoulder at 653 nm. This could be attributed to small aggregates present in solution. The spectrum of the dimers sample was different with a λ_{max} at 552 nm and a second peak at 650 nm. The shape and values of this spectrum were in accordance with the literature for a scattering spectrum of a solution of gold nanoparticles dimers [11].

If for larger particles it is possible to notice the difference in optical properties between single particles and their dimer assemblies using RLS spectroscopy even considering the large interparticle distance, then this technique could be considered as a useful tool to follow the formation or the dissociation of AuNP-DNA assemblies in real time.

5.1.2.3 Study of DNA hybridisation during dimer formation

As already explained in detail in previous chapters, DNA-AuNP assemblies were formed by taking advantage of the capability of DNA to assemble in a specific manner. As stated in the introductory chapter (see **Section 2.3**), dsDNA can be denatured by breaking the hydrogen bonds between the ssDNA when increasing the temperature. Only a little information about the mechanism of DNA-AuNP formation is available in the literature [12]. To investigate this phenomenon, large G_0 AuNPs (31.3 ± 0.4 nm) were analysed with scattering spectroscopy using a thermostatic cuvette holder.

The method was first tested using the scattering properties of temperature independent (Ludox) or dependent (rhodamine B) compounds. For these two chemicals,

scattering spectroscopy measurements were recorded from room temperature (25°C) to 70°C and back (see **Figure 5.8**).

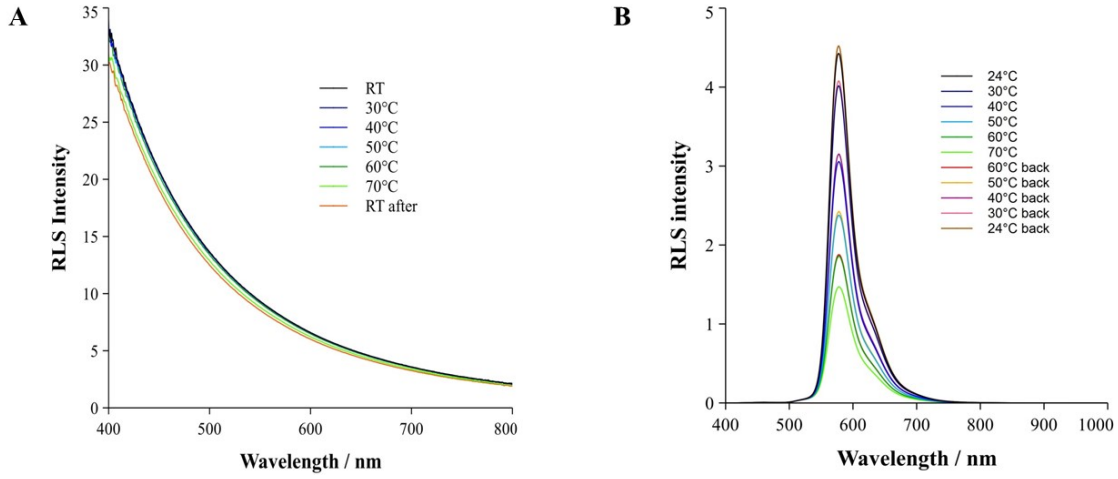

Figure 5.8. Raw **s**cattering spectra of **A)** Ludox and **B)** Rhodamine B when exposed to a temperature change

As expected, **Figure 5.8A** shows that temperature had no influence on the scattering spectra of Ludox. On the other hand, when a temperature increase was applied to rhodamine B the intensity of its scattering spectra decreased; the reciprocal was found upon increasing the temperature [13]. These preliminary experiments showed that the method was valid to evaluate the influence of the temperature on a sample by RLS spectroscopy. Furthermore, measurement of rhodamine B was undertaken in real time and at a constant temperature to measure the time needed by the sample to reach the desire temperature (50°C, 10 minutes, see **Appendix AI.1**). To ensure equilibrium of the sample for each temperature change, the sample was allowed to equilibrate for 15 minutes.

Finally, before starting measurements, G_0 particles stability in the presence of salt was studied to determine the best experiment conditions (see **Appendix AI.2**). Particles started to aggregate at 40 mM salt concentration. Therefore, for the temperature experiments, a salt concentration of 30 mM NaCl was chosen.

Before studying the association or dissociation of complementary DNA-AuNP monoconjugates into dimers, the first measurements were made on BSPP AuNPs, DNA-AuNP monoconjugates and DNA shell NPs. For each sample, three cycles were performed of temperature increase from 20 °C to 60 °C with a subsequent decrease to 20 °C (see **Figure 5.9**).

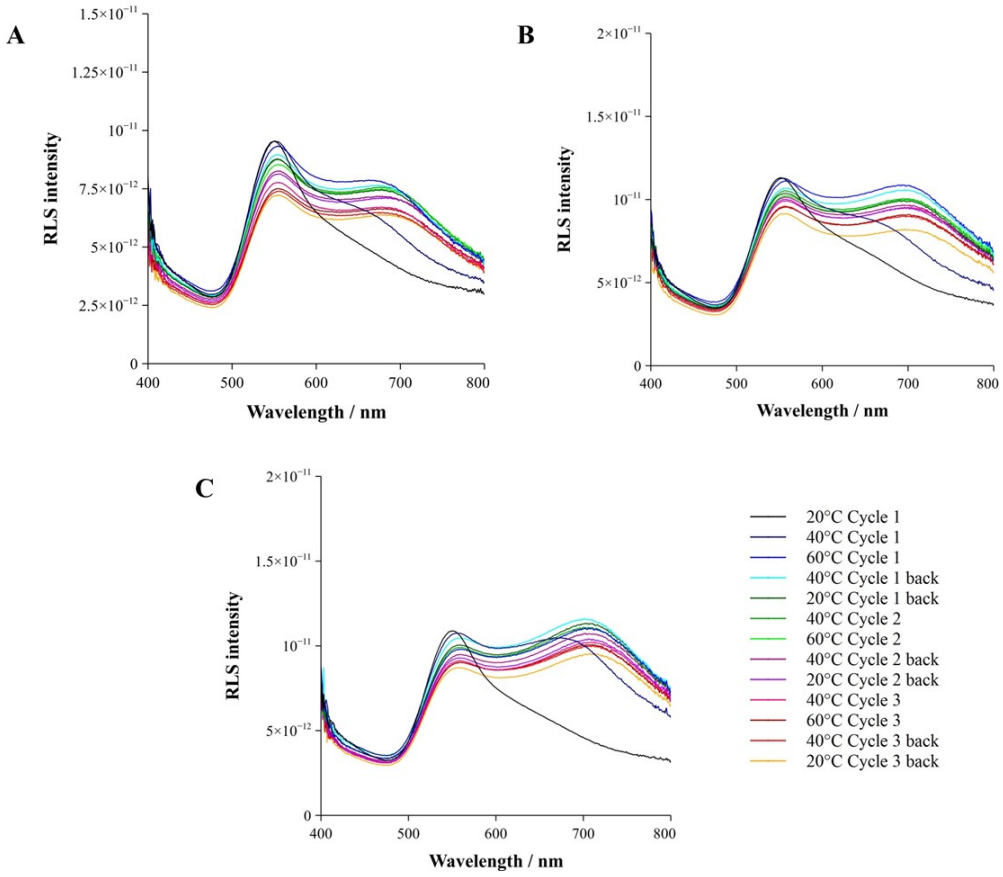

Figure 5.9. Evolution of RLS spectra of **A)** G_0 BSPP **B)** G_0 mono and **C)** G_0 multi particles with increasing temperature in phosphate buffer (30 mM NaCl)

For these three samples, similar results were obtained. However, in presence of NaCl, G_0 BSPP, G_0 DNA monoconjugates and G_0 DNA shell particles seemed to aggregate with an increasing temperature. A broad irreversible second peak around 700 nm appeared after 40 °C during the first cycle and exhibited the same intensity throughout the rest of the temperature cycles. As the appearance of this second peak was not reversible over the temperature cycle, it was clear that the particles aggregated. As preliminary experiments showed, particles were stable in 30 mM NaCl. Nevertheless, in the buffer condition, increasing the temperature seemed to make them aggregate. Unfortunately, in order to screen the negative charge of the ssDNA, it is necessary to keep a small amount of salt in the reaction during DNA hybridisation. This is why all experiments were carried out in 30 mM NaCl. All experiments were carried out in parallel using water. However, in this case no optical changes were observed (see **Appendix AI.3**)

To study the formation of AuNPs dimers through hybridisation of DNA strands, complementary monoconjugates, G_0 DNA A and G_0 DNA D, were mixed together and temperature cycles were performed (see **Figure 5.10A**).

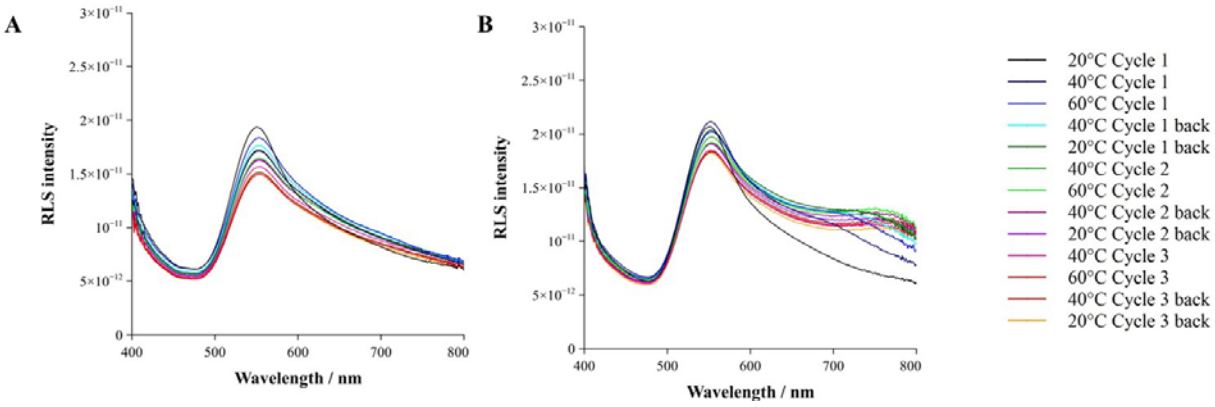

Figure 5.10. Evolution of RLS spectra of mixed **A)** G_0 monoconjugates A and D or **B)** G_0 DNA shell A and monoconjugates D with increasing temperature in 30 mM NaCl

Over the course of the experiment, the general shape of the scattering spectra of the G_0 NPs did not change. Nevertheless, the intensity of the peak at the λ_{max} clearly decreased. This phenomenon was not reversible and therefore was difficult to explain. A possible explanation of this intensity decrease was that some of the particles, due to the temperature increase, would have started sticking onto the cuvette walls.

Photothermal reshaping of gold nanoparticles using pulsed laser is a well-developed technique [14]. During these experiments the light source used was a halogen light. It was previously showed that spherical particles are highly stable when irradiated with low-power UV source [15, 16]. It is therefore unlikely that the light source used during these measurements caused the particles to reshape. The difference in particles behaviour in water (see **Figure AI.3**) or 30 mM NaCl buffer (see **Figure 5.9**) suggests a loss of stability due to the temperature, accelerated in presence of salt. However, it would be of great interest to record the scattering signal on a larger range (up to 1000 nm) to ensure that no reshaping is occurring during the measurements.

The use of RLS spectroscopy to follow and understand the formation of DNA-AuNP assemblies was employed. No clear signal of the formation of dimers or larger

assemblies was recorded. However, in the future, many aspects of the experiment could be altered in order to visualise the formation of assemblies; for example, the particles size (smaller particles or larger particles stabilised with a ligand) or the DNA system (lower melting temperature).

5.2 Photon time-of-flight spectroscopy

Two-photon photoluminescence emission spectra of DNA-gold nanoparticle monoconjugates and corresponding DNA-linked AuNP dimers were obtained via photon time-of-flight spectroscopy [17, 18]. This technique was combined with TPPL-FCS to simultaneously monitor the optical and hydrodynamic behavior of these nano-assemblies in solution, with single particle sensitivity and microsecond temporal resolution.

The 12.1 ± 0.3 nm DNA-linked AuNP dimers cannot readily be distinguished from the ssDNA-AuNP monoconjugates when steady-state light extinction and scattering spectroscopies were used (see **Sections 5.1.1 and 5.1.2**). Straightforward detection of the dimers was further complicated by their weak light scattering.

The experiments were carried out on various well-defined 12.1 ± 0.3 nm AuNP-DNA monoconjugates and corresponding linked AuNP dimers (the 'short-link' dimer AD-26 bp and the 'long-link' dimer BC-146 bp interparticle distance) (see **Sections 3.3.2** for experimental data and **4.4.2** for characterisation). **Figure 5.11** shows the TPPL spectra for the DNA-linked AuNP dimers, obtained using PTOFS.

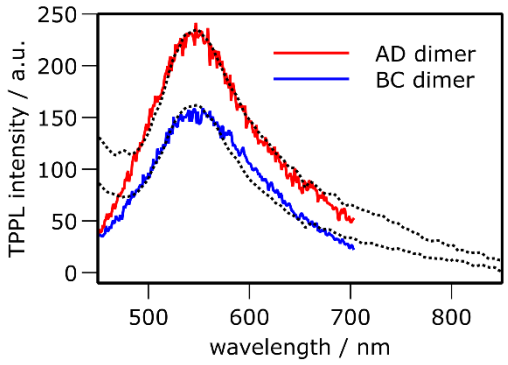

Figure 5.11 Two-photon photoluminescence spectra from AD and BC DNA-linked dimers. The dotted lines are the corresponding linear light scattering spectra, scaled for comparison.

Upon excitation of the nanoparticle solutions with 200 fs pulses of 800 nm light from a Ti-sapphire laser, an upconverted emission band is observed in the 450-700 nm range. The TPPL emission had a broad band peaking near 540 nm and reproduced the spectral shape of the linear light scattering spectrum. Such spectral similarity between photoemission and resonant light scattering is an observation generally seen with plasmonic nanostructures [17, 19, 20].

The mechanisms underlying the light emission seen by plasmonic nanostructures are still under debate, both for Stokes ('one-photon excitation') and anti-Stokes upconversion ('multi-photon excitation') emission which have been observed for plasmonic nanostructures [11, 17-19, 21]. In this work, the upconverted light emission observed under multi-photon excitation conditions was referred to as TPPL. This is also the term most regularly used in recent literature to refer to this phenomenon. Also, for most practical applications, the laser-excited light emission is indistinguishable from two-photon excited fluorescence.

A particularly attractive feature of the confocal measurement of TPPL in the set-up, was the possibility to simultaneously obtain information on the hydrodynamics of

the particles by analysing the TPPL intensity fluctuations in the confocal volume due to Brownian motion. TPPL-FCS is similar to fluorescence correlation spectroscopy, but instead of fluorescence it uses the multi-photon excited light emission from the plasmonic structures for probing the dynamics of the confocal volume [22-24].

Typical TPPL-FCS results for a ssDNA-AuNP monoconjugate and its corresponding DNA-linked AuNP dimer are shown in **Figure 5.12**.

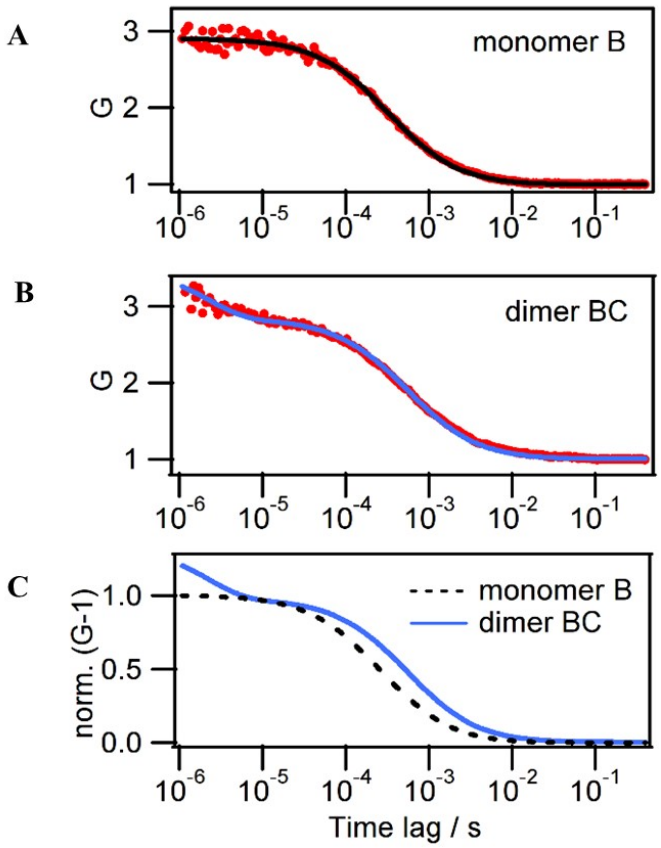

Figure 5.12. A) and **B)** TPPL intensity autocorrelation curves for ssDNA(B)-AuNP monoconjugates and long-link dimers BC, and fit using translational and rotation-translational diffusion, respectively **C)** best fits for monomer and dimer TPPL autocorrelation, rescaled to enable direct comparison, demonstrating the longer translational time of the dimers and the presence of a rotational component at short time lag

The autocorrelation curves of the TPPL intensity in the confocal observation volume clearly displayed different shapes between the AuNP-B monoconjugates and the AuNP dimers (see **Section 2.1.2** for theoretical background).

Experimental values of the diffusion coefficients, D_{trans} found for the four types of DNA-AuNP monoconjugates were all in the same range (DNA A, 2.3×10^{-11}, DNA B, 2.0×10^{-11}, DNA C, 2.3×10^{-11} and DNA B, 2.2×10^{-11} $m^2 s^{-1}$). As expected the values for dimers were slower with values of 1.6×10^{-11} and 1.1×10^{-11} $m^2 s^{-1}$ for dimers AD and BC. These values are further compared with microfluidics values in **Section 5.3**.

In the case of the dimers, the rotational diffusion coefficients were found to be $D_R = 7 \pm 0.8 \times 10^4$ s^{-1} for AD, and $D_R = 5.5 \pm 0.8 \times 10^4$ s^{-1} for BC. The noise on the autocorrelation at very short time lags resulted in a sizeable uncertainty on the time constant for rotational diffusion. However, in combination with the observation of a longer diffusion time, the appearance of this rapid rotational contribution demonstrated the hydrodynamic difference between ssDNA-AuNP monoconjugates and DNA-linked dimers: this was due to their different sizes.

The values obtained for the rotational diffusion coefficients D_R and the translational diffusion coefficients D_T for DNA-AuNP dimers may be compared to theoretical model values calculated for nanorods with diameter d = 12 nm and length L = 33 nm (AD) or L = 74 nm (BC), respectively. Following the hydrodynamic model by Tirado et al. the expressions of the translation diffusion coefficient and of the rotation constant were as in **Equation 5.2** [25].

$$D_T = \frac{k_b T}{3\pi\eta L}\left[\ln\left(\frac{L}{d}\right) + 0.312 + 0.565\frac{d}{L} - 0.100\ \frac{d^2}{L^2}\right]$$

$$D_R = \frac{3k_b T}{\pi\eta L^3}\left[\ln\left(\frac{L}{d}\right) - \ 0.662 + 0.917\frac{d}{L} - 0.050\ \frac{d^2}{L^2}\right]$$

Equation 5.2. Translation diffusion coefficient and rotation constant as described in the hydrodynamic model of Tirado at al.

The calculation yield to D_T = 2 x 10^{-11} m^2 s^{-1} and D_R = 7 x 10^4 s^{-1} for "AD-like" nanorods, and D_T = 1.3 x 10^{-11} m^2 s^{-1} and D_R = 1.4 x 10^4 s^{-1} for "BC-like" nanorods. These values were in the same order of magnitude and displayed the same trends as those experimentally obtained for the dimers, despite the rough approximation related to the shape of the object. The agreement with the simple model was better for AD dimer than for BC dimer. The former had the shorter linker between the two nanospheres, which may explain the better agreement. This result indicated that the hybridised DNA linker was indeed rigidly extended between the components of the structure.

The combined theoretical and experimental results for the translational diffusion coefficient of ssDNA-AuNP monoconjugates and DNA-linked AuNP dimers, illustrated that the diffusion coefficient of elongated objects (L = 33 nm and L = 74 nm for a width of 12 nm) cannot be estimated simply from the Stokes-Einstein equation when using the long axis as the hydrodynamic radius.

TPPL combined with PTOFS and FCS provided a sensitive method to detect and characterise even 'weakly plasmonic' assemblies which did not efficiently scatter light and whose plasmonic resonance did not show a clear difference between monoconjugate species and dimer assemblies. In contrast to linear optical spectroscopy, which was

carried out in typical spectroscopic cell volumes (3 mL), TPPL was measured in a small confocal volume, typically in the sub-picolitre range (~ 50 µl). This confocal configuration is compatible with detection in capillaries, such as those found in microfluidics or analytical chromatography. With these results, it could be suggested that the rotational component of the TPPL correlation function may probe the dimerisation of gold nanosphere-based DNA probes upon hybridisation, and transduce the presence and concentration of specific nucleic acid analytes.

5.3 Investigation of AuNP and DNA-AuNP diffusion properties

Part of the work presented in this section was published in: Johanna Midelet, Anne Débarre, Afaf H. El-Sagheer, Tom Brown, Antonios G. Kanaras, Martinus H.V. Werts. "Spectroscopic and hydrodynamic characterisation of DNA-linked gold nanoparticle dimers in solution using two-photon photoluminescence".*ChemPhysChem*. 2018, 19, 1-11.

In this section, diffusion coefficients of 12.1 ± 0.3 nm AuNP and DNA-AuNP samples were determined using a microfluidic 'H-filter'. The technique was based on determining the extent of the diffusive mass transfer from the flow of nanoparticle solution (Entry B) to the flow of pure solvent (Milli-Q water, Entry A), which were continuously injected at separate inputs of the microfluidic circuit and flowed in parallel after meeting at a 'T'-junction (see **Figure 5.13** and **Section 2.1.2** for background information). This method, previously applied to non-fluorescent food dyes and gold

nanoparticles, was adapted to include a spectroscopic flow cell which was used for in-line monitoring of the extinction spectrum of the output solution (Exit B)[26].

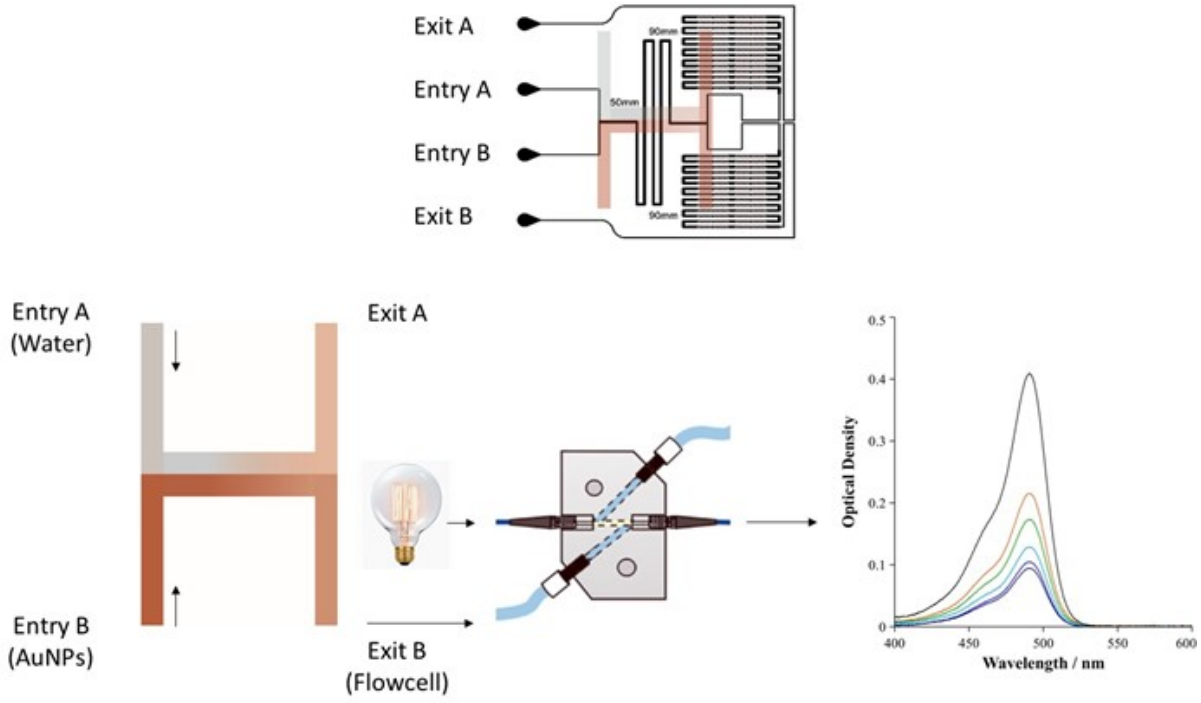

Figure 5.13. Schematic representation of the microfluidic 'H-filter' used for the diffusion coefficient measurements

Experimentally, as the OD was measured at the exit B the extent of diffusion, ξ_{exp} was described by **Equation 5.3**, with $\xi = 0$ corresponding to no diffusion and $\xi = 1$ to complete diffusion (the expression was slightly modified from the literature) [26].

$$\xi_{exp} = \frac{2\,OD_B}{OD_{tot}}$$

Equation 5.3. Expression of the experimental extent of the diffusion ξ_{exp} with ODtot, the optical density of the nanoparticle sample injected and OD_B the optical density at the exit B

Theoretically, the extent of the diffusion (ξ_{th}) can be expressed by **Equation 2.7**. This sum requires numerical evaluation. For sufficiently large values of $D\tau$ the series converges rapidly, in which case only a few terms are needed for a reliable result.

After collecting the data for ξ_{exp} at certain specified flow rates (U), D can be found by numerically solving $\xi_{exp} - \xi_{th} = 0$ using a dedicated python script ($0<i<5000$). Preliminary experiments were performed to validate the system by characterising the flow cell and the microsystem itself.

To make sure that the flow cell gave reliable measurements of the extinction spectra, a comparison between measurements issued from a standard UV-Visible cuvette and the flow cell was carried out using fluorescein and AuNPs (see **Figure 5.14**).

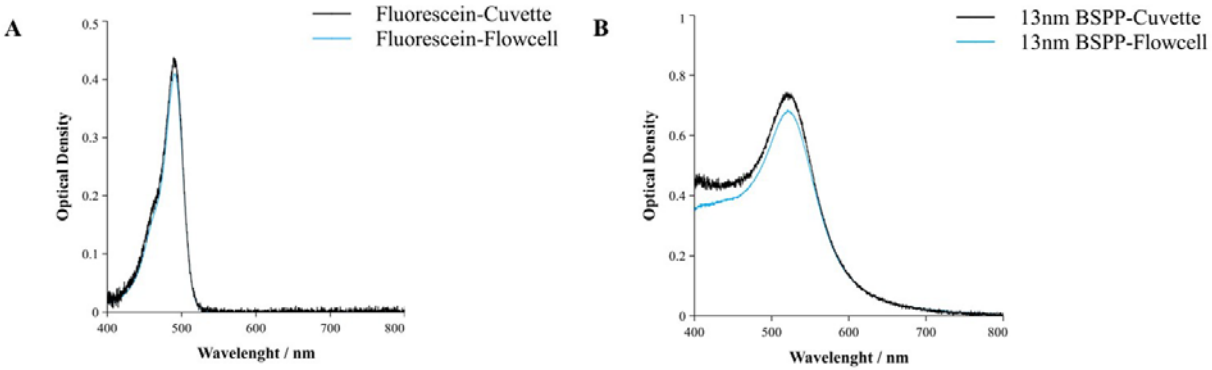

Figure 5.14. Comparison of extinction spectra using flow cell and UV-Visible cuvette for A) Fluorescein and B) 12.1 ± 0.3 nm BSPP AuNPs

As showed in the plots above, the flow cell gave similar results to the UV-Visible cuvette for the extinction spectra measurements performed. This quick experiment confirmed that it was reliable to use the flow cell to follow the diffusion process of the AuNPs in real time at the output of the microsystem.

To characterise the microsystem itself, measurements were performed using fluorescein to determine the interaction time τ (see **Equation 2.7**). Fluorescein is a xanthene dye with a well-known diffusion coefficient ($6.4.10^{-10}$ $m^2.s^{-1}$) [27]. At a given volumetric flow rate *U* ($m^3.s^{-1}$, sum of the two entering flow rates), the extent of diffusion ξ for a given diffusion coefficient D can be theoretically calculated. For this, it is convenient to convert the flow rate into a (device-independent) measurement of the interaction time.

To determine $\xi_{exp,}$ the maximum OD of the extinction spectra were measured over time for 5 different volumetric flow rates, 4, 10, 20, 30 and 40 µl.min^{-1} (see **Figure 5.15A** and **B**).

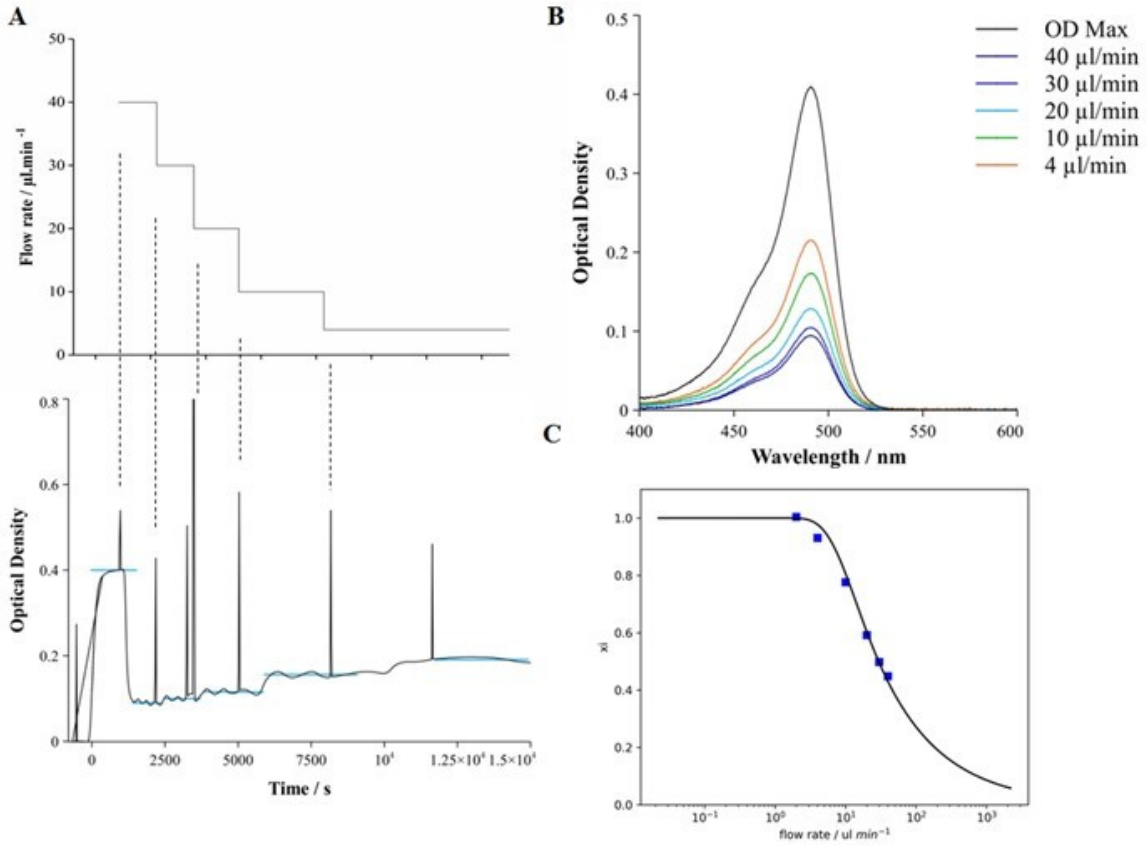

Figure 5.15. Determination of τ using fluorescein. A) Plot of the OD at λ_{max} over time (s) with the corresponding flow rates applied B) Extinction spectra of fluorescein after

stabilisation at different volumetric flow rate and C) Calculated extent of diffusion versus volumetric flow rate

Figure 5.15A, which shows the evolution of the OB_B at λ_{max} over time, from the highest 40 µl.min^{-1} to the lowest 4 µl.min^{-1} flow rate (the spikes observed correspond to the changes in volumetric flow rates). **Figure 5.15B** shows a typical extinction spectrum for each flow rate after equilibrium. The difference in intensity is due to the diffusion process. It can be note that as predicted, the particles diffused more when the flow was slower. For each flow rate after an equilibrium time, the plot started to plateau. An average value of the OD_B (symbolised by the blue straight lines on **Figure 5.15B**) was determined for each flow and used to calculate the ξ_{exp}. Finally, by making the theoretical plot of ξ_{th} *versus* volumetric flow rate fit with the experimental points (see **Figure 5.15C**), the value of interaction time τ was found to be $2.1.10^{10}$ m^{-2}.s^{1}. The same process was repeated for AuNP samples, using the determined τ and the diffusion coefficient, *D* as an unknown value.

Single (BSPP coated), DNA monoconjugates or DNA dimers gold nanoparticles of 12.1 ± 0.3 nm were introduced in the microfluidic system and their diffusion coefficients were determined. For each sample, as for the fluorescein, plots of the OD_B at λ_{max} *versus* time were recorded while varying the volumetric flow rates (see **Appendix AI.4**).

Finally, the experimental values of ξ_{exp} were plotted against the flow rates used and the fitting of these data using the equation for ξ_{th}, permitted the determination of the diffusion coefficient D for each sample. In order to allow comparison, all these data were plotted in the same graph (see **Figure 5.16**).

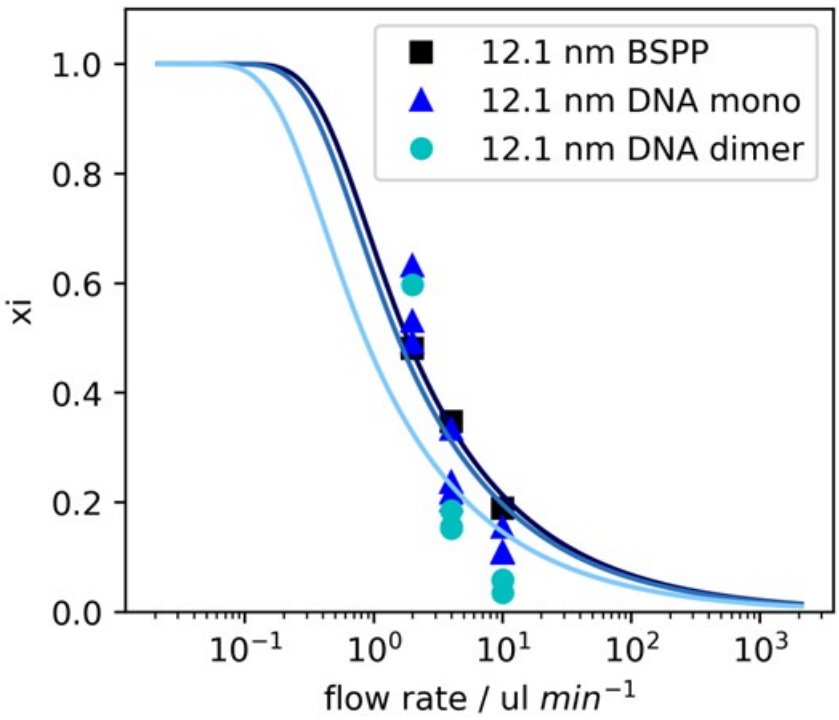

Figure 5.15. Comparison of the plot of ξ_{exp} *vs* flow rate for the different samples (Black squares: BSPP particles, dark blue triangles: DNA monoconjugate particles, light blue circles: DNA dimer particles) with theoretical curves (plain black, dark blue and light blue lines)

The value obtained for diffusion coefficients of the samples were respectively D= 4.1 ± $1.3.10^{-11}$ $m^2.s^{-1}$ for BSPP coated particles, 2.0 ± $0.8.10^{-11}$ m^2 s^{-1} for DNA monoconjugates particles and 0.6 ± $0.5.10^{-11}$ m^2 s^{-1} for DNA dimer particles.

Compared to small molecules, like dyes, the diffusion of the gold nanoparticles was at least one order of magnitude slower; this required very low flow rates for the set-up. This condition was difficult to stabilise, and prolonged times were necessary to reach a stationary state after changing the flow rate. This explains the large error bars, which particularly handicapped the determination of the dimer assemblies. The stability of the microfluidic measurement could be improved by further temperature stabilisation, use

of pressure-driven flow instead of syringe pumps and reduction of dead volume by integrating the observation flow cell in the microfluidic structure. In spite of these experimental difficulties, the diffusion coefficient of BSPP-coated AuNPs observed was in line with the value expected for a 12.1 ± 0.3 nm diameter sphere, using the Stokes-Einstein relation, i.e. $3.8.10^{-11}$ m^2s^{-1}. Moreover, it was observed that DNA-AuNP monoconjugates have a significantly lower diffusion coefficient than BSPP-AuNPs. The diffusion coefficient was further reduced in the case of the DNA-AuNP dimers.

Furthermore, it is interesting to compare the data obtained for the DNA coated samples through microfluidics and TPPL-FCS ($2.3 \pm 0.2.10^{-11}$ for monoconjugates and $1.1. \pm 0.3x\ 10^{-11}$ $m^2.s^{-1}$ for dimers) (see **Section 5.1.3**). The two methods agreed fairly well. The trend in diffusion coefficient between DNA-AuNP monoconjugates and DNA-linked AuNP dimers and the order of magnitude of the coefficient were reproduced by the TPPL-FCS measurements.

Diffusion coefficients were determined using a microfluidic system and the values obtained permitted the differentiation of the samples. The values of the coefficients decreased with the size increase of the assemblies tested. Furthermore, data collected using TPPL-FCS were in agreement with the microfluidic values.

5.4 Investigation of AuNP and DNA-AuNPs sedimentation properties

Part of the work presented in this section was published in: Johanna Midelet, Afaf H. El-Sagheer, Tom Brown, Antonios G. Kanaras, and Martinus H. V. Werts. "The sedimentation of colloidal nanoparticles in solution and its study using quantitative digital photography" *Part. Part.Syst. Charact*. 2017, 34,10.

The sedimentation behaviour of colloidal nanoparticles is influenced by nanoparticle hydrodynamics and gravitational and Brownian forces. An understanding of the sedimentation of nanoparticle solutions permits to achieve a rapid and visual analysis of size distribution and colloidal stability of newly synthesised colloids.

The sedimentation of nanoparticles was studied quantitatively using digital photography and a simple model based on the Mason-Weaver equation. First, the agreement between experimental time-lapse photography and numerical solutions of the model was studied for a series of spherical gold nanoparticles (see **Section 5.3.1**). The new method was then extended to study for the first time the gravitational sedimentation of DNA-AuNP dimers as a model for a system of a higher complexity structure (see **Section 5.3.2**). Finally, simple formulas were derived for estimating suitable parameters for the preparative centrifugation of nanoparticle solutions (see **Section 5.3.3**).

5.4.1 Sedimentation of spherical gold nanoparticles

The establishment of a concentration gradient in a dilute colloidal solution of independent, non-interacting particles in a homogeneous gravitational field is described by the Mason-Weaver equation (see **Equations 2.10** and **2.11**) [28]. The height position in the cell is given by z. The concentration of decanting particles C satisfies the Mason-Weaver equation, with boundary conditions.

In this work, **Equations 2.10** and **11** were solved numerically using a Crank-Nicolson finite-difference method. The initial conditions at t=0 were C= C0 for $0 \leq z \leq z_{max}$ and C= 0 elsewhere (see **Section 2.1.3** for background information).

Quantitative colour imaging for measuring concentration profiles in microfluidic channels, using an optical microscope and a dedicated CCD camera was previously published [26]. Here a digital camera provided the output of unprocessed ('RAW') image data, which was used to image gold nanoparticle solutions in spectroscopic cells in a temperature controlled environment. In these images the individual pixel values were proportional to the detected light intensity.

Intensity gradient profiles $I_{raw}(z)$ for all samples (and all colour channels) in each image of the time series were extracted by horizontal averaging over the visible optical window of the spectroscopic cells (see **Section 3.5.5** for experimental details). Pixel values of a selected black area were averaged for background subtraction, I_{dark}. Each image frame thus obtained its specific calibration of pixel size. The digital intensity profiles $I_{raw}(z)$ were then further treated numerically using the Python programming language with scientific extensions. Background corrected image profiles I(z) were obtained by subtraction of the near-zero dark background (see **Equation 5.4**).

$$I(z) = Iraw(z) - Idark$$

Equation 5.4. Formula used to subtract the dark background in each image

The top area of each extracted z profile, which does not contain liquid, was used for calculating I_0 by averaging. This permitted the correction of the slight frame-to-frame variations in illumination intensity. A linear baseline correction, $ODbase(z)=k_1z+k_2$ was applied globally to all time-frames for each sample. In all cases, the baseline correction was modest and not necessary to obtain useful results. The final corrected optical density is obtained using **Equation 5.5**. This Beer-Lambert-Bouguer formulation was employed despite the condition of monochromatic light not being rigorously fulfilled: the filters used in colour cameras define large spectral bands (width ~100 nm). A linear response of the optical density as a function of concentration was still obtained, provided that the extinction spectra of the samples was sufficiently large and their optical density was sufficiently low (OD < 1).

$$OD(z) = \log_{10}\left(\frac{I_0}{I(z)}\right) - ODbase(z)$$

Equation 5.5. Beer-Lambert-Bouguer formulation used to obtain the final corrected optical densities

Comparison of experiment with theory is achieved by converting the concentration profiles C(z) from the Mason-Weaver model into modelled optical density profiles, ODmodel(z) using an "effective extinction coefficient" which was referred to here as k_3 and can be adapted to rescale the model concentration profile to fit the experimental values (see **Equation 5.6**).

$$ODmodel(z) = k_3 C(z)$$

Equation 5.6. Expression used to convert the concentration profiles into modelled optical density profiles

Typical optical densities at the extinction maximum were in the range of 0.3-1. Under these dilute conditions, the ligands do not influence the sedimentation behaviour of the particles. Also, the only solvent parameters of relevance for sedimentation was the viscosity and the density; these were very close to those for pure water at low concentrations of stabilising ligand.

Experimental concentration profiles of several settling solutions of gold nanoparticles were obtained from digital photographs taken at different time points. A typical example, using commercial 40 nm gold nanospheres in water, is shown in **Figure 5.17**. The photographs for this series were taken over a 39 day period, and quantitative vertical optical density profiles were obtained using the method detailed in **Section 3.5.5**. In this work, we only use the green colour channel of the images, since this produces the strongest optical response for the red-coloured gold nanoparticles.

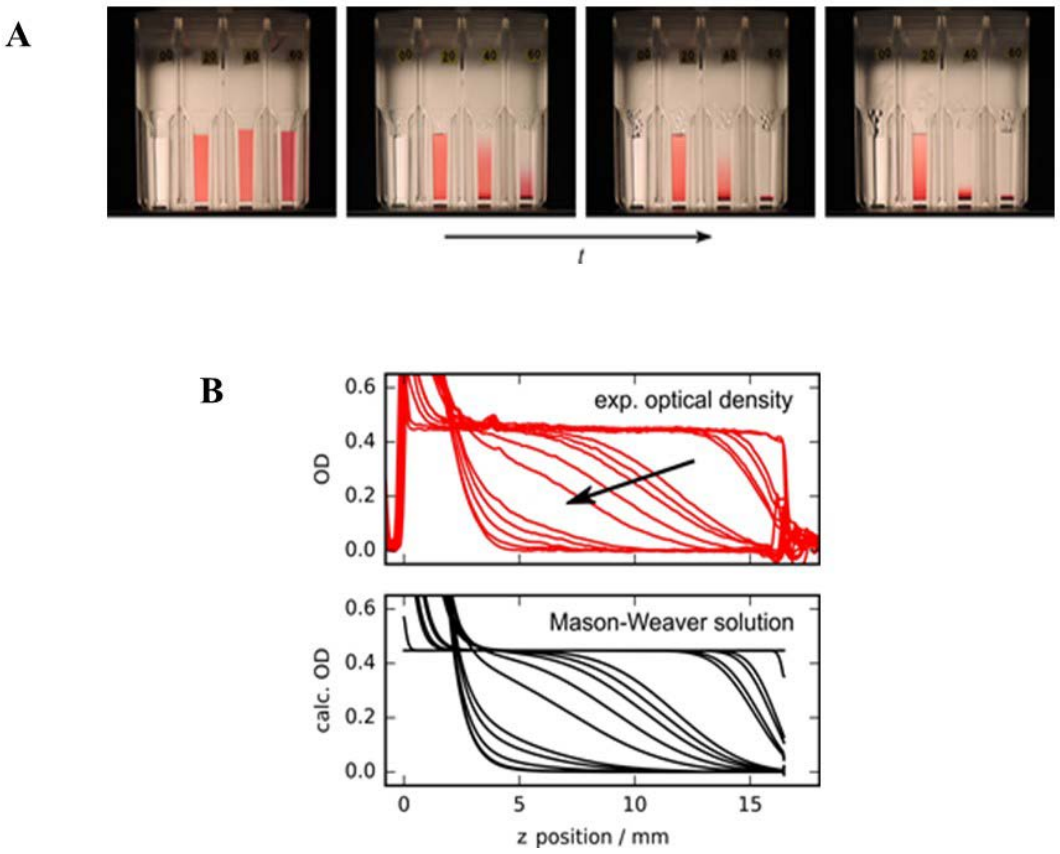

Figure 5.17. A) Digital photography of sedimentation over time of 20, 40, 60 nm colloidal gold in water. The cell at the left of each picture contains water only. Photos were taken at t= 0, 7, 14 and 35 days. **B)** Evolution of the vertical particle density gradient in an aqueous solution of 40 nm diameter gold nanospheres. Photos were taken at t = 0, 1 h, 21 h, 27 h, 44 h, 52 h, 7 d, 9 d, 11 d, 14 d, 21 d, 23 d, 28 d, 35 d, and 39 days. Top: experimental optical density profiles obtained from the intensity profiles. The arrow indicates the direction of time. Bottom: theoretical optical density profiles obtained numerically as the solution to the Mason-Weaver equation

In the same figure, the solution of the Mason-Weaver equation C(z,t) at the same timepoints t was shown. The diffusion and sedimentation coefficients were adjusted independently to obtain best agreement with the experimental observations. The values obtained, $D = 5.1.10^{-12}\ m^2.s^{-1}$ and $s = 7.9.10^{-10}$ s agree within 20 % of those expected from

the Einstein-Smolukowski-Sutherland and the Stokes relations for perfect 40 nm diameter gold spheres in water in the same conditions (see **Appendix AI.5**).

Furthermore, diffusion and sedimentation coefficients were obtained for the entire series of gold nanosphere diameters by fitting the Mason-Weaver solutions to the optical density profiles which evolve through time (see **Figure 5.18**).

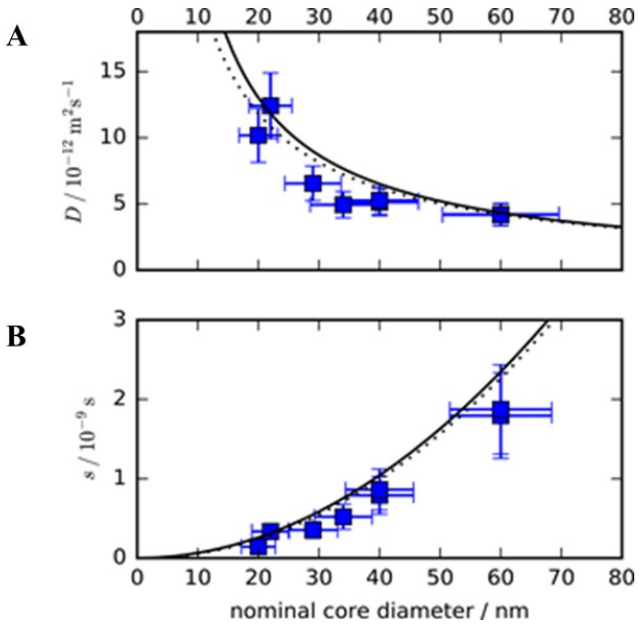

Figure 5.18. Diffusion *D* and sedimentation *s* coefficients obtained by analysing the evolving experimental density gradient of settling gold nanosphere solutions (square markers). **A)** The solid curves are the expected values for perfect golden spheres from the Stokes-Einstein-Sutherland equation and **B)** Stokes' law. The dotted curves are for gold spheres with a hypothetical 1 nm thick organic layer

These coefficients agree reasonably well (within 20%) with the predicted values. In addition to the predictions based on the gold core only, the expected diffusion coefficients for the gold core plus an extra 1 nm of ligand shell were calculated (ρ = 900 kg.m^{-1}, dotted curve in **Figure 5.18**). This second theoretical curve demonstrates that

the present simple method cannot distinguish between small differences in overall hydrodynamic radius and density.

In this section, the Mason-Weaver equation was confirmed as a valid model for the behaviour of simple gold nanoparticle solutions. Furthermore, the precision of the method was investigated. Improvements could be achieved by stabilisation of the illumination and the camera positioning.

5.4.2 Sedimentation of 12.1 nm DNA-AuNP dimers

After the initial demonstration of the quantitative analysis of time-lapse photography of settling spherical gold nanoparticles in water, a sample of purified DNA-linked dimers of 12.1 ± 0.3 nm diameter gold nanospheres was investigated (see **Figure 5.19**). This experiment illustrated that studying sedimentation can aid in the chemistry and characterisation of biomolecularly-scaffolded nanoparticle assemblies.

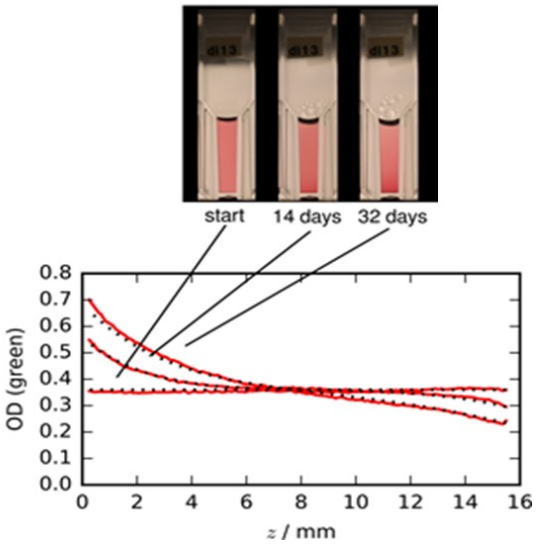

Figure 5.19. A) Composed image of the time-lapse photography of sedimenting DNA-linked gold nanosphere dimers (at 277 K). **B)** optical density traces as a function of vertical position in the cell, taken at various points in time (red solid lines); the black dotted curves are the solution to the Mason- Weaver equation

By adjusting the theoretical curves to the experimental data, $D = 5.8.10^{-12}\ m^2.s^{-1}$ and $s = 9.0.10^{-11}$ s were obtained for the diffusion and sedimentation coefficients, respectively. The sedimentation coefficient of DNA-linked dimers was slightly smaller than that of a bare 12.1 ± 0.3 nm monomer sphere. The extra mass from the second gold sphere was counterbalanced by more friction with the solvent due to the larger outer surface area of the dimer. The larger volume comes to a large extent from the DNA which has a much lower density than gold.

Additionally, the diffusion coefficient is lower than that of a 12.1 ± 0.3 nm monomer as a result of the larger hydrodynamic volume of the object. Gold has a much higher density than water, whereas the DNA linker has a density comparatively very close to that of water. Any extra volume taken up by the DNA linkage does not significantly contribute to the buoyant mass of the object, since the displaced water

volume is replaced with a substance having a density close to that of water. The buoyant mass of the dimer is therefore determined by the two gold cores.

The lower sedimentation coefficients lead to slower establishment of the gradient. However, in combination with the lower diffusion coefficient, it finally leads to a more pronounced, shorter density gradient. A further analysis of the hydrodynamic behaviour and the resulting combination of *D* and *s* of this type of assemblies is not within the scope of this work, but has received recent attention in the literature [30].

It is also interesting to note that the estimated time to obtain the final equilibrium gradient (at 277K, with 2 cm liquid height) is approximately of 200 days for both the monomers and the DNA-linked dimers. For analysing the transient concentration profile it is not necessary to wait that long, which demonstrates the interest of having the numerical solution to the Mason- Weaver at hand. Nonetheless, 30 days is still a long time, and these samples are better analysed with centrifuge-based techniques. In this context it is interesting to note that, the required centrifugal acceleration for many inorganic-core nanoparticles is well within range of standard laboratory centrifuges, instead of higher-speed specialised instruments (see **Section 5.3.4**).

5.4.3 Sedimentation of 47.4 nm DNA-AuNP dimers

The sedimentation process of larger particles and their dimer assemblies was also studied using the same process. G_1 BSPP, DNA monoconjugates, DNA shell and dimer particles were left to sediment for a week and digital pictures were taken at 0, 24, 48, 72 and 168 hours (see **Figure 5.20**).

Pictures were processed using the software Image J and graphs of the optical density versus the height of the cuvette were plotted for the different times.

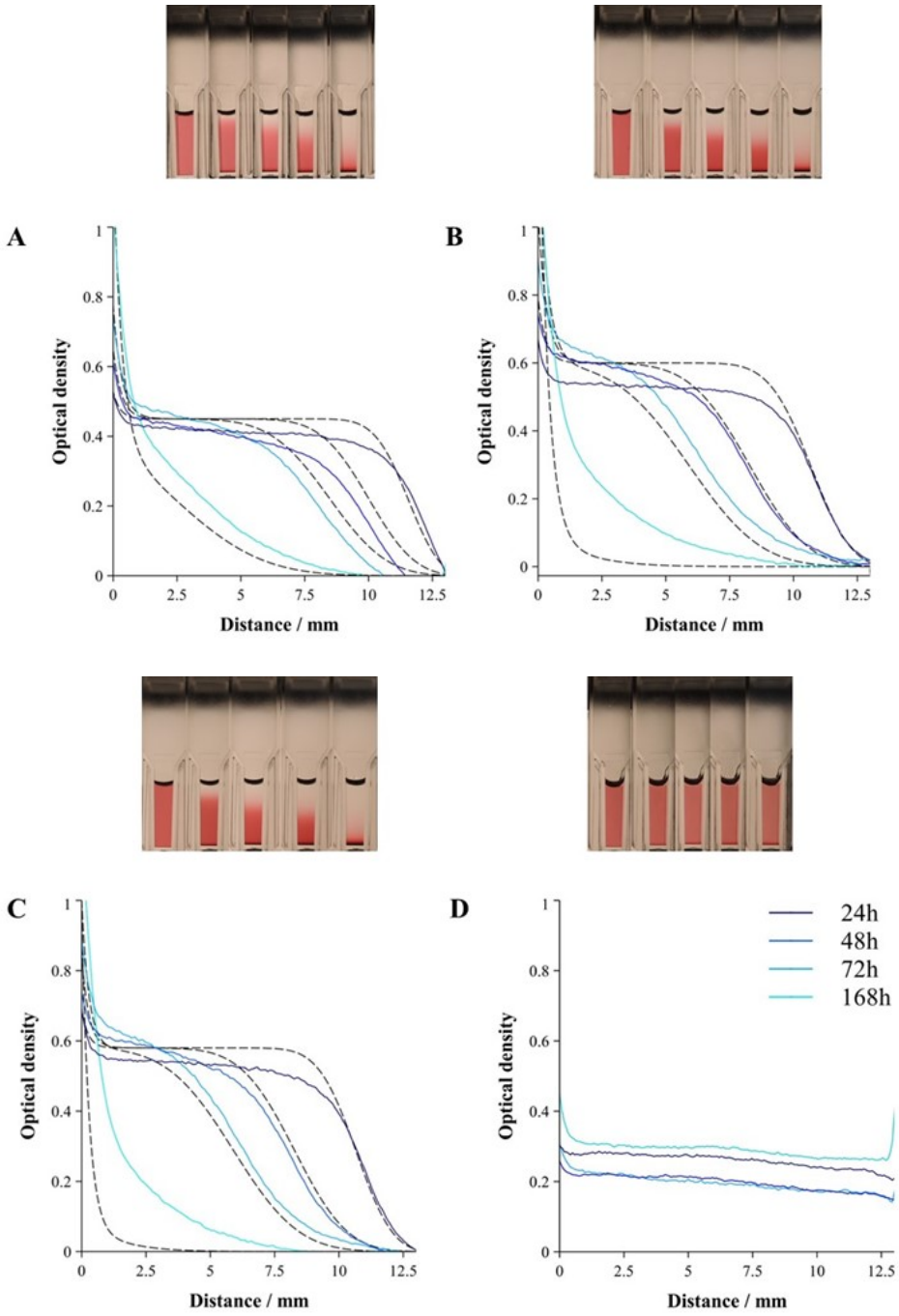

Figure 5.20. Digital pictures and plots of OD *vs* height of the cuvettes over time for samples **A)** G_1 BSPP B) G_1 DNA monoconjugates **C)** G_1 DNA shell and **D)** G_1 DNA dimers. Dotted curves correspond to the solution to the Mason-Weaver equation

Values of *D* and *s* were obtained for each sample. *D* was $6.5.10^{-12}$, 10.10^{-12} and 8.10^{-12} $m^2.s^{-1}$ for G_1 BSPP, G_1 DNA monoconjugates and G_1 DNA shell, respectively. And *s* was $1.8.10^{-9}$, $2.8.10^{-9}$ and $2.8.10^{-9}$ s. The final observed profile did not match the simulation in the case of G_1 monoconjugates and G_1 DNA shell. In order to draw clear conclusion, these experiments would need to be repeated.

Nevertheless, an interesting phenomenon was observed during this experiment. The solution of G_1 dimers did not sediment over the time period of the experiment. The hypothesis is that agarose gel is surrounding the dimer assemblies after their purification. This was confirmed by looking at the TEM images (see **Figure 5.21**).

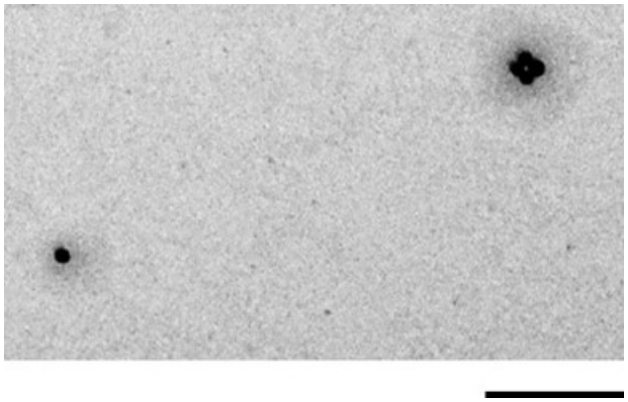

Figure 5.21. TEM pictures of G_1 dimers embedded in agarose gel. Scale bar is 500 nm

To purified G1 (47 ± 0.6 nm) gold nanoparticles, a 0.75 % agarose gel was employed. This low percentage seemed to affect the behaviour of the particles after purification. This experiment showed a direct application for the quantification of sedimentation using digital camera.

5.4.4 Application of the results to gold nanoparticles centrifugation

The results from the Mason-Weaver model may be used to generate initial approximate estimates for preparative and analytical centrifugation. For many nano-assemblies using high-density inorganic core materials, the centrifugal acceleration necessary for rapid sedimentation is well within the capabilities of standard table-top laboratory centrifuges. A centrifugal acceleration that is much higher than strictly necessary may have deleterious consequences for colloidal stability as the density of nanoparticles in the pellet may become very high, accelerating aggregation.

As an example the minimal centrifugal acceleration g_{cfg} needed to obtain sedimentation equilibrium for gold colloid solutions in a centrifuge within a given time t_{cfg}, was considered. By using **Equation 5.7** the centrifugal acceleration g_{cfg} necessary for the chosen centrifugation time t_{cfg} and a liquid height in the centrifuge tube z_{tube} can roughly be estimated.

$$g_{cfg} = \frac{1.4\, z_{tube}}{s\, t_{cfg}} \; or \; RCF = \frac{1.4\, z_{tube}}{g\, s\, t_{cfg}}$$

Equation 5.7. Centrifugal acceleration g_{cfg} necessary for the chosen centrifugation time t_{cfg} and a liquid height in the centrifuge tube z_{tube} This can be expressed as `relative centrifugal force', RCF = gcfg/g, where g = 9.81m.s^{-1}

Calculated rotational centrifugal force (RCF) values needed for complete centrifugation of different size of gold colloids in typical Eppendorf-type vials (z_{tube} = 3 cm), within t_{cfg} = 30 min were then used in centrifugation experiments.

In most cases the recommended centrifugal acceleration gave remarkably good results (see **Appendices A1.6 and 7**). Measurement of the UV-visible extinction spectra of the resuspended colloids confirms the visual impression that the calculated RCF values are indeed sufficient, and higher speeds for centrifugation are not necessary. In the case of 20 nm diameter gold spheres, centrifugation at slightly higher acceleration (~20%) was required to concentrate all particles near the bottom of the tube.

This work rationalises observations on the settling of nanoparticles in liquid solution in the framework of the Mason-Weaver model. This is illustrated by the quantitative agreement between this model and experimental digital photography for the time-evolution of the concentration gradient of suspended nanoparticles submitted to a gravitational field. A simple experimental protocol for observing the sedimentation process is established, using time-lapse digital photography of the samples in an undisturbed laboratory fridge in order to avoid thermally induced convection.

By fitting a numerical solution of the Mason-Weaver equation to the experimental concentration gradient, the diffusion and sedimentation coefficients *D* and *s* were obtained, without need to wait for complete equilibrium to be established. Early studies on sedimentation were mostly concerned with precise measurement of the equilibrium gradient, which only yields the buoyant mass mb of the particle as the sole parameter, not the separate contributions of diffusion and sedimentation coefficients [31, 32].

Any significant deviations from the predictions made by the Mason-Waver model would point to of stronger interparticle interactions, aggregation of individual objects, or changes in the properties of the liquid medium. It is important to be aware of such deviation as they may affect other aspects of the behaviour of the nanoparticles in liquid media, such as their interaction with biological entities. The practical insights and

simple quantitative expressions provided are of direct interest for wet-chemical synthesis, purification and application of functional nanoparticle assemblies.

In this chapter physicochemical properties of AuNPs in the range 5 to 50 nm in their single or DNA-AuNP dimers state were studied. Differences in there optical, diffusion and sedimentation properties were observed. For smaller particles, classic spectroscopic techniques (UV-Vis and RLS) did not permit to differentiate signals from single and dimer forms. Nevertheless, TPPL-FCS data showed the possibility to distinguish hydrodynamic differences between single and dimer forms. Furthermore diffusion and sedimentation properties of different type of particles were studied and compared using microfluidics and digital photography. As shown in **Table 5.1**, diffusion coefficient values obtained via three different techniques were in the same range and in agreement with the theory.

Table 5.1. Comparison of diffusion coefficient D (10^{-11} $m^2.s^{-1}$) values obtained using TPPL-FCS, microfluidics and digital photography.

Samples	**Theoretical value**	**TPPL-FCS**	**Microfluidics**	**Digital photography**
12.1 nm Au-DNA monoconjugates	1.99	2.30	2.00	N/A
12.1 nm Au-DNA dimers	N/A	1.10	0.6	0.58

5.5 References

1. Qian, Z. and D.S. Ginger, *Reversibly Reconfigurable Colloidal Plasmonic Nanomaterials*. Journal of the American Chemical Society, 2017. **139**(15): p. 5266-5276.

2. Macfarlane, R.J., et al., *Nucleic acid-modified nanostructures as programmable atom equivalents: forging a new "table of elements"*. Angewandte Chemie - International Edition, 2013. **52**(22): p. 5688-5698.

3. Zhang, C., et al., *A general approach to DNA-programmable atom equivalents.* Nature Materials, 2013. **12**(8): p. 741-746.

4. Chen, J.I.L., Y. Chen, and D.S. Ginger, *Plasmonic Nanoparticle Dimers for Optical Sensing of DNA in Complex Media*. Journal of the American Chemical Society, 2010. **132**(28): p. 9600-9601.

5. Lee, S.E., et al., *Reversible Aptamer-Au Plasmon Rulers for Secreted Single Molecules.* Nano Letters, 2015. **15**(7): p. 4564-4570.

6. Jain, P.K., et al., *Calculated absorption and scattering properties of gold nanoparticles of different size, shape, and composition: Applications in biological imaging and biomedicine*. Journal of Physical Chemistry B, 2006. **110**(14): p. 7238-7248.

7. Haiss, W., et al., *Determination of Size and Concentration of Gold Nanoparticles from UV−Vis Spectra.* Analytical Chemistry, 2007. **79**(11): p. 4215-4221.

8. Huang, X. and M.A. El-Sayed, *Gold nanoparticles: Optical properties and implementations in cancer diagnosis and photothermal therapy*. Journal of Advanced Research, 2010. **1**(1): p. 13-28.

9. Jain, P.K., W. Huang, and M.A. El-Sayed, *On the Universal Scaling Behavior of the Distance Decay of Plasmon Coupling in Metal Nanoparticle Pairs: A Plasmon Ruler Equation.* Nano Letters, 2007. **7**(7): p. 2080-2088.

10. Navarro, J.R.G. and M.H.V. Werts, *Resonant light scattering spectroscopy of gold, silver and gold-silver alloy nanoparticles and optical detection in microfluidic channels.* Analyst, 2013. **138**(2): p. 583-592.

11. Loumaigne, M., et al., *Optical extinction and scattering cross sections of plasmonic nanoparticle dimers in aqueous suspension.* Nanoscale, 2016. **8**(12): p. 6555-6570.

12. Sedighi, A., et al., *A Proposed Mechanism of the Influence of Gold Nanoparticles on DNA Hybridization.* ACS Nano, 2014. **8**(7): p. 6765-6777.

13. Rosenthal, I., P. Peretz, and K.A. Muszkat, *Thermochromic and hyperchromic effects in Rhodamine B solutions.* The Journal of Physical Chemistry, 1979. **83**(3): p. 350-353.

14. González-Rubio, G., A. Guerrero-Martínez, and L.M. Liz-Marzán, *Reshaping, Fragmentation, and Assembly of Gold Nanoparticles Assisted by Pulse Lasers.* Accounts of Chemical Research, 2016. **49**(4): p. 678-686.

15. Attia, Y.A., et al., *Photostability of gold nanoparticles with different shapes: the role of Ag clusters.* Nanoscale, 2015. **7**(26): p. 11273-11279.

16. Al-Sherbini, E.-S.A.M., *UV–visible light reshaping of gold nanorods.* Materials Chemistry and Physics, 2010. **121**(1): p. 349-353.

17. Loumaigne, M., et al., *The intrinsic luminescence of individual plasmonic nanostructures in aqueous suspension by photon time-of-flight spectroscopy.* Nanoscale, 2015. **7**(19): p. 9013-9024.

18. Loumaigne, M., et al., *Time-of-Flight Photon Spectroscopy: A Simple Scheme To Monitor Simultaneously Spectral and Temporal Fluctuations of Emission on Single Nanoparticles.* Acs Nano, 2012. **6**(12): p. 10512-10523.

19. Yorulmaz, M., et al., *Luminescence Quantum Yield of Single Gold Nanorods.* Nano Letters, 2012. **12**(8): p. 4385-4391.

20. Tcherniak, A., et al., *One-Photon Plasmon Luminescence and Its Application to Correlation Spectroscopy as a Probe for Rotational and Translational Dynamics of Gold Nanorods.* The Journal of Physical Chemistry C, 2011. **115**(32): p. 15938-15949.

21. Fernandes, R., et al., *Interactions of Skin with Gold Nanoparticles of Different Surface Charge, Shape, and Functionality.* Small, 2015. **11**(6): p. 713-721.

22. Magde, D., E.L. Elson, and W.W. Webb, *Fluorescence Correlation Spectroscopy .2. Experimental Realization.* Biopolymers, 1974. **13**(1): p. 29-61.

23. Elson, E.L. and D. Magde, *Fluorescence Correlation Spectroscopy .1. Conceptual Basis and Theory.* Biopolymers, 1974. **13**(1): p. 1-27.

24. Ries, J. and P. Schwille, *Fluorescence correlation spectroscopy.* BioEssays, 2012. **34**(5): p. 361-368.

25. Tirado, M.M., C.L. Martínez, and J.G. de la Torre, *Comparison of theories for the translational and rotational diffusion coefficients of rod‐like macromolecules. Application to short DNA fragments.* The Journal of Chemical Physics, 1984. **81**(4): p. 2047-2052.

26. Werts, M.H.V., et al., *Quantitative full-colour transmitted light microscopy and dyes for concentration mapping and measurement of diffusion coefficients in microfluidic architectures.* Lab on a Chip, 2012. **12**(4): p. 808-820.

27. Galambos, P. and F.K. Forster, *Micro-Fluidic Diffusion Coefficient Measurement*, in *Micro Total Analysis Systems '98: Proceedings of the uTAS '98 Workshop, held in Banff, Canada, 13–16 October 1998*, D.J. Harrison and A. van den Berg, Editors. 1998, Springer Netherlands: Dordrecht. p. 189-192.

28. Mason, M. and W. Weaver, *The Settling of Small Particles in a Fluid.* Physical Review, 1924. **23**(3): p. 412-426.

29. Schneider, C.A., W.S. Rasband, and K.W. Eliceiri, *NIH Image to ImageJ: 25 years of image analysis.* Nature Methods, 2012. **9**(7): p. 671-675.

30. Urban, M.J., et al., *Shape Analysis of DNA–Au Hybrid Particles by Analytical Ultracentrifugation.* ACS Nano, 2016. **10**(8): p. 7418-7427.

31. Perrin, J., *Mouvement brownien et molécules.* J. Phys. Theor. Appl., 1910. **9**(1): p. 5-39.

32. Johnston, N. and L.G. Howell, *Sedimentation Equilibria of Colloidal Particles.* Physical Review, 1930. **35**(3): p. 274-282.

Chapter 6. Seeded growth method for synthesis of gold nanoparticle assemblies

Conceptually, nanoparticle dimers are the simplest type of assembly and many strategies are already available for their synthesis [1-3]. In the case of gold nanoparticles, the most sophisticated and precise way to form gold nanoparticle dimers, trimers and tetramers is by using DNA scaffolds [4].

However, as highlighted in **Chapter 4** there are currently limitations for using this approach for the formation of dimers of large spherical (>30nm) and non-spherical gold nanoparticles. These include the difficulty of separating large spherical AuNPs with a discrete number of short DNA strands using gel electrophoresis, or the difficulty of functionalising anisotropic AuNPs with a discrete number of oligonucleotides [5, 6].

In this chapter, we present the use of a seeded-growth method as a solution for the synthesis of dimers of either large spherical or non-spherical (branched) gold nanoparticles. The first step of the synthesis involved the formation of small single or dimer gold nanoparticles, called seeds (see **Section 6.1**). These seeds were then employed in a growth process of nanoparticles (see **Section 6.2 and 6.3**) and the products were purified (see **Section 6.4**). The synthesis and optical properties of the assemblies were studied using optical spectroscopy (see **Section 6.5**). Finally in **Section 6.6**, a seeded-growth method was employed to metallise DNA on gold nanoparticles.

6.1 Synthesis of gold nanoparticles seeds

The synthesis of gold nanoparticle seeds is the first crucial step of every seeded growth method and has been widely investigated [7, 8]. In this chapter, AuNP-DNA linked dimer seeds were used for the first time as a template to grow larger nanoparticle dimers.

6.1.1 Single spherical seeds

Small spherical AuNPs were synthesised using a recently published protocol [9]. This protocol is different from the protocol employed in **Chapter 4** (see **Section 4.1.1**) to make 4.5 ± 0.4 nm particles. The difference between these particles is the stabilising agents used during their synthesis. After synthesis the seeds were capped with citrate and tannic acid. They were further stabilised by BSPP *via* ligand exchange. It was observed that they were easier to concentrate using centrifugation than the 4.5 ± 0.4 nm AuNPs originally synthesised with sodium borohydride. In **Figure 6.1** a TEM analysis was used to characterise particles size distribution. Analysis was performed on 1000 particles and their size plotted in a histogram (see **Figure 6.1B**). The average size of the particles was 5.7 ± 0.2 nm.

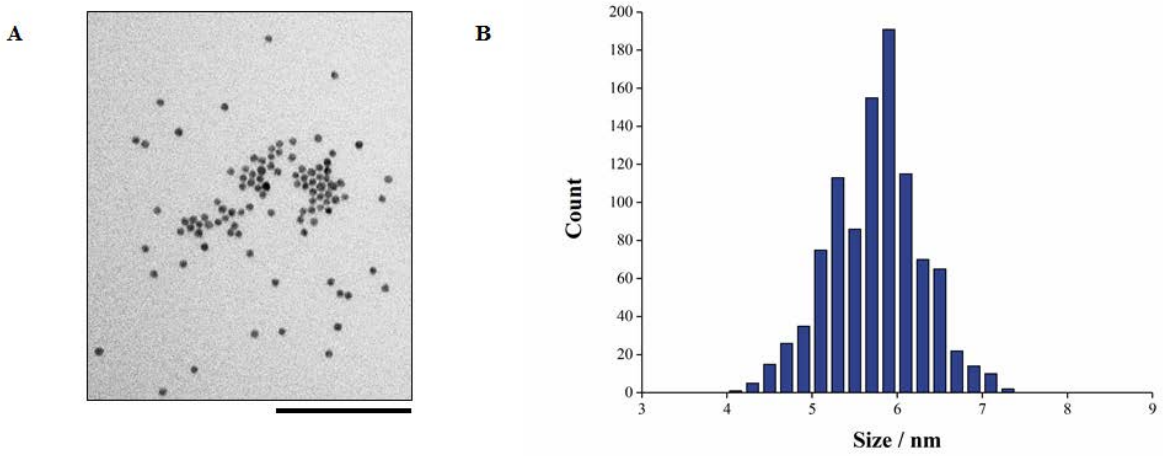

Figure 6.1. Characterisation of 5.7 ± 0.2 nm single spherical gold nanoparticle seeds **A)** Transmission electron microscopy image. Scale bar is 100 nm. **B)** Size distribution histogram

As seen on the TEM picture, the seed particles obtained have a narrow size distribution and are of spherical shape. Their optical properties were recorded and analysed using the same spectroscopic techniques presented in **Chapter 4**; these results will be given in **Section 6.5**. During the growth experiments reported in this chapter, these single seed particles were used as a reference to compare with dimer nanoparticle assemblies.

6.1.2 Dimer spherical seeds

To overcome current limitations with the self-assembly of DNA-large spherical or anisotropic AuNP particles, the seeded growth method was employed using dimers of 5.7 ± 0.2 nm spherical DNA-AuNP as seeds. These will be referred to as ‘dimer seeds’. Single particles, synthesised in **Section 6.1.1,** were functionalised as in **Section 4.3.1.1** with DNA strands Bcc and Ccc (see **Section 3.2.1.1** for sequences). These

strands were altered with clicking groups (DIBO and azide) to ensure the stability of the hybridisation over the seeded growth process [10]. In addition, they also carried a three-thiol anchor to bind more strongly the DNA to the gold surface (see **Section 2.3.2** for background information) [11]. Then, the building blocks were hybridised to form DNA-AuNP dimers with an interparticle distance of about 50 nm. After agarose gel electrophoresis purification, TEM analysis was carried out to characterise the dimer seeds (see **Figure 6.2**).

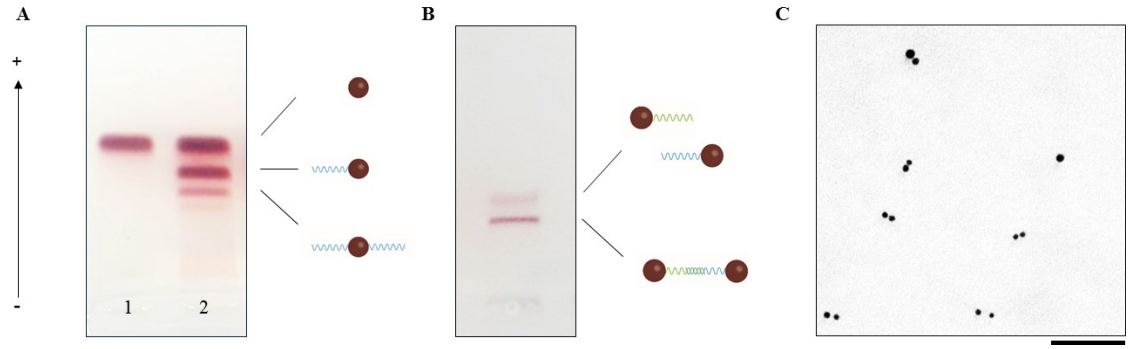

Figure 6.2. Characterisation of 5.7 ± 0.2 nm dimer spherical gold nanoparticle seeds **A)** Agarose gel for purification of DNA-AuNP monoconjugates **B)** Agarose gel for purification of DNA-AuNP dimers **C)** Transmission electron microscopy image. Scale bar is 100 nm

As described in **Chapter 4**, monoconjugates and dimers were separated and analysed using agarose gel electrophoresis (see **Figure 6.2A and B**). By analysing TEM pictures, it was found that 67 % of the assemblies present in solution were dimers. This value is higher than the one found for DNA strands without attached particles in **Section 4.2.3** (53%). This could be attributed to more stringent temperature control during the

hybridisation process. These dimer seeds were then utilised for the synthesis of large spherical and branched AuNP-DNA dimers (see **Sections 6.2 and 6.3**).

6.2 Growing of large spherical single and dimer gold-DNA nanoparticles

The protocol for synthesis of large spherical single and dimer DNA-AuNPs was adapted from a published protocol, originally used to produce gold nanorods [12]. Single and dimer DNA-AuNP seeds were introduced in a growth solution made of CTAB, gold salt and L-ascorbic acid and the reaction was left undisturbed to allow the particles to grow. The growth process of spheres instead of nanorods was achieved by removing the addition of silver from the original protocol. The absence of silver ions, selective surface blockers, allows particles to grow as spheres rather than rods (see **Section 2.2.2** for background information). The solutions quickly turned light pink, and were light purple by the end of the synthesis. A visual difference in colour between single and dimers particles was observed (see **Figure 6.3A**). Particles were purified from the excess CTAB using centrifugation and visualised using TEM (see **Figure 6.3B** and **C**).

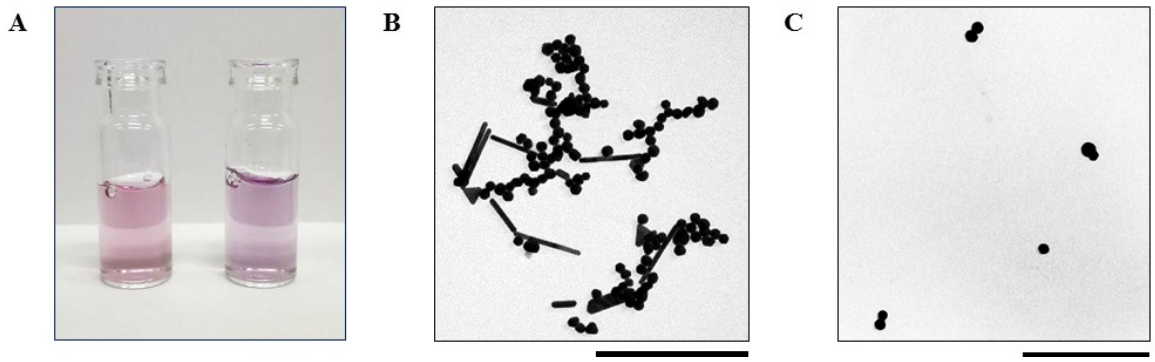

Figure 6.3. Characterisation of single and dimer grown spherical gold nanoparticles **A)** Photography of the final products after growing of single seeds (left) and dimer seeds (right) **B)** Transmission electron microscopy image of single grown spherical gold nanoparticles and **C)** Transmission electron microscopy image of dimer grown spherical gold nanoparticles. Scale bars are 100 nm

The difference in colours observed between the final solution of single and dimer particles was expected. A solution of large dimer nanoparticles with a small interparticle distance exhibits a different colour to single particles due to LSPR interaction (see **Section 2.1** for background information) [13]. The TEM micrograph for the grown single particles solution (see **Figure 6.3B**) showed an important diversity in shape with presence of triangles and rods. Nevertheless, particles effectively grew and measurement of 50 spherical particles present in the mix resulted in an average diameter of 46.4 ± 0.5 nm being calculated. As seen in **Figure 6.2C**, particles present in the dimers solution were grown; measurement of 50 particles gave an average diameter of 39.9 ± 0.6 nm. Also other structures (triangle/sphere, rod/sphere) were also observed on the grids. However, these were rare. No interparticle distance was observed in the grown dimer assemblies. However, the use of TEM to characterise yield or interparticle distance is not ideal due to the drying forces which occur during preparation of the samples [14].

After TEM analysis, it was clear that a purification method to separate the different species in solution (single and dimer particles) was beneficial. In fact, the purification of the various growing products would be beneficial for two reasons. Firstly, the yield of grown dimers obtained would be easier to define and secondly the accuracy of the measurement of optical properties rising from dimers would be increased. Therefore, samples were further purified and their optical properties were further studied (see **Sections 6.4 and 6.5**).

6.3 Growing of non-spherical single and dimer gold-DNA nanoparticles

Branched single and dimer DNA-AuNPs were synthesised using a published protocol [15]. Following the same principle as for spherical particles, single and dimer DNA-AuNP seeds were introduced into a growth solution made of CTAB, gold salt and L-ascorbic acid. An additional reagent, silver nitrate, was also incorporated to induce the formation of the branches at the gold NP surface (see **Section 2.2.2** for background information) [15]. The solution slowly turned from pale grey to light blue, for single particles, and to dark blue for dimers (see **Figure 6.4A**). This colour change gave a preliminary indication of the difference between the products. After purification from the excess CTAB, particles were visualised using TEM (see **Figure 6.4B and C**).

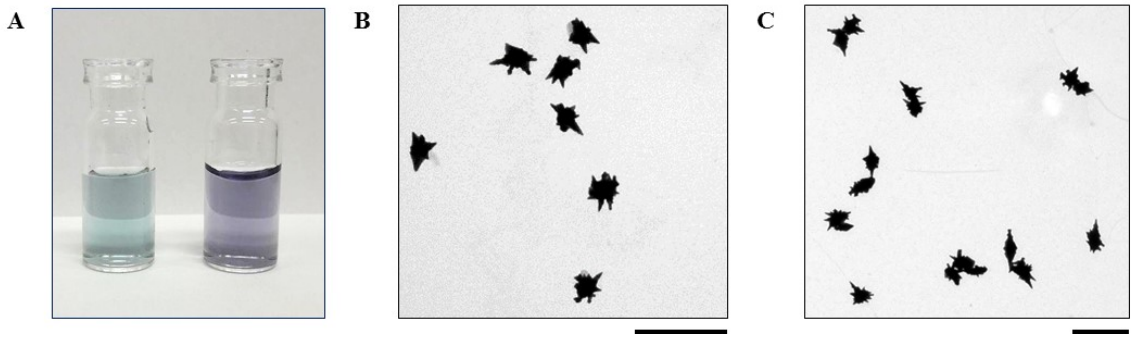

Figure 6.4. Characterisation of single and dimer branched gold nanoparticles **A)** Photography of the final products after growing single seeds (left) and dimer seeds (right) **B)** Transmission electron microscopy image of single grown branched gold nanoparticles and **C)** Transmission electron microscopy image of dimer grown branched gold nanoparticles. Scale bars are 100 nm

An important difference in colour was observed between the final solution of single and dimer particles. During the seeded growth process, this gave a good first indication that there was a difference between the products. The TEM image for the grown single particles solution showed well defined branched particles. These were present on the grid as predominantly single particles with some larger aggregates, probably due to the drying effect on the TEM grid [14]. After counting 50 particles, single branched particles were identified to be 118.6 ± 0.6 nm. During the dimer solution analysis, numerous grown branched dimer assemblies were observed on the grids. After counting 50 particles, their size was determined to be 123.5 ± 0.9 nm. When looking closely at the interparticle space between the dimers, some of them seemed to be linked through a tip. A plausible hypothesis is that the DNA was covered by gold and looked like a tip. Nevertheless, due to the drying forces occurring during the samples preparation, it was hard to confirm the presence of dimers using TEM analysis. To analyse the particles in solution and confirm the presence of dimer assemblies, the use of cryo-TEM would be useful and is envisaged for future experiments [16]. In this work,

spectroscopic techniques have been used to confirm the presence of dimer assemblies (see **Section 6.5)**. The purification technique employed for spherical particles was also applied to branched products (see **Section 6.4**).

6.4 Purification of grown DNA-gold nanoparticles

The experiments presented in this section were carried out with the help of Mr Oliver Freeman for his master degree thesis.

After the previous observations made on the TEM analysis, described above, a process for purification of the grown particles was developed. In the preliminary experiments, the use of depletion forces induced by the addition of cetyl trimethylammonium chloride (CTAC), normally used to separate gold nanorods from unwanted shapes, was investigated [17, 18]. Unfortunately, although this approach was successful for purifying single particles, it did not give satisfying results for the separation of dimer products. Agarose gel electrophoresis was selected as a method for purification, due to it being straightforward and efficient. After the seeded growth process, spherical and branched products were coated with CTAB. When attached to particles, this ligand did not permit separation with agarose gel electrophoresis as the particles were not stable in the TBE buffer used for agarose gel electrophoresis [19]. In order to increase the stability of the grown samples prior to electrophoresis, a ligand exchange between CTAB and a short DNA strand (strand S, see **Section 3.2.1.1** for sequence) was performed using a published protocol [20]. The grown particles, newly covered by a dense DNA shell (see **Sections 2.4.1** and **3.2.1.2** for background

information and experimental procedure), were separated by agarose gel electrophoresis and the different purified products were visualised using TEM (see **Figure 6.5**).

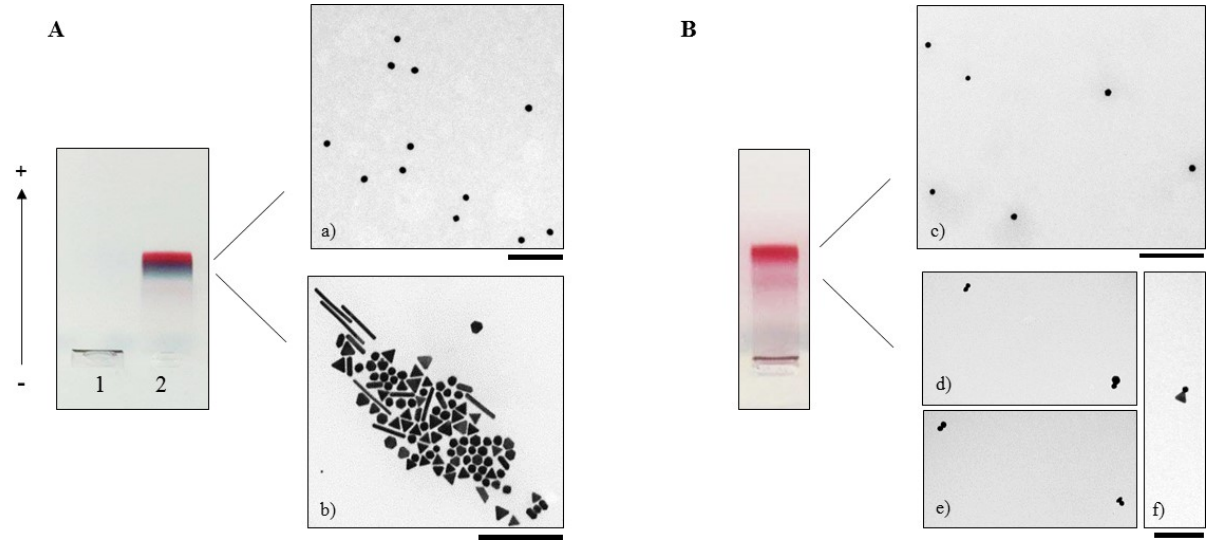

Figure 6.5. Agarose gel electrophoresis purification of **A)** single grown spheres and **B)** dimer grown spheres and TEM analysis of attributed bands. Scales bars are 500 nm

Figure 6.5A presents the purification of grown single spherical particles. Lane 1 of the gel shows CTAB coated grown single spherical particles which aggregated in the well. In lane 2, where DNA coated grown single spherical particles were run, two bands of different colours were observed. The upper one bright pink, contained spherical single AuNPs of 46.4 ± 0.5 nm, as seen in the TEM image. The lower band, dark blue, contained a mixture of other shapes including triangles, rods and polygons. The purification process was successful for single grown particles as the pink band was composed of spherical particles with 100% purity.

Upon analysis purification of the dimer grown assemblies (see **Figure 6.5B)** by agarose gel electrophoresis, two distinct pink bands were observed. As seen on the TEM images, the upper band contained single spherical particles and the lower band contained

dimer assemblies. Some of the observed dimer assemblies were hetero-shape dimers, for example the dimer made of a sphere and triangle, displayed in **Figure 6.5Bf**.

The purification procedure was also successful for the dimer grown spherical particles. Nevertheless, as observed on the gel in **Figure 6.5B**, the intensity of the dimer band was low compared to that of single particles. This indicates a lower yield of grown dimers. When measuring the actual intensity of the bands using ImageJ software, the dimer yield was determined to be 27%. As the yield of dimer seeds introduced in solution was 67%, a 40% loss in dimer yield occurred during the growing process. Three hypotheses could explain this phenomenon. Firstly, it is possible that the dimer seeds grew into a large single spherical structure. However, this idea can be discarded as the sizes of single and dimer grown particles were the same, showing that this hypothesis was unlikely. Secondly, the possibility of DNA denaturing in the acidic conditions of the seeded growth process was investigated. Polyacrylamide gel electrophoresis analyses on DNA, incubated in the synthesis conditions, were carried out. The results (see **Appendix AII.1**) showed that the DNA strands remained intact in the synthesis conditions for the length of time required for the synthesis. The final hypothesis, and most likely hypothesis, is that the DNA strands detach from the particle surface. However, even though a three thiol anchor had been added to the DNA strands to increase their affinity for the gold surface this may not be sufficient. Future discussions with the DNA experts from University of Oxford (Prof. Tom Brown, Nucleic Acids Research Group) could confirm this and attempts could be made to further modify the DNA strands to increase the DNA attachment to the gold nanoparticle seeds.

The difference in shape polydispersity between single and dimer particles during the growing process could be justified by the fact that dimer particles had already been through two agarose gel purification steps before being employed as seeds. To verify

this hypothesis, a seeded growth experiment was performed on single particle seeds with subsequent purification through agarose gel electrophoresis. On this gel, the blue band was fainter, therefore, less triangle and rods are present in the reaction (see **Appendix AII.2**). A lower shape polydispersity was observed in this sample. This experiment validated the hypothesis that grown dimer seeds do not have a polydispersed shape, as their seeds were pre-purified during their synthesis. Therefore, the seeds responsible for the formation of anisotropic grown particles might have been remove during the dimers purification [21].

The purification technique was then employed for branched nanoparticles. However, the results were not as conclusive as with the spherical particles. After electrophoresis, smeared bands were observed on the gel for both the single and dimer particles (see **Figure 6.6**).

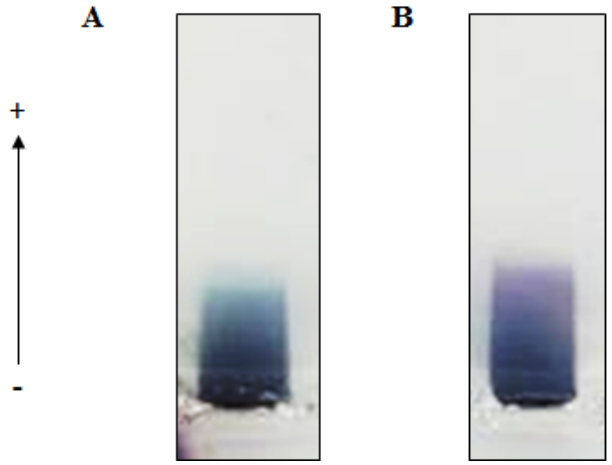

Figure 6.6. Agarose gel electrophoresis of **A)** single grown branched and **B)** dimer grown branched gold nanoparticles using agarose gel electrophoresis

The fact that the particles were running on the agarose gel proved that they carry a DNA shell (without DNA the particles would not migrate). Nevertheless, no clear band was observed. This smearing effect may be explained by the large diversity in shape and

size of the branched nanoparticles. No further purification was developed for branched nanoparticles. One future method could be to purify the nanoparticles using density gradient ultracentrifugation [22]. However, in this study, grown branched particles were analysed using spectroscopic analysis immediately after their synthesis (see **Section 6.5**).

The efficiency of the purification process for the spherical particles was further studied by analysing the optical properties of purified products for both single and dimer assemblies, using spectroscopy (see **Section 6.5.1**).

6.5 Spectroscopy for analysis

Electron microscopy is a useful technique to observe and analyse nanomaterials. Unfortunately, this technique does not give information about the actual state of the material in solution, because of the drying process on a surface. This is a particular disadvantage, especially when studying nanoparticle assemblies. However, spectroscopic techniques do permit the observation of a signal from the overall sample in its colloidal form. As performed in **Chapter 5** on DNA-AuNP assemblies synthesised *via* DNA hybridisation, extinction and scattering spectroscopies were employed to analyse the content of the grown AuNP solutions, previously described in **Sections 6.2** and **6.3** (see **Section 6.5.1**). Furthermore, real time spectroscopy was used to follow the growing process of the different types of particles (see **Section 6.5.2**).

6.5.1 Extinction and scattering measurements of grown AuNPs

Extinction and scattering spectra were obtained from seeds, grown spherical particles and grown branched particles, both in their single and dimer forms. Single and dimer grown spherical particle measurements are shown in **Figure 6.7A** and **B,** while single and dimer grown branched particles data are shown in **Figure 6.7C**. Scattering data for the branched particles are not shown as they were not useable after processing due to baseline recording error.

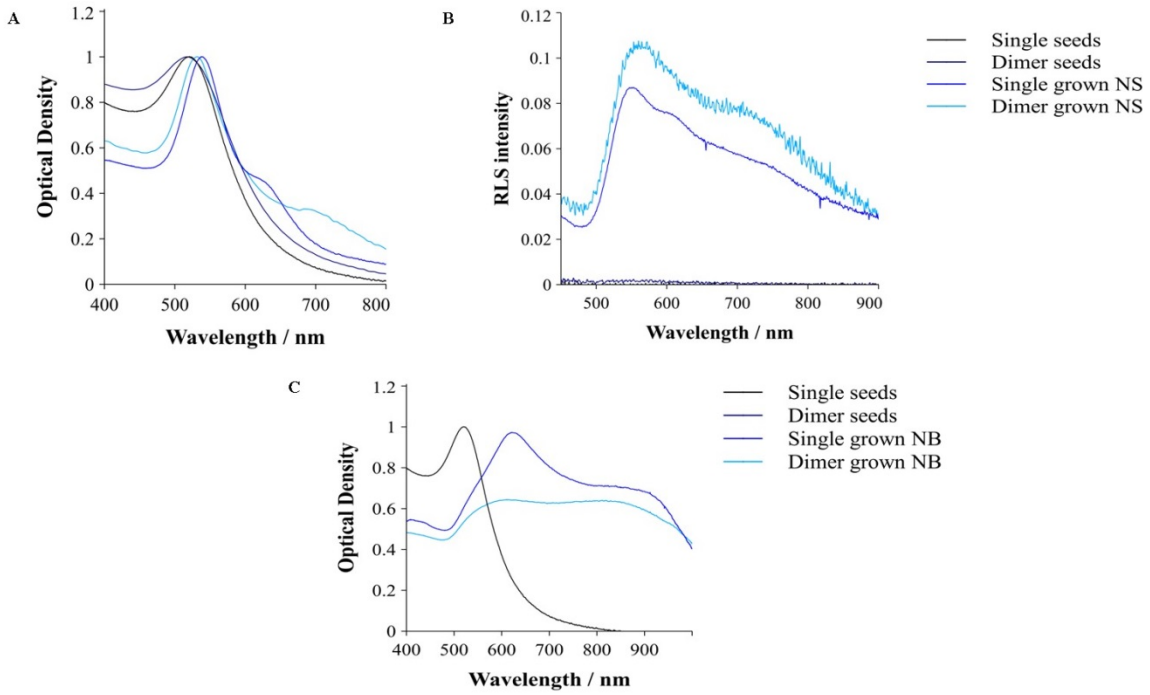

Figure 6.7. Extinction and scattering measurements of grown AuNPs **A)** Normalised extinction spectra of single and dimer seed and grown spherical particles **B)** Scattering spectra of single and dimer seeds and grown spherical particles and **C)** Normalised extinction spectra of single and dimer seeds and grown branched particles

Extinction spectra were normalised to 1 at their maximum in order to compare their shapes. Scattering spectra were processed using Ludox as a reference as described in **Section 2.1.1**.

As already pointed out in **Chapter 5**, extinction spectra for single and dimer seeds are extremely similar in shape with a maximum wavelength at 519 nm (see **Figures 6.7A or C**). In dimer seed assemblies, as the particles were extremely small (5.7 ± 0.2 nm) and far apart (around 50 nm), no interaction occurs. This results in a spectrum similar to single particles. The scattering response of the seed particles for both single and dimers were also discussed previously (see **Chapter 5**). An extremely weak signal was observed, as expected (see **Figure 6.7B**). In fact it is known that at the plasmon resonance, 20 nm spherical particles only scatter 1% of the incident photon flux [23].

The extinction spectrum of single grown spherical particles differs from the single seed nanoparticle spectrum. Importantly, a red shift of the maximum wavelength of 18 nm was observed. This shift is characteristic of the size of the particles increasing during the growing process [24]. Furthermore, in addition to the characteristic sharp peak of the LSRP at 537 nm, an extra shoulder at 630 nm was observed. This new peak appeared during the seeded growth process and is attributed to the non-spherical shapes present in solution (rods, triangles and polygons, see **Section 6.2**). As for single grown spherical particles, the spectrum of dimer assemblies exhibited a red shift of 13 nm compared to the dimer seed solution. This shift was smaller in comparison with single particles. This can easily be explained by the difference in the size of the individual particles in the dimer form, compared with single particles; the sizes were 39.9 ± 0.6 nm and 46.4 ± 0.5 nm, respectively. Moreover, a second peak was observed at 700 nm. This new peak did not appear in the spectrum of dimer seeds or single grown particles and was attributed to the LSPR interaction between the individual particles of a dimer. The spectrum can be described as a rod-like shape where a transversal and a longitudinal SPR was observed.

The scattering data of the spherical particles showed a distinct increase in size during the growing process, as displayed by the increase in scattering intensity between seed and grown signals (single and dimers). As for the extinction signal, the single grown particles spectra exhibited two peaks. A major peak at 550 nm was observed and was characteristic of spherical particles. A shoulder at 610 nm was also observed which was attributed to the presence of non-spherical particles in the single grown spherical solutions.

The scattering spectrum of the dimer grown spherical particles showed two distinct peaks. The first peak was at 562 nm and the second at 735 nm. The shape of the dimer spectrum was in accordance with data from the literature and is in line with the presence of dimer assemblies in solution [13].

Extinction data from the single branched nanoparticles showed a characteristic shape with a peak at 620 nm. As suggested in the literature, this fairly broad peak could be attributed to the transversal SPR of the branches themselves [25]. A second peak, due to the elongated shape of the particle branches, is normally observed in the near infrared (NIR) [26]. Extinction data from the dimer branched nanoparticles was similar to that of the single nanoparticles and also showed a characteristic shape with a peak at 620 nm. Nevertheless, this peak was less distinct. Even if a difference between single and dimers was noted, measurements would have to be carried out with a spectroscopic instrument more sensitive in the NIR to delineate this further. As branched nanoparticles have heterogeneous structures, it would also be best to study their optical properties using single particle spectroscopy [25].

Extinction and scattering spectroscopy data for the single and dimer grown spherical particles were in agreement with the theory and the TEM analysis presented

in **Sections 6.2** and **6.3**. The formation of large dimer spherical gold nanoparticles was confirmed by the spectroscopic analysis. The data also showed interesting results regarding the growing of branched particles.

The grown spherical particles purified by agarose gel electrophoresis were also characterised by spectroscopy (see **Section 6.4**). Unpurified samples and the different products extracted from the agarose gel were studied and data are shown in **Figure 6.8**.

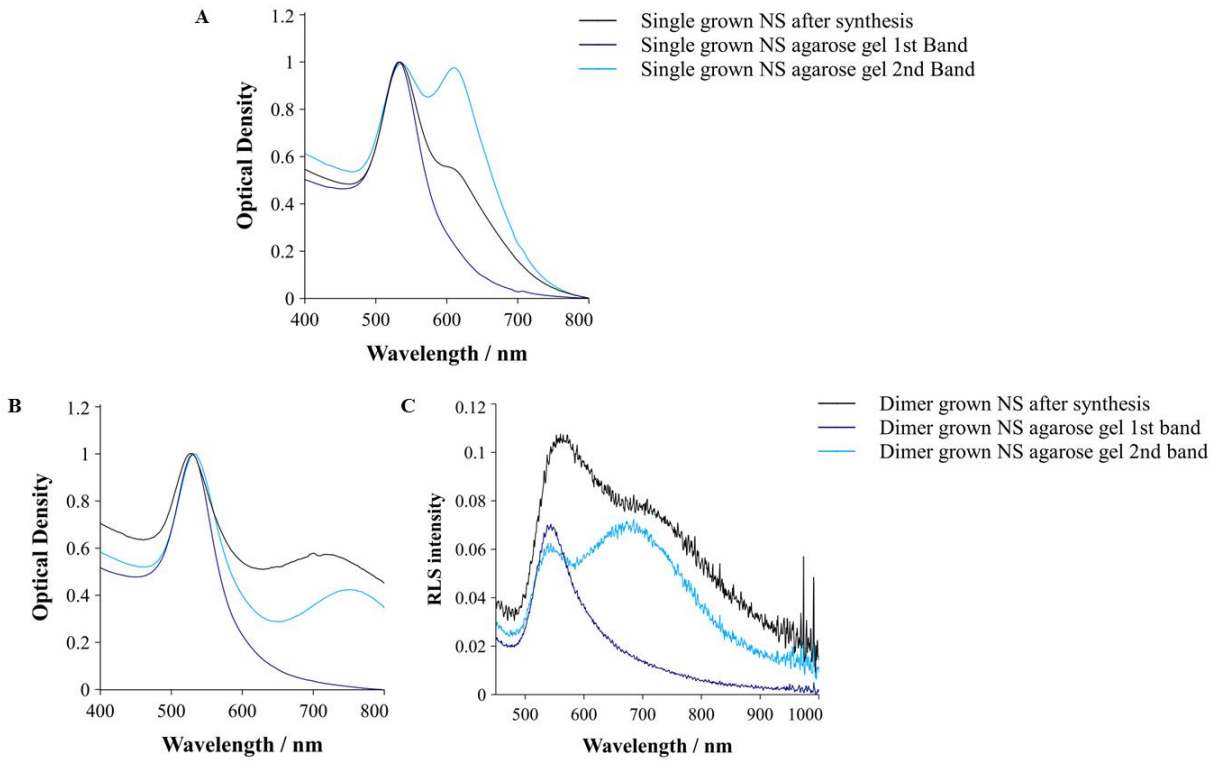

Figure 6.8. Spectroscopy analysis of the purification process. **A)** Normalised extinction spectra of purified single grown spherical particles **B)** Normalised extinction spectra of purified dimer grown spherical particles and **C)** Normalised scattering spectra of purified dimer grown spherical particles

Figure 6.8A shows the extinction spectra of single grown spherical particles before and after purification. The particles contained in the upper pink band in **Figure**

6.5A exhibited a sharp peak at 534 nm. This shape and value is coherent with 46 nm spherical gold nanoparticles. The spectrum from the lower blue band showed two peaks. One was at 534 nm and is due to the quasi spherical polygon particles in solution. The second peak was at 610 nm and was attributed to the optical response of the anisotropic shape in solution. The clear increase in intensity of this second peak, which is absent in the upper band spectrum, indicates the success of the purification process.

The dimer solution was investigated in more detail using light scattering spectroscopy in addition to extinction spectroscopy. In **Figure 6.8B**, all spectra presented a sharp peak at 530 nm. This peak was attributed to the extinction of 40 nm spherical particles. It can thus be concluded that the first band in the dimer agarose gel (see **Figure 6.5B**) only contained single spherical monodispersed particles. The spectrum of the dimers showed two peaks as in the non-purified sample. Nevertheless, in the dimer spectrum the second peak at 752 nm was more defined than for the non-purified sample. This phenomenon indicates the purification of the large spherical gold nanoparticle dimers. The scattering measurements presented in **Figure 6.8C** are in agreement with this analysis. While the first band of the gel show a spectrum comparable to the one described by Mie theory for 40 nm spherical gold nanoparticles, the one from the second band was similar to scattering spectra depicted in the literature for large spherical gold nanoparticles [13].

The use of spectroscopy permits the analysis of the newly grown assemblies in solution, to confirm the formation and purification of the dimer assemblies. In order to understand more about the synthesis process, the same techniques were employed to follow it in real time.

6.5.2 Time-resolved spectroscopic measurements

To investigate the seeded growth process and adjust the synthetic protocol, the optical response of particles was recorded in real time using extinction and scattering spectroscopy. This was achieved by undertaking the growing process directly in the spectroscopic cuvettes. In the case of RLS measurements, appropriate dilutions of all the reagents were made to avoid signal saturation. As shapes of the different spectra have already been discussed in the previous section (see **Section 6.5.1**) no further comments will be added. The spherical particles, single and dimers, were studied first and the results are shown in **Figure 6.9**.

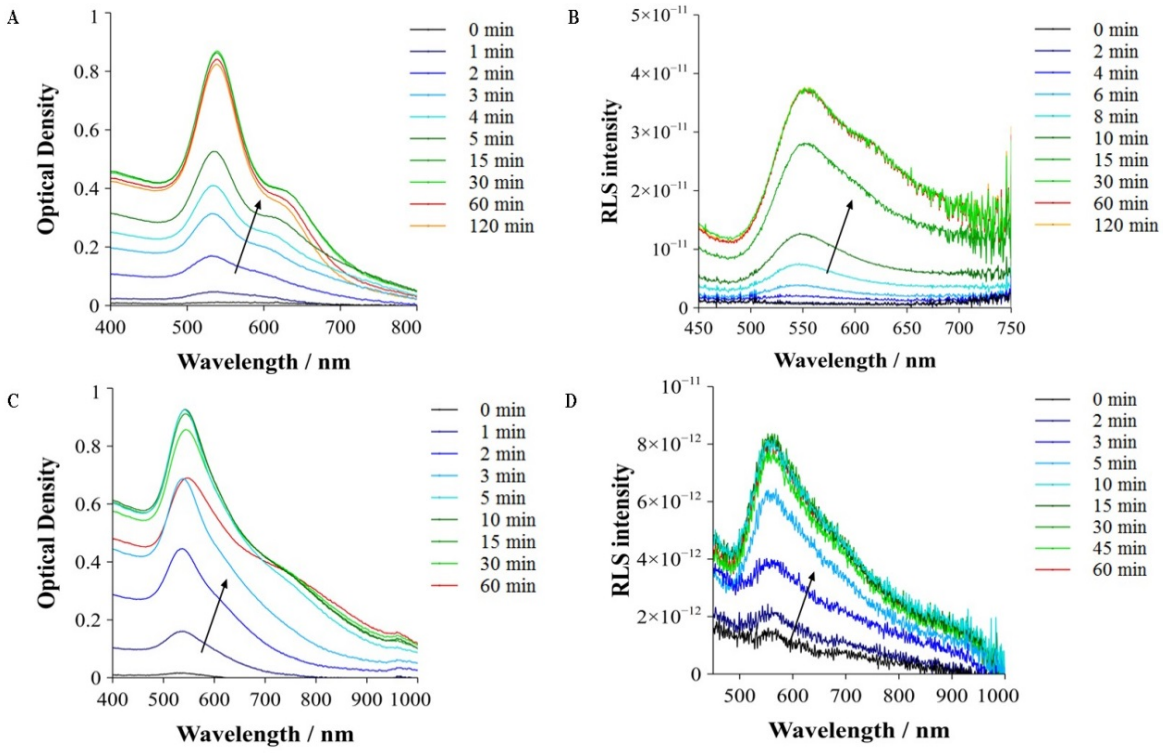

Figure 6.9. Time-resolved measurements of spherical particles during the growing process **A)** Extinction and **B)** scattering spectra of single grown spherical AuNPs **C)** Extinction and **D)** scattering spectra of dimer grown spherical AuNPs

According to the extinction spectra in **Figure 6.9A,** the completion of the single spherical particle's growing was attained as early as 15 minutes. No further increased of optical density of the sample was observed after this time. Therefore, on basis of this analysis, the growing process could be considered to be complete. However, when looking at the scattering data, the growth seems to need at least 30 minutes to be completed. This difference can be explained by the difference in sensitivity between the two techniques, with the RLS technique being more sensitive towards changes in particle diameter. It could also be envisaged that the dilution of the mixture played a role and slowed the reaction down.

Based on these measurements, the growth of dimers was then followed over 60 minutes. The extinction spectrum of the dimer assemblies at 60 minutes showed a decrease in optical density at 547 nm and an increase at 758 nm. As the particles grow, the interparticle distance decreased and the LSPR interaction become stronger. Therefore, less single particle signal at 547 nm was observed, but there was more dimer signal at 758 nm recorded. This observation illustrates the formation of dimers by growing in the solution in real time. Scattering data for the dimers did not show this process. The spectra were not modified after 10 minutes. Further experiments should be carried out using a larger time scale in order to confirm the formation of dimers by RLS.

The same experiments were carried out, as above, for branched particles, for both single and dimer particles; the results are shown in **Figure 6.10**.

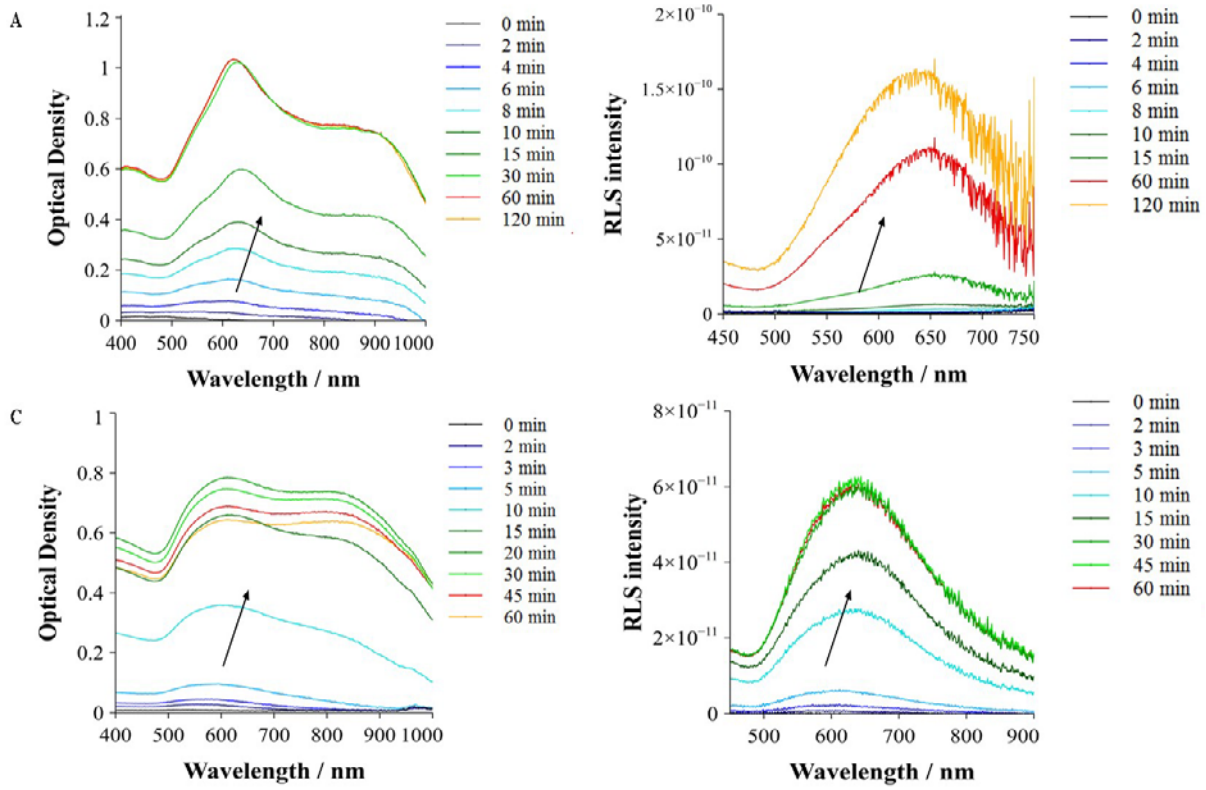

Figure 6.10. Time-resolved measurements of the growth process of branched particles during the growing process **A)** Extinction and **B)** scattering spectra of single grown branched AuNPs **C)** Extinction and **D)** scattering spectra of dimer grown branched AuNPs

Extinction spectra in **Figure 6.10A** showed that the seeded growth process for single branched particles is completed after 30 minutes. Nevertheless, according to the scattering measurements, modification of the particles shape is likely to last for at least 120 minutes. The most plausible explanation for this delay is that the branches of the particles keep elongating after 30 minutes, changing the scattering response of the solution.

The results for the dimer assemblies were different from those for the single ones. On one hand, extinction data showed that the growing process for dimer assemblies was terminated at around 60 minutes. However, the scattering data stayed constant after 30 minutes. While these data are hard to interpret, the decrease of the

optical density at 603 nm in **Figure 6.10C** gives a good indication that the dimers had formed. This signal, attributed to the single branched particles, decreased after 20 minutes, showing a decrease of signal coming from the single particles. The hypothesis is that a signal above 1000 nm due to plasmon interactions might be observed in parallel to this diminution. As stated above, complementary measurements within this range (>1000 nm) would have to be conducted with another instrument.

It was possible to follow the kinetics of the seeded growth process and estimate when the syntheses were completed. Even if the growing process in each case started quickly (signal started to increase after only 2 minutes), its completion seemed to take around 60 minutes for spherical particles and 120 minutes for branched ones. These data are important for future work where experiments adjusting the time can be used to tune the size of the assemblies. For example, in order to obtain smaller assemblies, the synthesis would need to be quenched early on in the process (<10 minutes).

6.6 Preliminary work toward a new method for DNA metallisation

Preliminary experiments have been undertaken to apply seeded-growth method to DNA metallisation. As described in the background chapter (see **Section 2.5**), DNA metallisation is the action of crystallising metal atoms inside or around a DNA template [27]. This method could be employed to achieve the synthesis of designed anisotropic gold nanoparticles bearing a controlled number of branches [28].

In this section, the long DNA A (86 bp) which was used as template was attached to small gold nanospheres. A recently published protocol has been used in order to start investigating the feasibility of using the seeds previously synthesised in **Section 4.4.1** in DNA metallisation experiments [28]. Six different types of particles were used in this seeded growth protocol. The first three were made of 5.7 ± 0.2 nm particles, capped with BSPP and bearing from zero to two DNA templates. The following three were capped with a DNA shell (Strand S, see **Section 3.2.1.1** for sequence) and had from zero to three DNA templates. The synthesis consisted of incubating the seeds with a gold salt solution and the reducing agent hydroxylamine hydrochloride for 15 minutes. The DNA shell was added to the surface of the seeds to assess if it had an impact on the metallisation of the DNA template. The hypothesis was that the negatively charge DNA shell would repeal the DNA template from sticking to the gold nanoparticle surface via electrostatic repulsions. It was assumed that the DNA shell linked to the surface via thiol bonds would be more efficient that the negative BSPP molecules and the metallisation of the DNA would therefore be improved. First experiments were carried out using ssDNA. TEM analysis of the different metallised seeds can be observed in **Figure 6.11**.

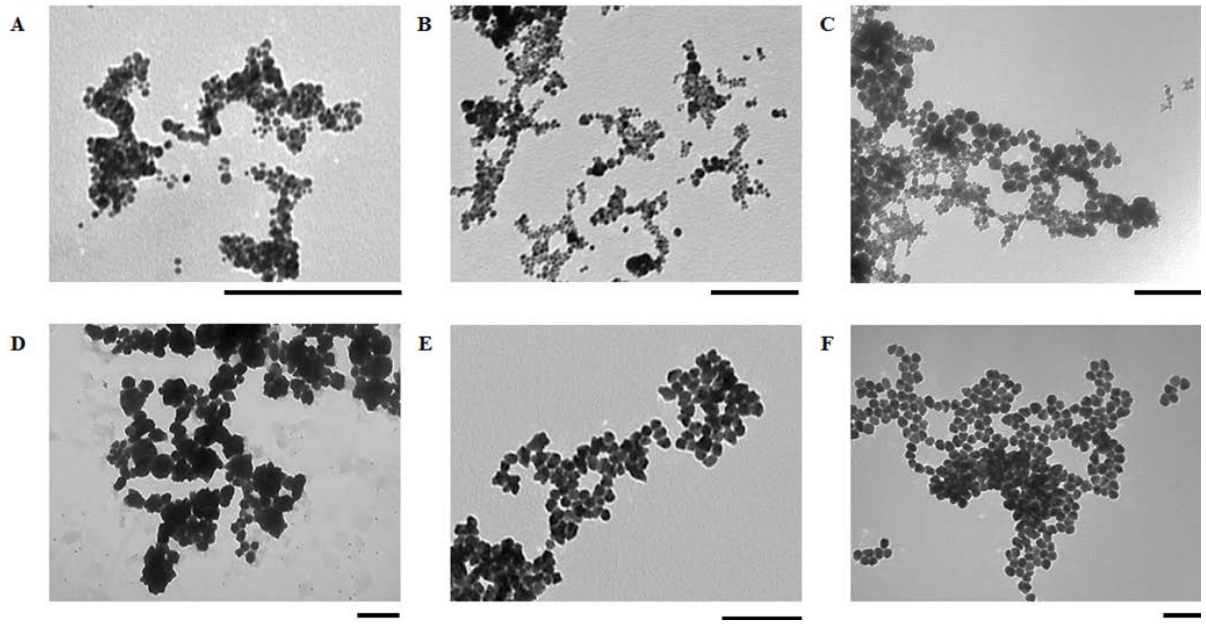

Figure 6.11. DNA metallisation using different types of seeds. **A)** 5.7 ± 0.2 nm BSPP AuNPs, **B)** 5.7 ± 0.2 nm BSPP monoconjugates AuNPs, **C)** 5.7 ± 0.2 nm BSPP DNA diconjugates AuNPs, **D)** 5.7 ± 0.2 nm DNA shell AuNPs, **E)** 5.7 ± 0.2 nm DNA shell monoconjugates AuNPs, **F)** 5.7 ± 0.2 nm DNA shell diconjugates AuNPs. Scales bares are 200 nm

The first general observation from these images is that the DNA metallisation of the long template was not achieved as no single or di-branched particles can be observed in any of the pictures in **Figure 6.11B, C, E** or **F**. All syntheses achieved with BSPP coated particles (see **Figure 6.11A to C**) showed particles which were polydispersed in size. The addition of the DNA shell seemed to have increased the size and shape disparity in the samples, as seen in **Figure 6.11 D to F**. Therefore, the growing could be directed by the presence of the DNA shell at the surface of the seeds.

Even if the primary aim of these first experiments, to precisely metallised DNA template was not achieved, it gave valuable information about the use of a DNA shell at the surface of the seed to enhance size and shape monodispersity. No further analysis were carried out on these materials.

In this chapter, the success of the new synthesis for large spherical or non-spherical gold nanoparticle dimers, based on seeded growth method, was confirmed by full spectroscopic and electrophoretic analysis. This work constitutes a solid base for the development of the technique. Future work and outcomes will be discussed in **Chapter 7**.

6.7 References

1. Alivisatos, A.P., et al., *Organization of 'nanocrystal molecules' using DNA.* Nature, 1996. **382**: p. 609.
2. Diaz Fernandez, Y.A., et al., *The conquest of middle-earth: combining top-down and bottom-up nanofabrication for constructing nanoparticle based devices.* Nanoscale, 2014. **6**(24): p. 14605-14616.
3. Liu, X., et al., *Au–Cu2–xSe Heterodimer Nanoparticles with Broad Localized Surface Plasmon Resonance as Contrast Agents for Deep Tissue Imaging.* Nano Letters, 2013. **13**(9): p. 4333-4339.
4. Harimech, P.K., et al., *Reversible Ligation of Programmed DNA-Gold Nanoparticle Assemblies.* Journal of the American Chemical Society, 2015. **137**(29): p. 9242-9245.
5. Claridge, S.A., et al., *Isolation of discrete nanoparticle - DNA conjugates for plasmonic applications.* Nano Letters, 2008. **8**(4): p. 1202-1206.
6. Tan, S.J., et al., *Building plasmonic nanostructures with DNA.* Nature Nanotechnology, 2011. **6**: p. 268.
7. Gole, A. and C.J. Murphy, *Seed-Mediated Synthesis of Gold Nanorods: Role of the Size and Nature of the Seed.* Chemistry of Materials, 2004. **16**(19): p. 3633-3640.
8. Watt, J., et al., *Effect of Seed Age on Gold Nanorod Formation: A Microfluidic, Real-Time Investigation.* Chemistry of Materials, 2015. **27**(18): p. 6442-6449.
9. Piella, J., N.G. Bastus, and V. Puntes, *Size-Controlled Synthesis of Sub-10-nanometer Citrate-Stabilized Gold Nanoparticles and Related Optical Properties.* Chemistry of Materials, 2016. **28**(4): p. 1066-1075.
10. Heuer-Jungemann, A., et al., *Copper-free click chemistry as an emerging tool for the programmed ligation of DNA-functionalised gold nanoparticles.* Nanoscale, 2013. **5**(16): p. 7209-7212.
11. Li, Z., et al., *Multiple thiol-anchor capped DNA–gold nanoparticle conjugates.* Nucleic Acids Research, 2002. **30**(7): p. 1558-1562.
12. Nikoobakht, B. and M.A. El-Sayed, *Preparation and growth mechanism of gold nanorods (NRs) using seed-mediated growth method.* Chemistry of Materials, 2003. **15**(10): p. 1957-1962.

13. Loumaigne, M., et al., *Optical extinction and scattering cross sections of plasmonic nanoparticle dimers in aqueous suspension.* Nanoscale, 2016. **8**(12): p. 6555-6570.

14. Barrow, S.J., et al., *Surface Plasmon Resonances in Strongly Coupled Gold Nanosphere Chains from Monomer to Hexamer.* Nano Letters, 2011. **11**(10): p. 4180-4187.

15. Day, H.A., et al., *Controlling the three-dimensional morphology of nanocrystals.* Crystengcomm, 2010. **12**(12): p. 4312-4316.

16. Busson, M.P., et al., *Optical and Topological Characterization of Gold Nanoparticle Dimers Linked by a Single DNA Double Strand.* Nano Letters, 2011. **11**(11): p. 5060-5065.

17. Scarabelli, L., et al., *A "Tips and Tricks" Practical Guide to the Synthesis of Gold Nanorods.* The Journal of Physical Chemistry Letters, 2015. **6**(21): p. 4270-4279.

18. Park, K., H. Koerner, and R.A. Vaia, *Depletion-Induced Shape and Size Selection of Gold Nanoparticles.* Nano Letters, 2010. **10**(4): p. 1433-1439.

19. Hanauer, M., et al., *Separation of Nanoparticles by Gel Electrophoresis According to Size and Shape.* Nano Letters, 2007. **7**(9): p. 2881-2885.

20. Shi, D.W., et al., *A facile and efficient method to modify gold nanorods with thiolated DNA at a low pH value.* Chemical Communications, 2013. **49**(25): p. 2533-2535.

21. Park, K., et al., *Optimizing Seed Aging for Single Crystal Gold Nanorod Growth: The Critical Role of Gold Nanocluster Crystal Structure.* Journal of Physical Chemistry C, 2016. **120**(49): p. 28235-28245.

22. Chandra, K., et al., *Separation of Stabilized MOPS Gold Nanostars by Density Gradient Centrifugation.* ACS Omega, 2017. **2**(8): p. 4878-4884.

23. Navarro, J.R.G. and M.H.V. Werts, *Resonant light scattering spectroscopy of gold, silver and gold-silver alloy nanoparticles and optical detection in microfluidic channels.* Analyst, 2013. **138**(2): p. 583-592.

24. Bastus, N.G., J. Comenge, and V. Puntes, *Kinetically Controlled Seeded Growth Synthesis of Citrate-Stabilized Gold Nanoparticles of up to 200 nm: Size Focusing versus Ostwald Ripening.* Langmuir, 2011. **27**(17): p. 11098-11105.

25. Nehl, C.L., H. Liao, and J.H. Hafner, *Optical Properties of Star-Shaped Gold Nanoparticles.* Nano Letters, 2006. **6**(4): p. 683-688.

26. Khoury, C.G. and T. Vo-Dinh, *Gold Nanostars For Surface-Enhanced Raman Scattering: Synthesis, Characterization and Optimization.* The journal of physical chemistry. C, Nanomaterials and interfaces, 2008. **2008**(112): p. 18849-18859.

27. Burley, G.A., et al., *Directed DNA Metallization.* Journal of the American Chemical Society, 2006. **128**(5): p. 1398-1399.

28. Ma, X., et al., *Gold nanocrystals with DNA-directed morphologies.* Nature Communications, 2016. **7**.

Chapter 7. Conclusion and Outlook

If the typical colours of gold nanoparticles have fascinated men for centuries, their properties are still under vigorous scientific investigations. It has been established and modelled that the size and shape of gold nanoparticles influence their optical properties [1]. This phenomenon goes even further when particles interact with others in 2 or 3D structures[2].

Since Alivisatos and Mirkin introduced the use of oligonucleotides as scaffold for self –assembled gold nanoparticles, the field has shown a vibrant interest [3, 4]. Nevertheless much progress in term of diversification of the library of assemblies is still to be made. This would enable researchers to obtain new materials exhibiting new properties.

The aim of this thesis was to synthesise programmed DNA-AuNP assemblies and to study their physicochemical properties.

A summary of the main results for each chapter is presented in **Section 7.1**, while a discussion about future work can be found in **Section 7.2**.

7.1 Summary of results

In **Chapter 4**, particles of different sizes (4.5, 12.1, 31.3 and 47.4 nm) were successfully synthesised. The smaller ones (4.5 and 12.1 nm) were functionalised with a specific number or a dense shell of DNA depending on their applications. A new strategy to functionalise the larger particles with a specific number of DNA was developed. The strategy showed promising results using 12.1 nm AuNPs. Unfortunately it could not be applied to larger particles due to their lack of stability. DNA-AuNP dimer assemblies were successfully synthesised using the previous building blocks. Some trimers were also synthesised but they quantity was not appropriate for measurement of optical, diffusion or sedimentation properties. The physicochemical properties of all the other gold nanoparticles or DNA-AuNP conjugates synthesised were investigated.

In **Chapter 5**, physicochemical properties of AuNPs in the range 5 to 50 nm in their single state or as DNA-AuNP assemblies were studied. Extinction and scattering spectroscopies of the smallest particles did not permit differentiation between single and assembled gold nanoparticles. This was due to the small sizes of the NPs (low scattering properties) and the large interparticle distance in dimer assemblies. Diffusion coefficients were measured using microfluidics and TPPL-FCS. Both techniques gave similar results and unlike the spectroscopy it was possible to distinguish between single and dimers AuNPs. The sedimentation process of various particles was quantified using digital photography and results were successfully applied to centrifugation experiments.

Lastly in **Chapter 6**, a new synthesis for large spherical or branched gold nanoparticle dimers, based on seeded growth method, was developed. If the synthesis process seemed to have work effectively, the results regarding the yield and the

purification of pure large spherical or branched gold nanoparticle dimers were less successful (especially for the branched). Furthermore, extinction and scattering spectroscopies were used to characterise the final products, the synthesis process and the purification step. As this work constituted a solid base to show the success of the technique, some future work will be discussed in **section 7.2**.

7.2 Outlook: Future work

The results achieved in this thesis gave further information about the properties of gold nanoparticles and DNA-AuNP assemblies. Nevertheless, this work also left some unresolved hypothesis. This section contains the main ideas for further potential investigations.

In **chapter 4**, only DNA-NP homodimers in size, shape and composition were synthesised. In order to develop the library the next step would be to create first, using the same process, hetero-sized structures (see **Figure 7.1**).

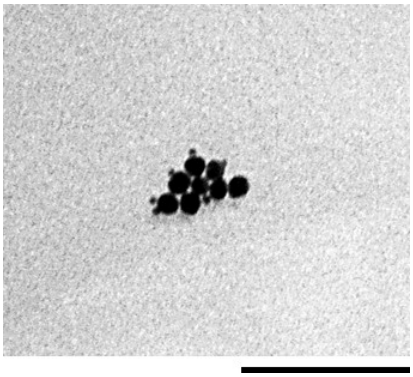

Figure 7.1. TEM pictures of gold nanoparticles heterodimers of 4.5 and 12.1 nm. Scale bar is 100 nm

The next degree of complexity would be to also synthesise heterodimers in shape and composition. Furthermore, as described in **Chapter 2**, the four strand DNA system used in this project was originally designed to form tetrahedron structures. The next step would therefore to synthesised first homogenous and then heterogeneous larger assemblies as trimers or tetrahedron. Optical characterisation of these kind of assemblies using the techniques employed in this thesis (UV-Vis, RLS, PTOFS, and TPPL-FCS, see **Chapter 5**) would give interesting information regarding the behaviour of mutli-properties assemblies. In order to facilitate the interaction between the different particles and be able to detect more plasmon coupling in assemblies, the DNA system used could be revised.

In **Chapter 5**, microfluidics showed the capacity to measure diffusion coefficients and differentiate between single and dimer assemblies. As particles can be synthesised in microfluidics, it would in theory be possible to create a synthesis/functionalisation/purification microfluidic circuit which would synthesised and purified DNA-AuNP assemblies in a continuous flow [5].

The seeded growth method developed in **Chapter 6** to synthesise large or anisotropic DNA-AuNP dimers presents a lot of potential. After increasing the stability of the binding between DNA and the particles surface, the method could be extended to different particle shapes (rods, triangles, cubes). Numerous experiments were carried on to synthesised gold nanorods dimers but none was successful. The complexity of the assemblies can also be developed by using trimer or tetrahedron seeds as starter points. Preliminary experiments of visualisation of grown assemblies in solution have been carried on, at the ENS Rennes in collaboration with Clyde Midelet. Dimers of branched grown gold nanoparticles were introduced in a simple microfluidic channel and dark-field video was recorded. Particles were observed in real-time and some of them seemed

to be constituted by two single particles (they exhibited a stronger intensity) (see **Figure 7.2**).

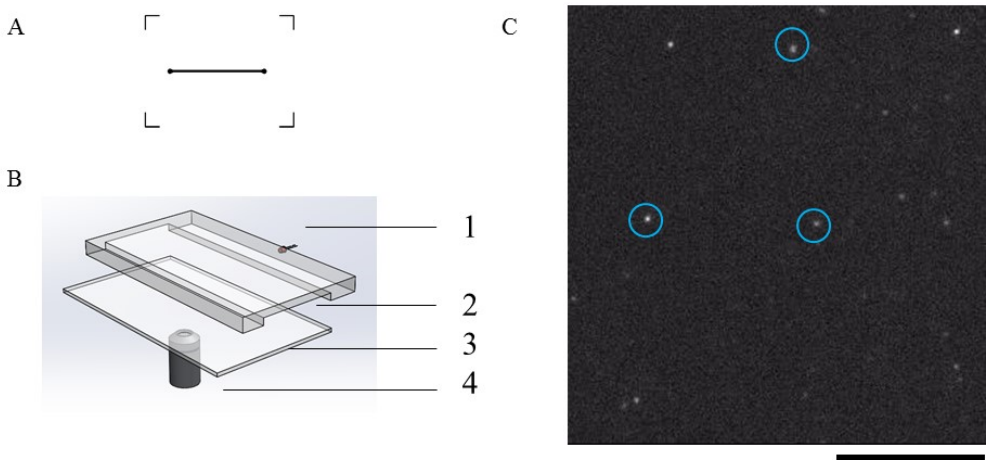

Figure 7.2. A) Schematic representation of the microfluidic channel used in the experiment. **B)** Details of the microfluidic apparatus, with 1: Light-emitting diode (LED) illumination (625 nm), 2: micro channel PDMS, 3: microscopy glass and 4: microscope objective (x20). **C)** Snapshot of the dark-field microscopy video recorded. Scale bar is 10 µm

It is interesting to note that when LED illumination of different wavelengths (525, 590, 605 nm) were used no signal was observed. This could be useful to analyse the composition of solutions assuming that single and assembled particles have different optical responses. Real time dark field microscopy could be further incorporated in the synthesis/functionalisation/purification microfluidic circuit mentioned above to characterised in real time the grown assemblies directly in microfluidic channels [6].

Finally, DNA metallisation could be employed to metallised DNA onto DNA-AuNP assemblies synthesised in this work. Different protocols are available to cover DNA with gold or silver. Particles and assemblies can be designed using specific metallisation of DNA as for example gold nanoparticles bearing silver branches.

7.3 References

1. Eustis, S. and M.A. El-Sayed, *Why gold nanoparticles are more precious than pretty gold: Noble metal surface plasmon resonance and its enhancement of the radiative and nonradiative properties of nanocrystals of different shapes*. Chemical Society Reviews, 2006. **35**(3): p. 209-217.

2. Wang, L., et al., *Dynamic Nanoparticle Assemblies*. Accounts of Chemical Research, 2012. **45**(11): p. 1916-1926.

3. Mirkin, C.A., et al., *A DNA-based method for rationally assembling nanoparticles into macroscopic materials*. Nature, 1996. **382**(6592): p. 607-609.

4. Alivisatos, A.P., et al., *Organization of 'nanocrystal molecules' using DNA*. Nature, 1996. **382**: p. 609.

5. Chen-Hsun, W., et al. *Synthesis of gold nanoparticles using microfluidic reaction systems*. in 2007 7th IEEE Conference on Nanotechnology (IEEE NANO). 2007.

6. Thiele, M., et al., *Combination of microfluidic high-throughput production and parameter screening for efficient shaping of gold nanocubes using Dean-flow mixing*. Lab on a Chip, 2017. **17**(8): p. 1487-1495.

Appendices. Supplementary information

AI. Supplementary information for Chapter 5

In **Section 5.1.2.3**, RLS was used to study the DNA hybridisation during dimer formation. In order to evaluate the time needed for samples to reach the set up temperature in the thermostatic cuvette holder, the evolution of RLS intensity at λ_{max} of a Rhodamine B sample was followed.

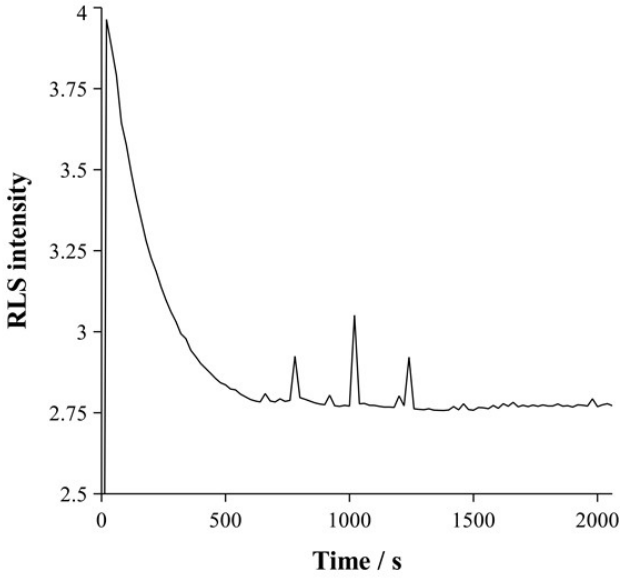

Figure AI.1. Evolution of RLS intensity at λmax of Rhodamine B sample at a constant temperature of 50 °C

When temperature is applied to Rhodamine B its RLS intensity decreases. As observed in **Figure AI.1** the RLS intensity of the Rhodamine B plateaued after 625 s (≈ 10 minutes).

Furthermore prior to hybridisation experiments, the stability of G_0 AuNPs in the presence of salt was studied.

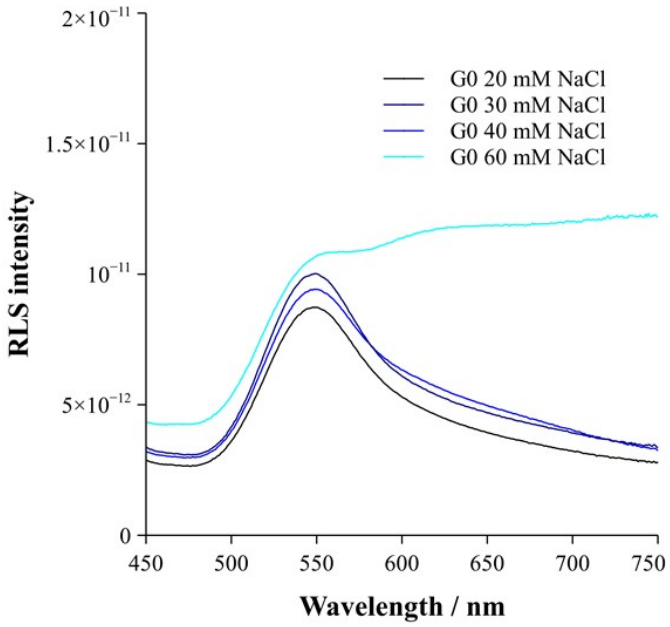

Figure AI.2. Evolution of RLS spectra for G_0 BSPP with increasing NaCl concentration in phosphate buffer

In **Figure AI.2**, a shoulder around 600 nm showed that particles started aggregating in the solution containing 40 mM NaCl. This phenomenon was even clearer at 60 mM NaCl.

To study the influence of the buffer during the hybridisation process all experiments were also carry out in Milli-Q water.

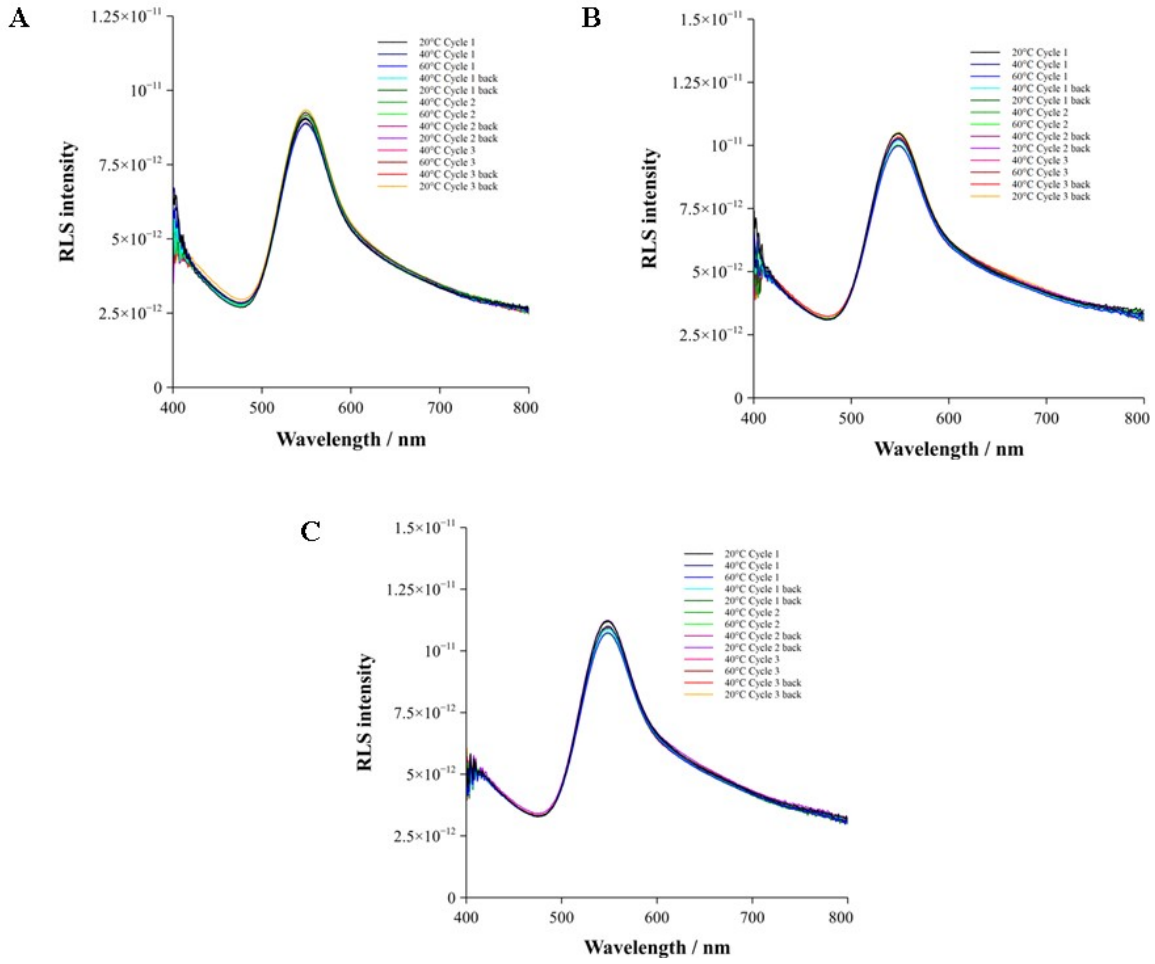

Figure AI.3. Evolution of RLS spectra of **A)** G_0 BSPP **B)** G_0 DNA monoconjugates and **C)** G_0 DNA shell particles with increasing temperature in Milli-Q water

No particular change was observed when studying the evolution of RLS spectra of G_0 BSPP, G_0 DNA monoconjugates and G_0 DNA shell particles with increasing temperature in Milli-Q water (see **Figure AI.3**).

In **Section 5.2**, diffusion properties of AuNP and DNA-AuNP assemblies were studied using microfluidics.

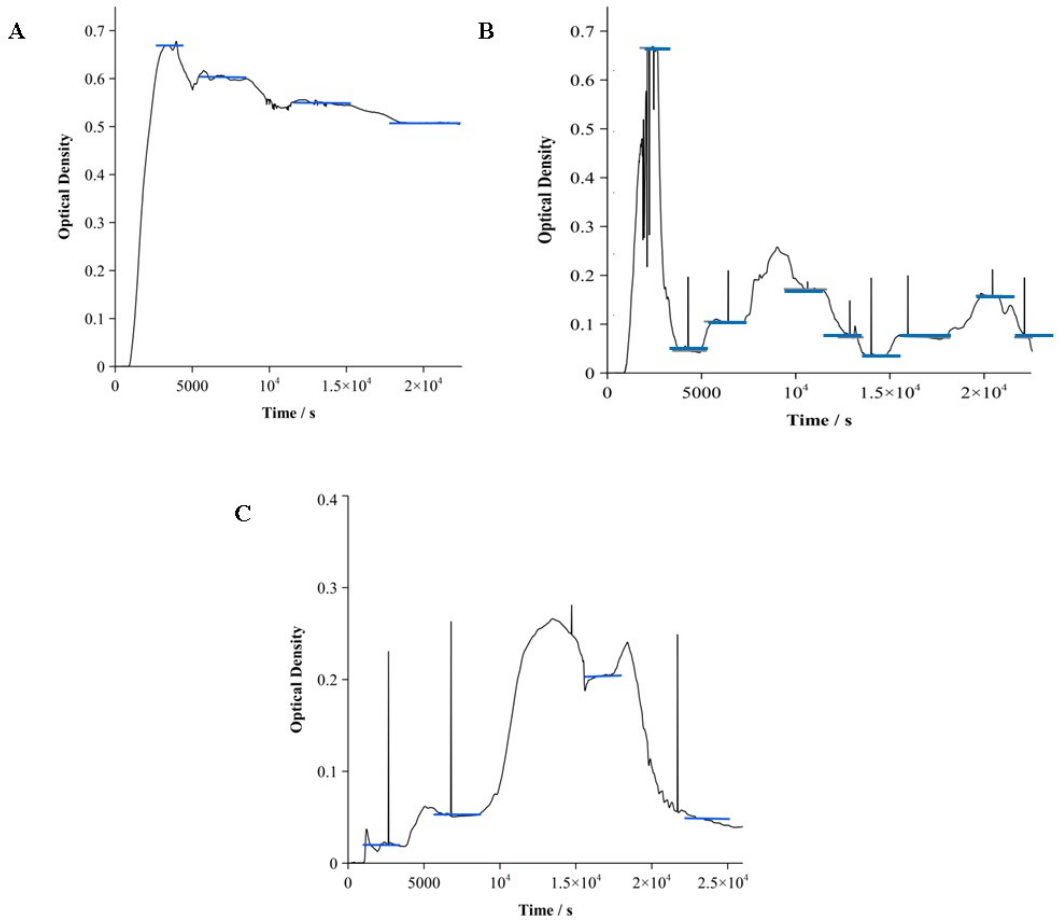

Figure AI.4. Evolution of OD_B at λ_{max} *versus* time (s) for 12.1 ± 0.3 nm **A)** BSPP AuNPs **B)** DNA monoconjugates and **C)** DNA-AuNP dimers at different flow rates

Blue lines in the lots of **Figure AI.4** represent the average value for OD_B at λ_{max} for given flow rates. These values were then used to determine the ξ_{exp} and by extension the diffusion coefficients.

In **Section 5.4**, sedimentation properties of AuNP and DNA-AuNP assemblies were investigated using digital photography. From these observations, suitable parameters for the preparative centrifugation of nanoparticle solutions were estimated.

AuNP diameter (nm)	***D*** **(10^{-12} $m^2.s^{-1}$)**	***s*** **(10^{-9} s)**
13	19.9	0.116
20	13.0	0.274
40	6.48	1.10
50	5.18	1.71
60	4.32	2.47
80	3.24	4.38
100	2.59	6.85
150	1.73	15.4

Figure AI.5. Calculated diffusion *D* and sedimentation *s* coefficients for gold nanoparticles in water using the Einstein-Smolukowski-Sutherland and Stokes relations (277 K, 1.56 mPa.s)

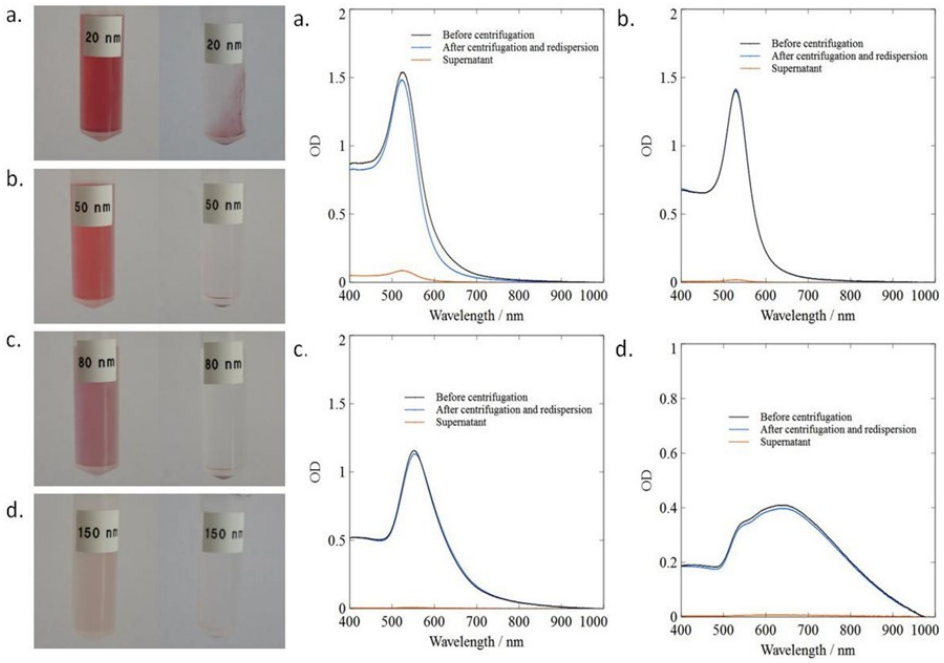

Figure AI.6. Photographs (left) and extinction spectra (right) before and after the centrifugation of gold nanoparticles in water, for 30 min at the centrifugal acceleration recommended by the Mason-Weaver model. A) 20 nm (4931 x g). B) 50 nm (789 x g). C) 80 nm (308 x g) and D) 150 nm (88 x g)

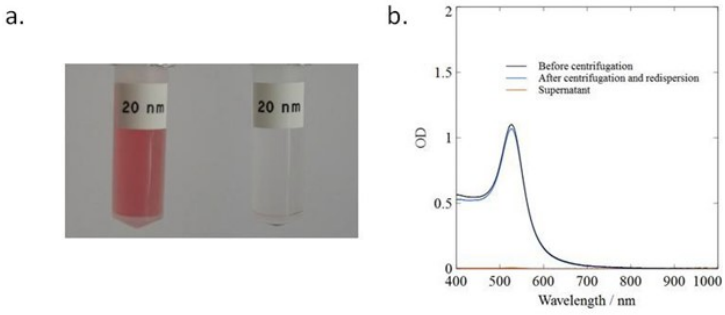

Figure AI.7. Centrifugation of 20 nm gold nanoparticles in water, for 30 min at 6000 x g, 20% higher than Mason-Weaver recommendation

At the exception of the 20 nm, for all AuNPs the recommended centrifugal accelerations gave excellent results (see **Figure AI.5**). For 20 nm AuNPs, an increase of 20 % on the recommended acceleration also gave satisfying results.

AII. Supplementary information for Chapter 6

In **Section 6.4**, grown dimer assemblies are purified using agarose gel electrophoresis. A lost in dimers yield was observed. In order to understand if the DNA system used to assemble the dimers was stable in the synthesis condition a PAGE was run.

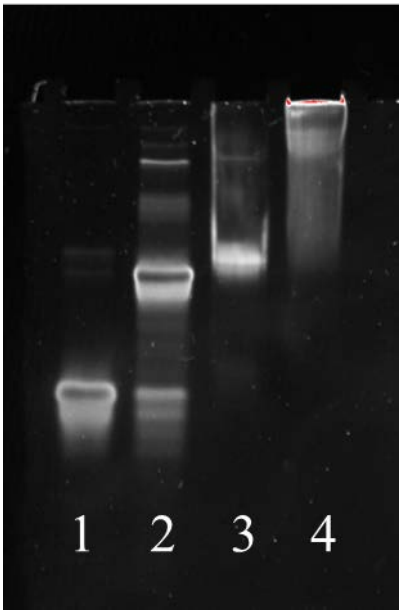

Figure AII.1. Investigation of the effect of the growing conditions on single and double strand DNA system (DNA Bcc and Ccc) by native 6% PAGE. Lane 1, strand Bcc, reference for ssDNA in phosphate buffer. Lane 2, duplex Bcc-Ccc, reference for dsDNA in phosphate buffer. Lane 3, duplex Bcc-Ccc in growth media without Au. Lane 4, duplex Bcc-Ccc in growth media with gold

As it could be observed in lane 3 no degradation of the duplex Bcc-Ccc was observed when incubating in the growth media without the Au salt. The smeared signal observed in lane 4 was due to the presence of the Au salt and not degradation.

The difference in shape polydispersity between single and dimer grown particles were investigated by using purified single seeds.

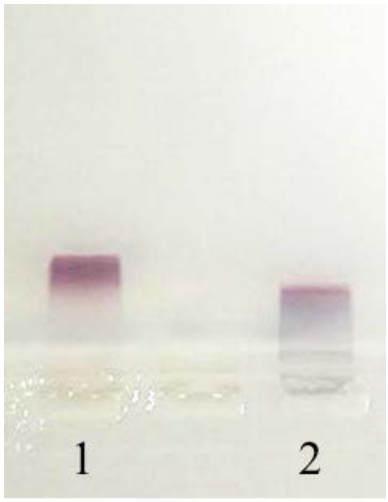

Figure AII.2. Agarose gel to study the influence of the seeds purification on the growing process. Lane 1 shows single 5.7 ± 0.2 nm seed AuNPs purified twice by agarose gel electrophoresis. Lane 2 shows single grown assemblies synthesized using the purified seeds

If compare to **Figure 6.5A**, lane 2 of this gel (see **Figure AII.2**) did not show a distinctive blue band. This result is attributed to a reduction of the shape polydispersity.